TIMELY AND UNIFORM APPLICATION OF CURING MATERIALS

John T Kevern, PhD, PE, F.ASCE, FACI, LEED AP
Division of the Natural and Built Environment
University of Missouri-Kansas City

Dan Zollinger, PhD
Professor, Civil & Environmental Engineering
Texas A&M University

Danny X. Xiao, PhD, PE, ENV SP
Department of Civil and Environmental Engineering
University of Wisconsin-Platteville

WisDOT ID no. 0092-22-03

September 2025

RESEARCH & LIBRARY UNIT

WISCONSIN HIGHWAY RESEARCH PROGRAM

WISCONSIN DOT
PUTTING RESEARCH TO WORK

Technical Report Documentation Page

1. Report No. WHRP 0092-22-03	2. Government Accession No.	3. Recipient's Catalog No.
4. Title and Subtitle TIMELY AND UNIFORM APPLICATION OF CURING MATERIALS		5. Report Date September 2024
		6. Performing Organization Code
7. Author(s) John T Kevern; Dan Zollinger; Danny X. Xiao		8. Performing Organization Report No. If applicable, enter any/all unique numbers assigned to the performing organization.
9. Performing Organization Name and Address University of Missouri-Kansas City, 5110 Rockhill, Kansas City, MO 64110 Texas A&M University, 201 Dwight Look Engineering Building, College Station, TX 77843 University of Wisconsin-Platteville, 1 University Plaza, Platteville, WI 53818		10. Work Unit No. 11. Contract or Grant No. WHRP 0092-22-03
12. Sponsoring Agency Name and Address Wisconsin Department of Transportation Research & Library Unit 4822 Madison Yards Way Room 911 Madison, WI 53705		13. Type of Report and Period Covered Final Report October 2022 ~ September 2024 14. Sponsoring Agency Code

15. Supplementary Notes
If applicable, enter information not included elsewhere, such as translation of (or by), report supersedes, old edition number, alternate title (e.g. project name), or hypertext links to documents or related information.

16. Abstract

This research project was undertaken to assess the current state of membrane-forming curing compound application in Wisconsin. In particular, the impact of rate of application and timing of application was assessed against various concrete and pavement properties. Laboratory testing provided anticipated baseline concrete performance for a variety of potential environmental conditions. Four field sites were assessed during the 2023 and 2024 construction season. Laboratory results showed that for most environmental conditions sufficient application rate is more important than uniformity. However, at the highest evaporative conditions both coverage rate and consistency are important. Concrete tested at 0.5 inches below the surface was agnostic to environmental conditions, supporting definition of the cure-affected zone as between 0.5 in. and the surface. The field research involved simple observations of construction timing and measures of how much curing compound was applied along with chilled mirror humidity profiles, shrinkage, ground penetrating radar (GPR), and joint activation and movement assessment. Test sections were installed with high and low coverage during early morning and later afternoon paving, and when possible, included an extended delay. The results showed that application rate and timing can be controlled in the field and were highly correlated to shrinkage, joint activation, and slab movement. A stepped implementation process is provided in Section 6 which begins with the easiest and fastest steps to achieve, followed by recommended improvements. The knowledge, technology, and data processing capabilities exist to move into the era of fully managed performance engineered curing.

17. Key Words Concrete paving, Concrete construction, Concrete Curing, Concrete Sensors	18. Distribution Statement No restrictions. This document is available through the National Technical Information Service. 5285 Port Royal Road Springfield, VA 22161

19. Security Classif. (of this report) Unclassified	20. Security Classif. (of this page) Unclassified	21. No. of Pages 130	22. Price N/A

Form DOT F 1700.7 (8-72) Reproduction of completed page authorized

TIMELY AND UNIFORM APPLICATION OF CURING MATERIALS

Final report

September 2024

Principal Investigator
John T. Kevern, Professor
University of Missouri-Kansas City

Co-Principal Investigator(s)
Dan Zollinger, Professor, CMS
Danny Xiao, Associate Professor
University of Wisconsin-Platteville

Research Assistant(s)
Etienne Beya Nkongolo

Authors
John T Kevern, Dan Zollinger, Danny X. Xiao

Sponsored by
Wisconsin Department of Transportation (WisDOT)

U.S. Department of Transportation

Office of the Assistant Secretary for Research and Technology

Preparation of this report was financed in part through funds provided by the Wisconsin Department of Transportation through its Highway Research Program (WHRP 22-03)

Disclaimer

This research was funded through the Wisconsin Highway Research Program by the Wisconsin Department of Transportation and the Federal Highway Administration under Project 0092-22-03. The contents of this report reflect the views of the authors who are responsible for the facts and accuracy of the data presented herein. The contents do not necessarily reflect the official views of the Wisconsin Department of Transportation or the Federal Highway Administration at the time of publication.

This document is disseminated under the sponsorship of the Department of Transportation in the interest of information exchange. The United States Government assumes no liability for its contents or use thereof. This report does not constitute a standard, specification or regulation.

The United States Government does not endorse products or manufacturers. Trade and manufacturers' names appear in this report only because they are considered essential to the object of the document.

EXECUTIVE SUMMARY

This research project was undertaken to assess the current state of membrane-forming curing compound application in Wisconsin. In particular, the impact of rate of application and timing of application was assessed against various concrete and pavement properties. Laboratory testing provided anticipated baseline concrete performance for a variety of potential environmental conditions. Four field sites were assessed during the 2023 and 2024 construction season. The acceptable type and rate of application of membrane-forming curing compound (MFCC) is highly variable across the US. This is not because concrete curing behavior is vastly different in different states, moreover, from a review of the literature and assessment of current methods, no quantifiable process existed at the beginning of this research to assess if sufficient MFCC had been applied for the environmental conditions. The thinking is that the current practices are generally fine, but with the feeling that more can be done. Consequently, the research plan involved simple and accessible measures which can be implemented today along with more advanced measurements for future consideration.

The laboratory portion evaluated moisture loss and surface hydration for a wide range of simulated environmental conditions, quality of MFCC application, and timing. A new technique of embedded resistance was developed to assess the differences between the cure-affected zone and the bulk or interior of the concrete. Results showed that for most environmental conditions, having sufficient MFCC but non-uniformly applied is more beneficial than insufficient and uniform coverage. However, at the highest evaporative conditions both coverage rate and consistency are important. Another interesting finding is that when MFCC is applied too early, when significant bleed water is present, the long-term evaporation rate is much higher due to dilution of the MFCC. Also, the concrete tested at 0.5 inches below the surface was agnostic to environmental conditions, supporting definition of the cure-affected zone as between 0.5 in. and the surface.

The field portion of the research involved simple observations of construction timing and measures of how much MFCC was applied along with chilled mirror humidity profiles, shrinkage, ground penetrating radar (GPR), and joint activation and movement assessment. For the initial sites the timing of application, speed of curing cart, and consistency of application were too highly variable to draw any strong research conclusions. So during the second observational visit the research team worked with the cart operator to improve consistency and reduce the variability. Of likely the most important outcome for the research, this small intervention provided excellent control of coverage. For subsequent sites test sections were installed with high and low coverage during early morning and later afternoon paving, and when possible, included an extended delay. The results showed that application rate and timing can be controlled in the field and were highly correlated to shrinkage, joint activation, and slab movement. The Evaluation Index (EI) parameter was utilized and showed that the optimum application rate can be determined from the anticipated weather conditions and that real-time monitoring using a weather station, relative humidity, and embedded resistance can confirm the applied MFCC is producing the desired concrete conditions. Finally, GPR can be used to confirm complete coverage.

A stepped implementation process is provided in Section 6 which begins with the easiest and fastest steps to achieve, followed by recommended improvements. The knowledge, technology, and data processing capabilities exist to move into the era of fully managed performance engineered curing.

Contents

List of Figures

List of Tables

1 INTRODUCTION

Curing of concrete is the act process to maintain an appropriate temperature and moisture content in concrete for a defined period so that the concrete develops the desired material properties (Vandenbossche,1999; ACI 308, 2016). Most simply, curing of concrete promotes increased hydration of Portland cement through control of moisture loss and sometimes of temperature (Powers, 1947). Curing of concrete occurs immediately after concrete is placed and finished and requires the maintenance of favorable conditions both at depth and near the surface for an extended period. According to American Concrete Institute (ACI) committee 308, concrete possesses a near-surface cure-affected zone which is strongly related to surface durability which is differentiated from curing and performance of the interior, bulk concrete. As concrete may result in numerous different shapes and volumes, the amount of exposed surface area is quite different between a pavement slab and a foundation. It can be argued that if curing is only a surface effect, curing has a minimal impact on the strength of large elements. All the classic data showing loss of strength related to curing is based on small cylinders and the effect is sample size dependent. For slabs, the effect of curing is observed in the surface layer including abrasion resistance, resistance to scaling, and diffusion. Curing effectiveness is related in part to various concrete pavement distress types such as plastic and drying shrinkage, cracking, scaling, joint spalling, and freeze-thaw deterioration. Some construction specifications such as Wisconsin Construction and Materials Manual, American Society for Testing and Materials (ASTM) among others do not provide proper configuration to qualify curing effectiveness characteristics in terms of the type of performance expected from a given environment. Most specifications for membrane-forming curing compound application require an application rate of 100-200 ft^2/gallon with little regard for field conditions or moisture needs of the concrete. Although ASTM C309 curing compound selection criteria have been identified, researched, and found to have utility for curing compound approval, none of the criteria described above have been systematically related to pavement performance or even a performance-related parameter that is practical and measurable under field conditions. Additionally, ASTM C156 guidance presents some limitations such as being conducted on smooth mortar samples, conducted under fixed ambient conditions (temperature, relative humidity, and wind speed), and a fixed application rate. Quality concrete curing is achieved through uniform and proper curing within the top few inches of the exposed surface with actual field performance poorly linked to quality assurance practices.

1.1 Problem statement

Concrete pavement is designed to provide a long service life. However, concrete curing regime affects the durability of concrete. Concrete curing using Membrane Forming Curing Compound (MFCC) is widely used by State Departments of Transportations (DOTs), due to less maintenance and low cost compared with water curing or covering with plastic sheeting. However, there is no existing method for quantifying or systematically evaluating the quality or effectiveness of curing in the field. Many specifications rely on the curing application rate which is the quantity of curing compound that can be applied on a specific surface area of concrete pavement, and for some other States DOTs the acceptance of the curing compound application depends on the inspector experience and quality standards such as uniform coverage compared to white paper sheet. Therefore, this study is exploring ways to provide a methodology that can be used as quality control, capable of measuring or monitoring the effectiveness of MFCC applications in the field.

1.2 Projects objectives

The study entails the qualification of curing compound application effectiveness relative to effects on long-term performance of concrete pavement. Curing quality combined with weather conditions at the time of construction are important factors in the performance and durability of concrete pavements. Adequately cured concrete has adequate moisture for continued hydration and development of strength, volume stability, resistance to freezing and thawing, and abrasion and scaling resistance.
The main objectives are:

- Observing and recording when and how uniformly the curing materials are applied by assessing representative concrete pavement projects in Wisconsin,
- Documenting how curing compound application times and coverage relate the development of distress (such as: shrinkage, cracks, scaling, or delamination) on concrete pavement, and
- Developing a measurable methodology to establish optimal times and assess uniform application.

2 LABORATORY WORK

2.1 Introduction

The laboratory portion of this research aims to link concrete pavement performance measures with application rate and application quality along with the evaluation of new curing compound assessment techniques. Beside limiting evaporation, MFCCs provide additional benefits of increasing solar radiation reflectance (Vandenbossche, 1999). The Wisconsin Department of Transportation (WisDOT) requires the use of wax or resin curing compounds within Type 2A/B according to the ASTM C309 specification. The laboratory work was intended to provide an understanding of concrete pavement behavior, cured at different application rates, curing conditions and application time. By expanding the tested conditions, a curing table can be developed to encompass the range of anticipated weather and curing performance and provide application rate envelopes to achieve the desired performance. For every concrete batch produced the baseline properties (unit weight, air content, slump, setting time, compressive strength, and surface resistivity) were determined to ensure consistency between the batches. Surface profile degree of hydration determined the hydration evolution between the cured affected zone and the interior of concrete, concrete moisture retention capacity was determined for all the curing conditions, and lastly, a continuous resistance technique test was developed to assess the effectiveness of curing compound in real time.

2.2 Experimental design and testing

The variables investigated in the laboratory were time of curing compound application, application rate and quality, and lastly curing conditions. For each of the evaporative conditions, four curing compound application rates were evaluated (uncured, non-uniform 180 sf/gal, uniform 180 sf/gal, uniform 400 sf/gal). WisDOT requires an application rate of 150 sf/gal for textured and tined pavement. The application rate for textured and tined pavement needs to be higher than for smooth surfaces to account for the additional surface area. The lighter rate of 180 sf/gal was used in the laboratory since the samples were too small to accurately reproduce tining. Curing application timing was varied (immediately after the final surface finishing while bleed water was present and at initial set when no bleed water was present). At least for the laboratory specimens, the point at which bleed water was no longer present coincided with initial set. Testing included concrete batch quality control (slump test, air content and unit weight), Box Test, surface profile degree of hydration, setting time (Vicat apparatus and Ultrasonic Pulse Velocity), compressive strength, surface resistivity, moisture loss (ASTM C156), and embedded resistance. The curing compound used was a poly alpha methyl styrene (PAMS) based product meeting ASTM C309 Type 2B meeting WisDOT specification. The laboratory concrete mix design used (**Table 1**) represented a WisDOT Grade "A" mixture using Type IL cement and limestone aggregate developed using the WisDOT DT2221 optimal mix spreadsheet. Since the status and availability of Supplementary Cementitious Materials (SCMs) is highly variable, the mixture utilized only cement for the broadest applicability in the future. The concrete batch size was 1.5 cubic feet, and the mixture was dosed with Air Entrainer Agent and polycarboxylate water reducer. Aggregate quality control was maintained by washing coarse aggregate and oven drying both fine and coarse aggregate 24 hours before mixing. Four application rates used are shown in **Figure 1**, where A represents the uncured specimens or 0 ft^2/gal, B represents specimens cured at 400 ft^2/gal applied using a brush, C: non-uniformly applied 180 ft^2/gal applied using a pump sprayer, and D represents 180 ft^2/gal uniformly applied using a pump sprayer. A full list of the laboratory tests is shown in **Table 2**.

Laboratory specimens for moisture loss and the associated tests had MFCC applied to the surface with edges and bottom covered by the plastic mold. The assumption is that all the measurable moisture is lost through the surface. In practice the edges of a concrete pavement are coated with MFCC while the

bottom is open for moisture to be lost through absorption to the aggregate base or gained by the humidity movement from the ground. Similarly, lab samples represent a much smaller volume of material than for a full-depth slab and have less total moisture to evaporate. As such, moisture loss measured or specified for lab testing cannot be directly linked to expectations for field concrete performance.

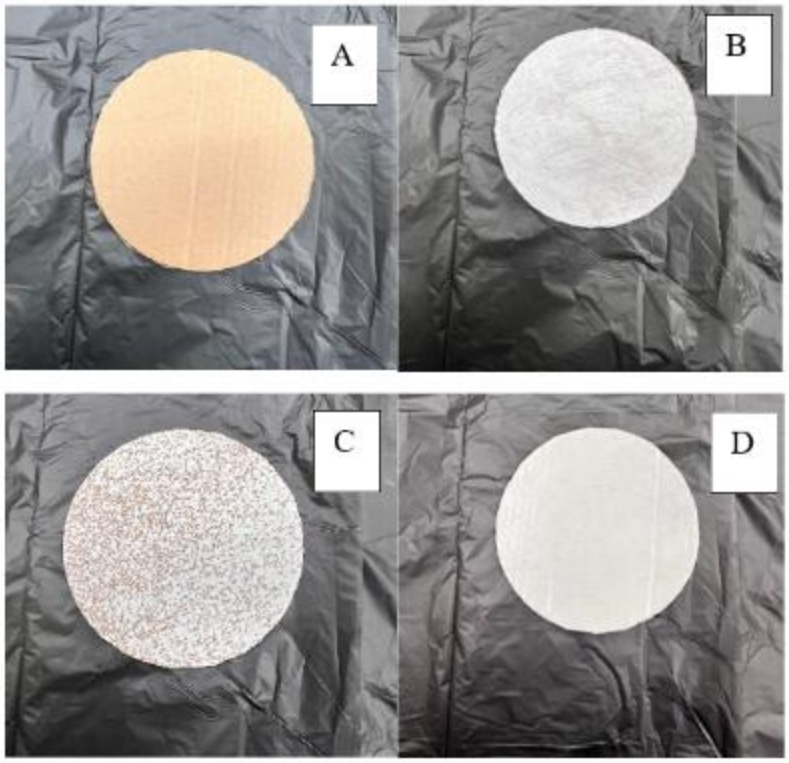

Figure 1. Different types of application rates, A: uncured specimens, B: 400 ft2/ gal (400U), C: non-uniform 180 ft2/ gal (180 NU), and D: 180 ft2/ gal (180U)

Table 1. Laboratory Concrete Mix design (pcy: pounds per cubic yard)

Materials	Mixtures (pcy)
Cement 1L	545
Fine aggregate	1340
Intermediate aggregate	1170
Coarse aggregate	650
Water	220
w/cm	0.42

Table 2. Laboratory tests

Tests	Specification	Significance
Slump test	ASTM C143	Workability
Air content	ASTM C231	Baseline performance for the mixture
Unit weight	ASTM C138	Baseline performance for the mixture
Box test	CP-63-19	Baseline performance for the mixture (workability)
Compressive strength	ASTM C31/ ASTM C39	Baseline performance for the mixture
Surface resistivity	AASHTO T358	Baseline performance for the mixture
Vicat apparatus	ASTM C191/C403	Provides baseline setting behavior in relation to curing compound application timing.
Ultrasonic Pulse Velocity	N/A	Provides baseline setting behavior in relation to curing compound application timing.
Degree of Hydration	N/A	Provides an actual measure of influence of curing on concrete condition
Moisture loss	ASTM C156	Provides a comparison to the gold standard curing compound test.
Embedded resistance	N/A	Measure the difference between cured affected zone and concrete interior.

2.2.1 Ultrasound Pulse Velocity

Ultrasound Pulse Velocity (UPC) was tested on concrete 4 in. x 8 in. concrete cylinders. The cylinder mold was placed in a plastic frame, where transducers were placed on top and bottom in contact with the cylinder as shown in **Figure 2.** To create contact between the top transducer with the surface of the concrete, a plexiglass disc was used. A commercial gel coupling fluid was applied to both transducers. The UPV works by measuring the time it takes for the ultrasonic wave to travel from the transmitter to the receiving transducer. Velocity of fresh concrete is relatively low and increases with time as concrete starts to set and microstructure densifies.

Figure 2. Vicat apparatus (left) and UPV (right) used for setting time

2.2.2 Moisture Retention Test

The moisture retention test was completed first on mortar following the ASTM C156 standard to verify the performance of the selected MFCC and later the same procedure was followed on concrete with the exception of varying curing compound application time, application rate, and the curing condition as shown in **Table 3**. The effect of application rates was investigated by applying MFCC at four different application rates 0 (uncured), 400 ft^2/gal (400 U) uniformly applied using a brush, 180 ft^2/gal non-uniformly (180 NU) applied using a pump sprayer, and l80 ft^2/gal (180 U) uniformly applied using a pump sprayer. The effect of application time was investigated by applying curing compound right after the final surface finishing (approximately 30 minutes after mixing and 120 minutes before the initial set) and after the bleed water was no longer present (after the initial set). Lastly, the effect of curing conditions was investigated by curing concrete specimens in a temperature and humidity-controlled environmental chamber set at 10 different combinations of evaporation rates. Concrete weight was recorded every 24 hours throughout the 72 hours of curing to determine moisture loss following ASTM C156.

Table 3. Factorial design for Moisture retention test

Application time and rates		Curing condition		
Curing time (t)	Application rates (ft^2/Gal)	Temperature (F)	Relative Humidity (%)	Evaporation rate (lbs/ft^2/hr)
Before Initial Set	0	100.4	32	0.1576
After Initial set	400		75	0.0594
	180 NU		50	0.0833
	180 U	90	32	0.1125
			75	0.0388
			50	0.0318
		70	32	0.0185
			75	0.0009
		50	50	0.0015

2.2.3 Cylinder and Surface profile degree of hydration.

The degree of hydration (DoH) was performed using methods proposed by Fagerlund (2009). The DoH was determined from samples used to determine concrete strength at the ages of 1, 3, 7, and 28 days. The compressive strength samples were cured in lime water and represent the best possible hydration as a control. Immediately after the compressive strength test, concrete samples were crushed. These samples were ground using a mortar and pestle to a uniform fine powder and sieved using sieve number 30. The second set DoH herein identified as surface profile degree of hydration was determined using concrete samples cast in 6 in. diameter x 3 in. tall cylinder molds. The surface profile DoH was determined by measuring the DoH from the powder obtained from a depth of 1/16th in. and at 0.5 in from the surface (**Figure 3)**. After casting, the specimens were left in the laboratory condition until the bleed water was gone and curing compound was applied at the four different application rates (Uncured, 400U, 180 NU and 180 U). Samples were then stored in a controlled temperature and relative humidity environmental chamber set at 10 different evaporation rates. DoH was then determined at the age 1, 3, and 7 days of curing. DoH was determined from the collected powder through ignition where 5 g of the ground sample was placed in a ceramic crucible and in an oven at 105 °C for 2 hours to obtain the weight of the free evaporable water. Then, samples were placed in a furnace at 1000 °C for 1 hour to obtain the weight of the non-evaporable water. The non-evaporable water was taken as the mass loss between 105 °C and

1000 °C, the measurements were corrected to account for loss on ignition of the cement. The quotient w^0_n/c (which is the chemically bound water at complete hydration of cement quantity) of 0.25 was assumed in this study as shown in **Equation 1** and supported by **Equation 2** and **Equation 3** (Fagerlund, 2009).

Figure 3. Concrete after grinding to collect the powder used for degree of hydration (A), The mechanical grinder used (B)

$$\alpha = \frac{\boldsymbol{Wn}}{\frac{\boldsymbol{C\,effective}}{\frac{\boldsymbol{W_o^n}}{\boldsymbol{C}}}} \qquad \textbf{Equation 1}$$

Where: α = degree of hydration in percentage, W_n is the amount of chemically bound water determined.

$$\boldsymbol{Wn = W_d + W_i - Csample * (Agg._{LOI} + Cement_{LOI} * K)} \qquad \textbf{Equation 2}$$

Where: W_d is the weight of sample after drying, W_i the weight of the sample after ignition or burning in the oven set at temperatures of 1832 Fahrenheit, C_{sample} is the weight of cement in the concrete power determined following the mixture proportions and lastly K is the aggregate to cement ratio.

$$\boldsymbol{Csample_{effective} = (1 - g) * \frac{Wi}{1 - 0.44 * g}} \qquad \textbf{Equation 3}$$

Where: g is the limestone content in cement for the Type IL cement used in this study (the limestone content was 12%), the ratio W_o^n was 0.25 assuming that during hydration cement chemically binds about 25% by weight of water.

2.2.4 Embedded resistance

Embedded resistance was measured using a 2-pin array arrangement which contained a non-conductive plastic frame holding 4 stainless steel probes, 2 for each depth (surface and 0.5 inches) as shown in **Figure 4**. Two of the probes were just in contact with the surface of the concrete and the others were embedded 0.5 in (12.5 mm) into the concrete below the cure-affected depth. The sides of the probes were protected using nylon sleeves to ensure that data was collected only from the concrete at the probe tip. The frame was set 1 in. above the surface to allow the free movement of air on the concrete surface. An arbitrary cutoff of 160 kΩ/cm was selected as the maximum resistance value for recording resistance based on the range of initially observed results and the precision drift of the equipment. Samples for embedded resistance testing were cast in 6 in. x 3 in. cylinder molds. Embedded resistance was measured on the same environmental conditions and application rates as shown previously.

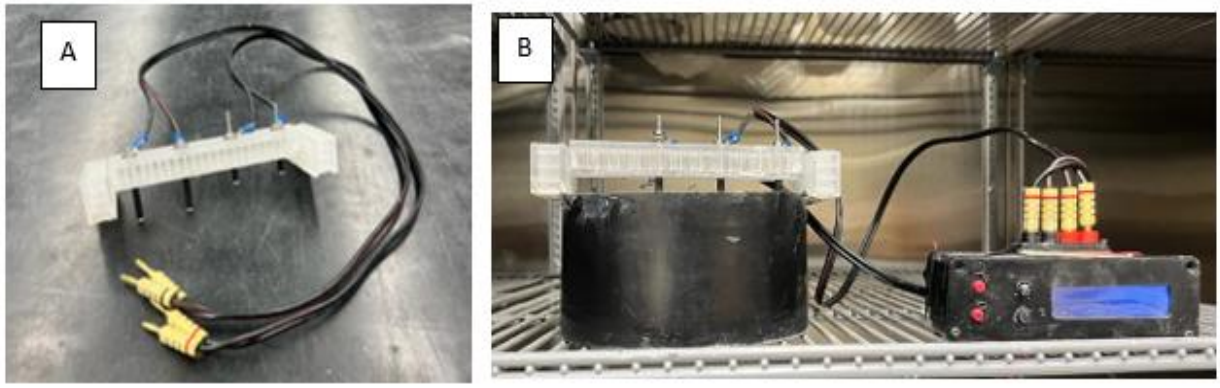

Figure 4. Embedded resistance test setup

2.3 Laboratory Results

2.3.1 Concrete Baseline Properties

Many (>60) concrete batches were produced for this study. Air content, unit weight, slump test, and setting time were measured for all the batches produced. Average values are shown in **Table 4.** The compressive strength was 6000 psi at 28 days of lime water curing from triplicate testing according to ASTM C39. The concrete surface resistivity of the same samples was 15 kΩ-cm, classified as moderate chloride ion permeability by AASHTO T277 (ASTM C1202).

Table 4. Average value of the concrete baseline properties

Slump, (in)	Unit weight (pcf)	Air content (%)	Initial set (min)	Final set (min)
1.5	149.5	5.2	155	240

2.3.2 Box Test Results

The box test is a simple, visual technique to quickly assess the edge-holding ability through a slipform paver. The box test mold was made of nonabsorbent plywood of 1 $ft^{3,}$ and a vibrator was used in a sequence of 3 seconds downward without touching the bottom of the box and 3 seconds vertical, the result of the test is shown in **Figure 5**. The concrete produced falls in category 1 and had less than 10 % of surface voids. The result shows that the concrete batch mixture responded well to the vibration with good edge holding.

Figure 5. Box test results

2.3.3 Moisture Loss Results

For moisture loss testing four evaporative conditions are shown representing the range of evaporative conditions tested in **Figure 6**. The data presented are average values from triplicate testing. The low evaporative condition was performed at 50°F and 75% RH with an estimated evaporation rate of 0.0009 lbs/ft^2/hr. The medium evaporative condition was performed at 70°F and 50% RH with an estimated evaporation rate of 0.0318 lbs/ft^2/hr. The moderate evaporative condition was performed at 90°F and 50% RH with an estimated evaporation rate of 0.0833 lbs/ft^2/hr. The high evaporative condition was performed at 100°F and 32% RH with an estimated evaporation rate of 0.1576 lbs/ft^2/hr. As expected, the moisture loss from the samples increased with higher evaporative conditions with the uncured samples having the greatest moisture loss. The effect of application rate and quality became more pronounced with increased evaporation rate. At the lowest two evaporation rates uniformity and rate were not significant factors. At the highest two evaporation rates, uniformity was less important than application rate. From a practical standpoint in the field, it is more important to ensure enough MFCC is being applied before focusing on uniformity. Unfortunately, uniformity is rather simple to visually assess where application rate is not.

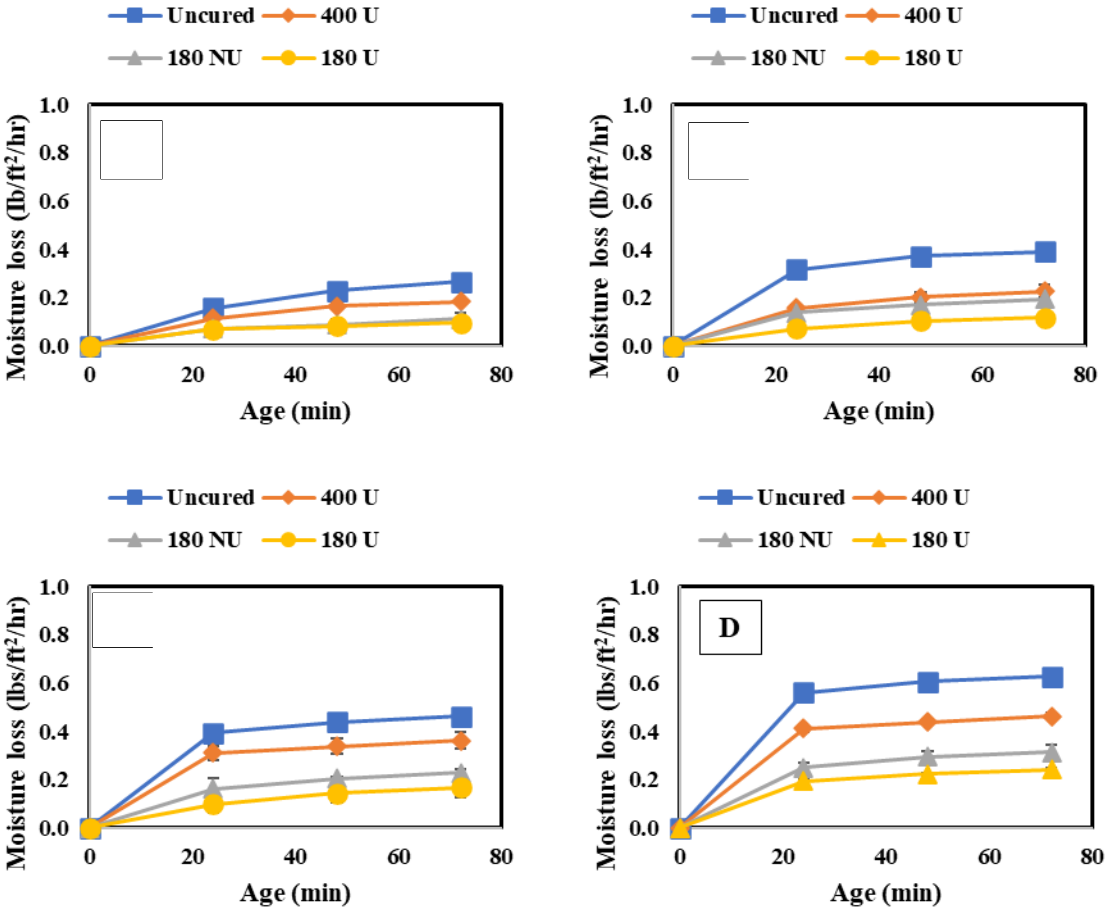

Figure 6. Moisture loss data for four selected curing conditions. A: Low Evaporation condition; B: Medium Evaporation condition; C: Moderate Evaporation condition and D: High Evaporation condition.

The effect of application time was investigated by comparing the moisture loss behavior of concrete when MFCC was applied directly after the final surface finishing (120 minutes before the initial set) or at the initial set (210-240 minutes from the time when cement met water). It should be noted that

the evaporative conditions of the laboratory are quite low resulting in a much longer time for bleed water to evaporate. The comparison was performed by comparing moisture loss after 72 hours of curing for all the four application rates identified as Uncured, 400 U, 180 NU and 180 U and four curing conditions. **Figure 7** shows the lowest results, **Figure 8** for the medium, **Figure 9** for the moderate, and **Figure 10** for the highest evaporative conditions. In all cases the samples where MFCC was applied while bleed water was present had the greatest moisture loss. While some of the difference can be attributed to evaporation during the 120 minutes between the before and after condition, the additional moisture loss is more evaporation. It has been well-described that in all but the harshest conditions, most of the bleed water is reabsorbed as pores empty during hydration (Henkensiefken et al., 2009). Applying the MFCC to wet concrete likely dilutes the chemicals and creates a more permeable final film. Whatever the mechanism, it is important to ensure MFCC is applied after bleed water is no longer present. While the timing is important, slow loss of bleed water corresponds to low evaporative conditions which are much less sensitive to curing effects and likely not of high importance.

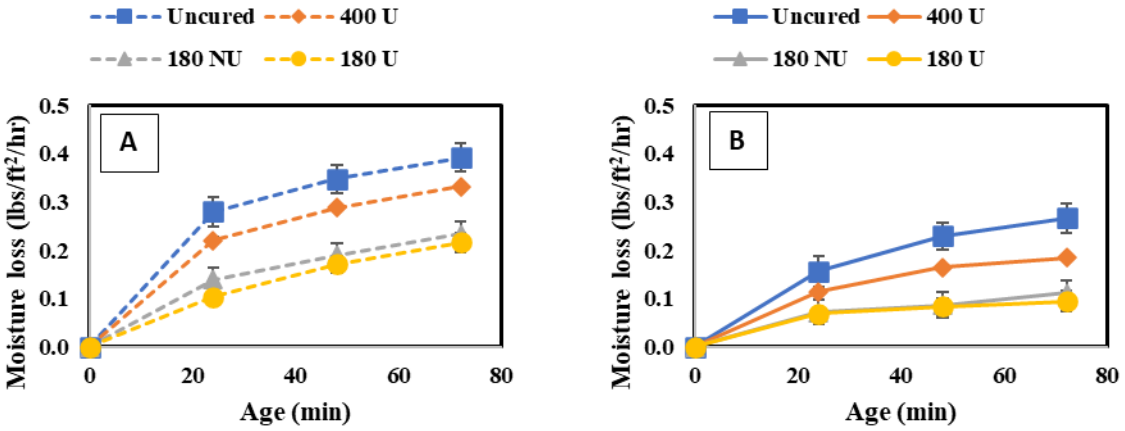

Figure 7. Moisture loss for Low evaporative conditions (50F 75%), (A) Before Initial set (B) After Initial set.

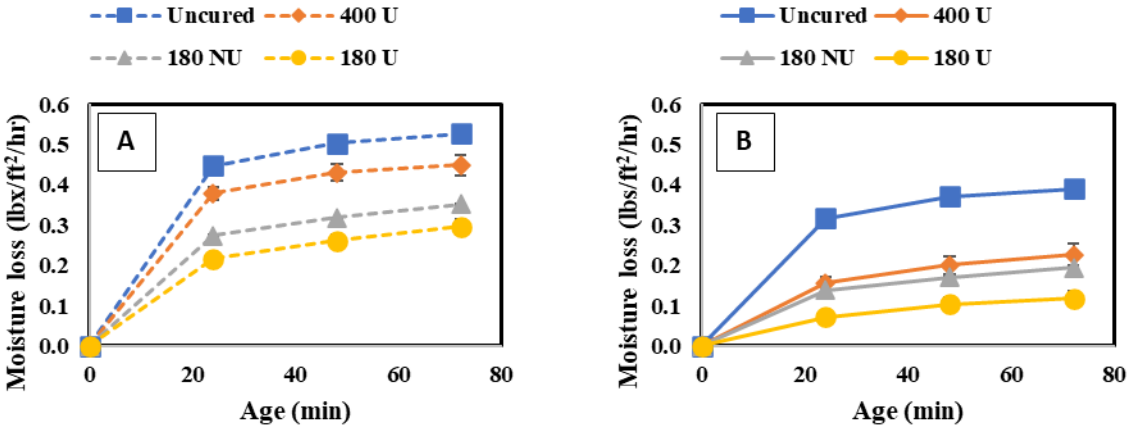

Figure 8. Moisture loss for Medium evaporative conditions (73F 50%), (A) Before Initial set (B) After Initial set

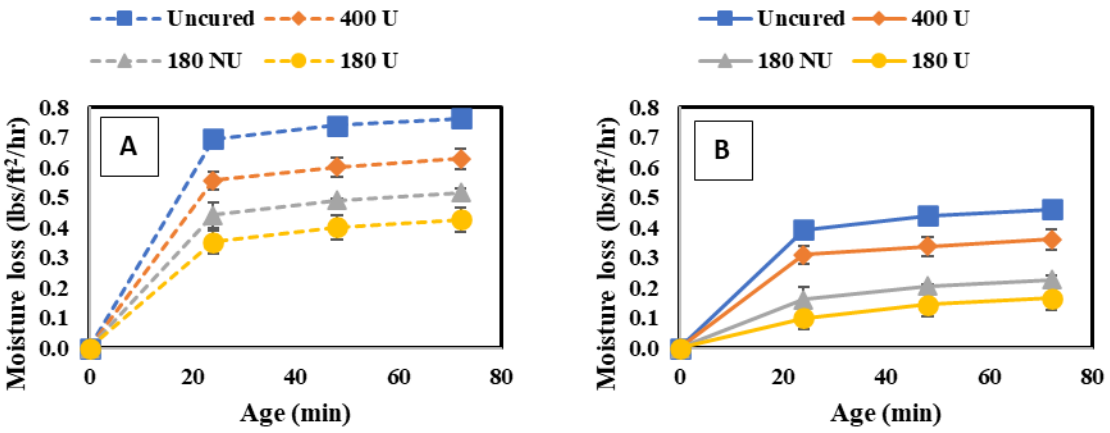

Figure 9. Moisture loss for Moderate evaporative conditions (90F 50%), (A) Before Initial set (B) After Initial set.

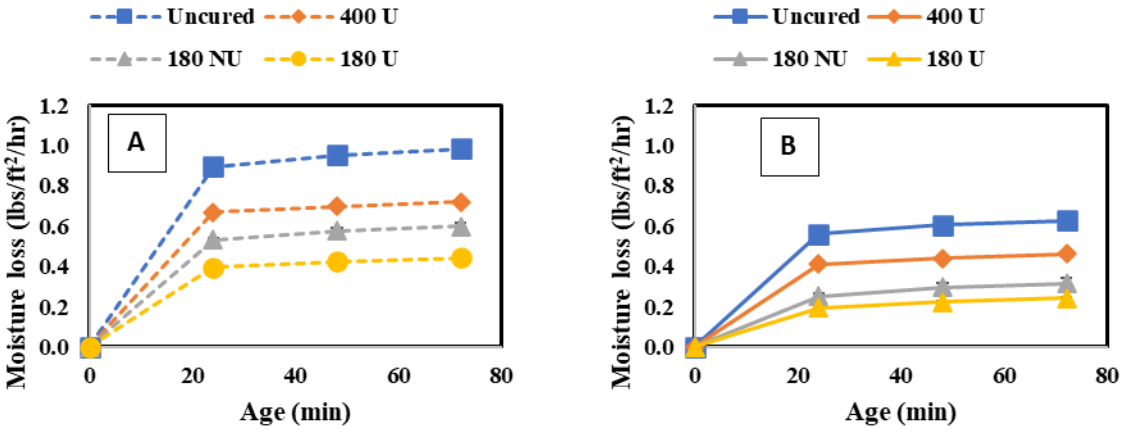

Figure 10. Moisture loss for High evaporative conditions (100F 32%), (A) Before Initial set (B) After Initial set.

2.3.4 Degree of Hydration Results

DoH was determined for the near surface and at 0.5-inch depth for all the four selected evaporative conditions with results shown in **Table 5.** As expected, DoH increased with time with the lowest evaporative conditions producing the highest DoH and better curing producing the highest DoH. The DoH at the 0.5 in. depth was statistically similar for all treatments, environmental conditions, and ages suggesting that the cure-affected zone does not extend to 0.5 inches.

Table 5. Surface profile degree of hydration for all four curing conditions.

Age (day)	Uncured				400 U			
	Low	Medium	Moderate	High	Low	Medium	Moderate	High
1	42.35	38.58	38.38	37.56	43.90	43.72	43.90	41.07
3	47.48	45.47	40.72	39.79	50.89	50.64	47.32	46.06
7	53.09	50.84	44.60	40.29	56.83	54.59	53.95	52.38
Age (day)	180 U				Interior Degree of Hydration			
	Low	Medium	Moderate	High	Low	Medium	Moderate	High
1	52.36	49.82	47.42	45.11	53.53	55.57	55.57	55.57
3	56.36	54.02	52.99	50.00	56.57	55.89	56.04	56.36
7	67.29	66.41	63.84	65.95	68.39	67.89	67.75	68.20

2.3.5 Embedded Resistance Results

Embedded resistance results are shown for the four selected evaporative conditions with low shown in **Figure 11**, medium in **Figure 12**, moderate in **Figure 13**, and high in **Figure 14**. As expected, the embedded resistance results coincide with both moisture loss and degree of hydration with the lowest evaporative conditions rising slowly and high evaporative conditions much more quickly. Interestingly the importance of curing rate over uniformity observed from the moisture loss specimens was also observed for embedded resistance with uniformity only becoming significant at the highest evaporation rate. The resistance values at the 0.5-inch depth were again similar for all treatments and environmental conditions further reinforcing that 0.5 inch is below the cure-affected zone.

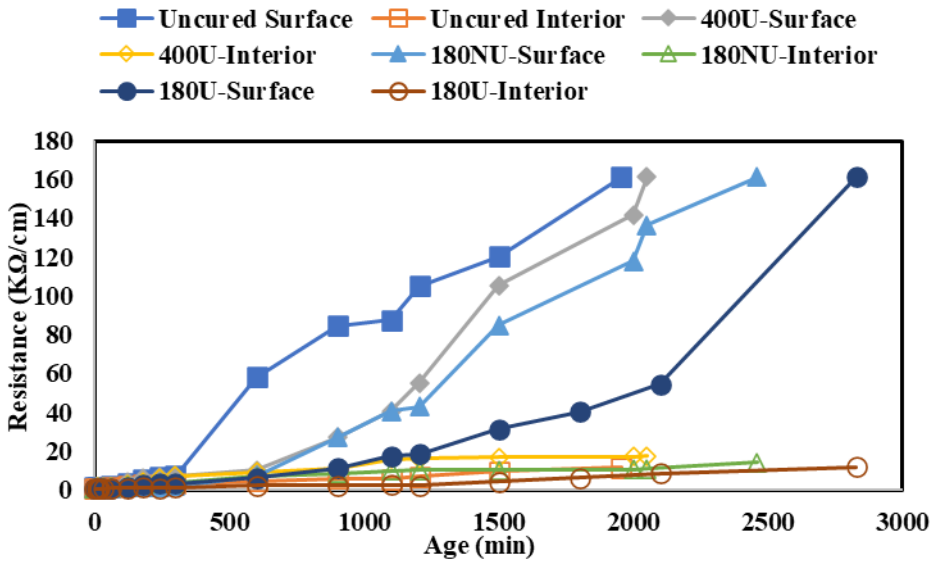

Figure 11. Resistance for low evaporative condition (50F,75% RH) Interior refers to probe inserted at 0.5 in.

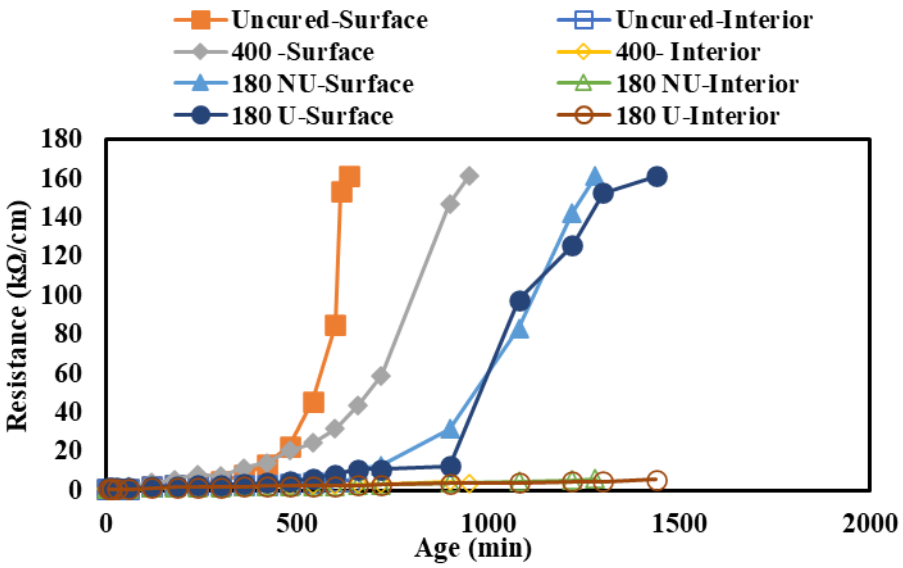

Figure 12. Resistance for Medium evaporative condition (74F,50% RH) Interior refers to probe inserted at 0.5 in.

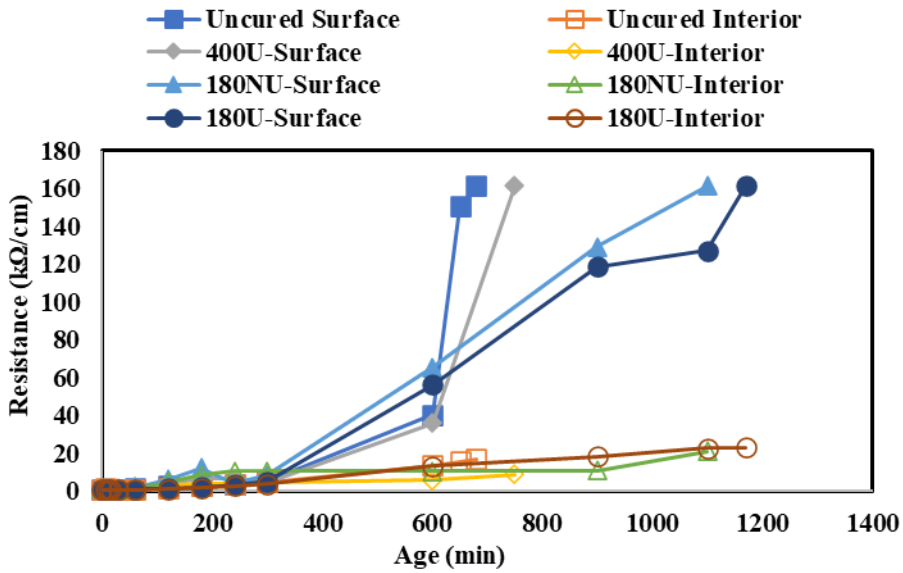

Figure 13. Resistance for Moderate evaporative condition (90F,50% RH) Interior refers to probe inserted at 0.5 in.

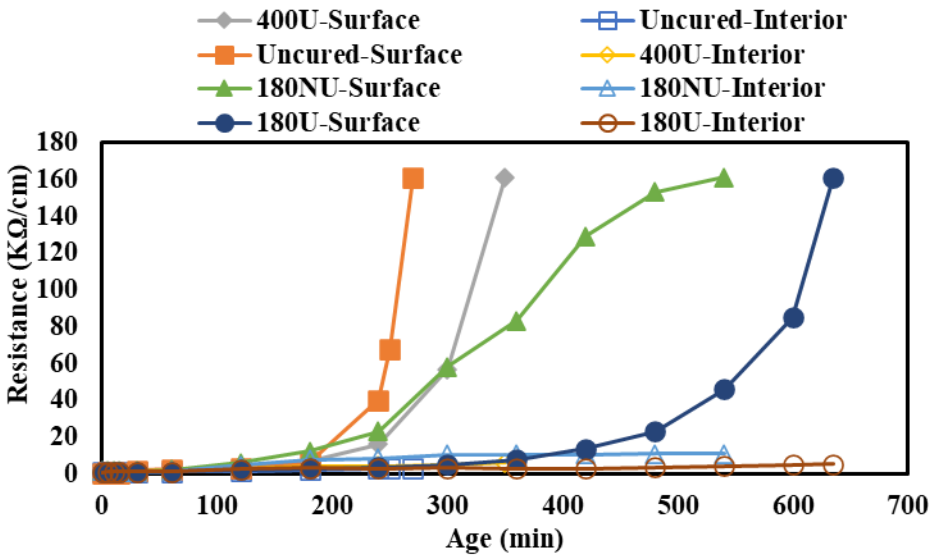

Figure 14. Resistance for High evaporative condition (100F,32% RH) Interior refers to probe inserted at 0.5 in.

2.4 Summary

The laboratory work was performed to investigate concrete behaviors under different treatments and environmental conditions and important observations include:

- Considering the amount of bleed water evaporated between completion of initial finishing and present at the ideal time to apply MFCC (after bleed water was no longer present), moisture loss was higher when MFCC was applied while bleed water was present.
- Moisture loss, degree of hydration, and embedded resistance all correlated with higher moisture loss, lower DoH, and increased resistance with increased evaporation rates.
- When comparing application quality, it was more important to have enough MFCC over less, uniformly applied as demonstrated by the superior performance of the 180NU compared to 400U samples.
- Results at the interior location of 0.5 in. were insensitive to MFCC application quality or environmental condition supporting that location as a good baseline outside of the cure-affected zone.
- Embedded resistance testing was supported by both moisture loss and DoH. Embedded resistance is a much simpler and quicker test to perform and could be a suitable surrogate for both.

3 FIELD OBSERVATIONAL VISITS

3.1 Overview

The concrete curing process is fundamental to concrete performance and durability. Concrete is cured to create uniform hardened properties development from the curing affected zone and the interior of concrete. Quality curing is achieved when a correct amount (application rate) of qualified curing compound is applied uniformly and in a timely fashion. Unfortunately achieving this is challenging due to the lack of appropriate techniques to assess concrete curing effectiveness in real time. Specific quantification of curing is elusive, some DOTs such as Minnesota and Texas use the rather ambiguous white paper sheet examination. As shown in the previous laboratory testing, the rate appears more significant than uniformity under the most important and highest evaporative conditions. During the summer paving season of 2003 and 2024 four observational site visits were made to assess the current state of the practice and assess the influence of some limited curing practice modifications. Among the tests utilized included a weather station that provided the relative humidity data at the surface of concrete, inside concrete at a determined depth through which curing quality or performance is evaluated by comparing curing quality between the ambient, filtered, and sealed conditions. A Ground Penetrating Radar (GPR) was used to assess the uniformity of curing based on the variance displayed within the dielectric measurements. Additionally, embedded resistance technique was developed by the research team and allows quantification of performance differences between the surface and interior concrete in addition to more simple assessment of application. The sites and observation dates are shown in **Table 6**.

Table 6. Site visit description

		Dates	
Site location	Road ID	From	To
Mequon	I-43	11-May	13-May
New London	STH-15	30-May	3-Jun
Wausau	STH-29	29-Aug	2-Sep
Haugen, 2024	STH-53	24-Jun	27-Jun

3.2 Testing Methodology

Three field visits were undertaken during the summer of 2023. Activities included recording of time delay of curing compound application, rates of application, weather conditions, and various other construction data. Caltrans Test CT535 was used to determine the localized application rate. Visual inspection/rating was used as a low-cost technique for identifying potential defects which can be easily compared with GPR results. When possible, the application rate was adjusted. Sections were observed during the morning and afternoon of the placement to assess temperature effects.

Field testing was conducted at each site designated for field monitoring for curing effectiveness. Data collection was obtained using various testing methods and techniques as subsequently described. Testing of curing compounds was carried out with two primary objectives: (1) to establish and prove superior performance and (2) to ensure a close and consistent correlation between laboratory and field results.

The American Concrete Institute (ACI) 308 nomograph was used to characterize the effect of weather with respect to evaporation potential (PE), which considers ambient temperature, relative humidity, concrete temperature, and wind velocity (**Figure 15**). This nomograph can also be represented by the following Equation 4:

$$PE = [70^{2.5} - \left(\frac{RH}{100} \times T^{2.5}\right)] \times (1 + 0.4 \times W) \times 0.00001$$

Equation 4

Where:

PE = potential of evaporation rate, lbs/ft^2/hr.
RH = the relative humidity of ambient conditions, %.
T = the temperature of ambient conditions, ˚F.
W = the wind velocity of ambient conditions, mph.

3.2.1 Application Rate (area/volume method)

The application rate was determined using the area/volume method where the volume of curing compound utilized during a particular run was measured by assessing the tank volume before and after and determining the length of application using a distance wheel. This method only determines how much MFCC was left in the spray nozzles with variables such as spray bar height, wind speed, and nozzle spray efficiency controlling how much was applied to the pavement surface.

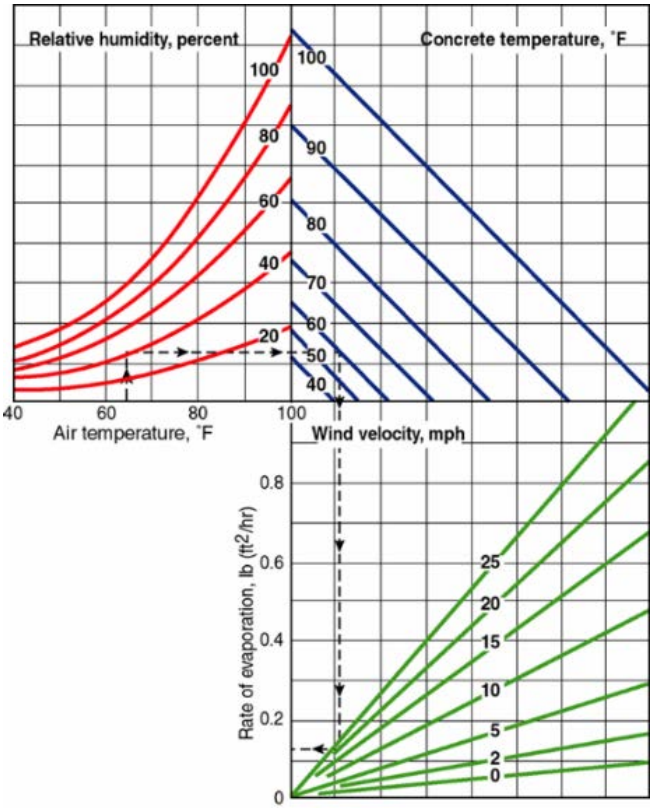

Figure 15. Nomograph in the ACI 308 Guide

3.2.2 Caltrans CT535

Caltrans CT 535 was used to assess how much MFCC was applied to the pavement. Caltrans CT 535 uses absorbent pads placed along the pavement approximately three feet from the edges at a random interval over 50 ft length ahead of the spraying cart as shown in **Figure 16**. Per CT535, 6 mil plastic was glued to the back of the pads to prevent absorption of moisture from the pavement. The test pads are removed from the pavement as soon as the spraying cart has passed over and mass is determined using a high-precision scale
Figure **17**). Then knowing the area and the mass of the test pads before and after MFCC application, and the density of the MFCC, the application rate is computed. This test assumes uniform application across the width of the pavement.

Figure 16. Caltrans CT 535 set-up. (Left) absorbent pads before curing compound application (Right): Absorbent pads after curing compound application.

Figure 17. Caltrans CT535 data collection stages

3.2.1 Concrete Maturity Meter

The quality of a given curing compound was evaluated using a concrete moisture-based maturity based on dew point temperature technology. This data was obtained by using a prototype of the Advanced Concrete Maturity Meter (ACMM) 2200 unit made by Petra Integrity Innovations. A detailed view of the 2200 unit is shown in **Figure 18**. This device can measure temperature data pertinent to the relative humidity under different environmental conditions. Therefore, three sensors are used, one records the ambient relative humidity, and the other two measure the dew point temperatures inside each of the two chambers (one being the filtered and the other sealed). Dual precision chilled-mirror dew point sensors measure the curing process utilizing measurement algorithms developed to verify the optimal moisture-based maturity of the curing environment. Chilled-mirror dew point sensors provide an absolute value for moisture, contrary to relative humidity sensors, which depend upon the temperature in their operation.

Their use eliminates a large margin of error generated by the wide temperature variations naturally occurring in the concrete curing process. A high-performance data acquisition system provides an instantaneous display of the measurements and computations of the concrete curing process, as well as data collection for archiving and further analysis. The model has the capacity to store several months'

logged data. Data are displayed on a LCD display and/or can be transmitted by USB or wirelessly, to a computer or phone for instant readout viewing and archiving.

Each of the dual dew point sensors are positioned in a sampling chamber that is embedded in the concrete (**Figure 19**). As moisture migrates from the concrete into the sampling chamber, the moisture equilibrates to a consistent level within each chamber to the vapor pressure within the pores of the concrete. This provides a measurement of the relative humidity representative of the suction level within the concrete.

Figure 18. The Concrete Maturity Meter (Petra 2200 Unit)

A Petra 2200 unit was installed at specific locations to measure the temperature and moisture data in the concrete pavement during the hardening and curing period. This unit recorded dew point (Tdp) and dry bulb (Tdp) temperatures at 15-minute intervals. Soon after placement of the concrete slab, measurements were initiated. Two brass sampling chambers were placed in the concrete slab to provide temperature data at specific depths (1/2" and 4¼") using the sampling chambers, noted previously, configured to measure the T_{dp} and T_{dp} below the membrane formed by the curing compound at the indicated depths. The top measurement represents the vapor pressure at the surface of the concrete immediately below the curing medium as is referred to as the filtered condition. The other location, positioned deeper in the pavement as shown in **Figure 19**, is obtained to gain representation of the moisture gradient forming with depth where this reading is closer to a fully sealed condition. Assessment of the effectiveness of a compound involves the comparison between the moisture conditions (filtered and sealed) under the curing medium.

Figure 19. Approach in Measuring Curing Effectiveness Using Chilled Mirror Technology

3.2.2 EI Measurements

The moisture-based concrete maturity is a parameter that indicates how curing has progressed based on its relationship to moisture, temperature, age, and strength gain. Accordingly, temperature-based maturity is conventionally an index that depends on only time and the concrete temperature. Since this form of maturity is not an efficient indicator of curing effectiveness, a moisture-modified maturity function is utilized. A modification factor is considered for numerical computation of the effects of moisture on the equivalent concrete curing time:

$$\boldsymbol{\beta_H = \left[1 + (a - aH)^b\right]^{-1}} \qquad \textbf{Equation 5}$$

Where:

βH = moisture modification factor,
H = relative humidity of the concrete,
a = coefficient = 5, and
b = coefficient = 1

This modification factor is used to modify the maturity index as:

$$\boldsymbol{M_H = \beta_H \sum_0^t (T - T_0)\Delta t = \frac{\sum_0^t (T - T_0)\Delta t}{1 + (5 - 5H)}} \qquad \textbf{Equation 6}$$

Where:

MH = the moisture-modified maturity at age t of concrete,
T = the average concrete temperature, °C, during time interval Δt,
T_0 = datum temperature (usually taken to be -10 °C),
t = elapsed time (hours or days), and
Δt = time interval (hours or days).

To evaluate the effectiveness of curing compounds, EI is introduced as an index based on the adjusted maturity model:

$$\boldsymbol{EI = \frac{t_f - t_a}{t_s - t_a}} \qquad \textbf{Equation 7}$$

Where:

t_f = the equivalent age of concrete under filtered curing conditions,
t_s = the equivalent age of concrete under sealed curing conditions, and
t_a = the equivalent age of concrete under ambient curing conditions

3.2.3 Use of NDT Method

As previously indicated, one purpose of curing is to maintain free moisture for hydration. Consequently, the amount of free water in the concrete surface could be an index to assess the effectiveness of a given curing compound. The dielectric constant (DC) is directly related to the free moisture content and the degree of hydration of concrete. Thus, by establishing a relationship between the dielectric constant and the capability of curing compounds to maintain free moisture on the concrete surface, another index to evaluate effectiveness emerges. The dielectric constant, or permittivity, is measured by determining the travel time of a microwave within a medium by use of a device, such as a percometer, as shown in **Figure 20**. The specifications of the percometer are listed in **Table 7**. Permittivity is measured by the change in the electrical capacity of the medium in contact with the electrode (probe). The dielectric constant is a way to potentially assess curing effectiveness over a broad area since the results from the ACMM are only for a specific location.

Figure 20. The Adek$_{TM}$ Percometer and the Probe

Table 7. Specifications for the Percometer.

Measuring range						
Probe Type	**Frequency (MHz)**	**Dielectric Constant (ε_r)**	**Electrical Conductivity, $\pm\mu S/m$**	**Temperature, ˚C**	**Measurement Accuracy ε_r**	**Recommended Application**
Surface Probe	40-50	1 ~ 32	0 ~ 2000	-40 ~ +80	± 0.1+1%	Laboratory use, Tube Suction Test

DC data was also taken using a Pavescan 1.0 air-coupled Ground Penetrating Radar (GPR) unit, as shown in **Figure 21**, manufactured by GSSI. This device was useful for making field measurements taken repeatedly, soon after placement of the concrete during the hardening process. The GPR unit was equipped with an air-launched antenna supported to the side of the cart and a portable computer attached to the cart handle for data collection and storage purposes. The software pre-installed in the computer can instantly calculate the DC for the surface concrete along with spatial location, as the cart is pushed over the pavement surface. At the initial setting, the moisture content at the concrete surface was very high, so, the DC measurements were correspondingly higher as well. Gradually, DC measurements began to decrease over a 24-hour period.

Figure 21. Modified GSSI Pavescan 1.0 GPR Used in Field Testing (left) on the side of new concrete, (right) on top of hardened concrete

Dielectric data was collected and the mathematical expression to represent the dielectric value (ξ) with time is:

$$Ln\left(1-\frac{\xi}{\tau}\right)=-\left\{\frac{\beta}{t}\right\}^{\alpha} \qquad \textbf{Equation 8}$$

Where:

ξ Measured dielectric constant (DC)
t Time, hrs
τ Practical maximum limit of ξ for concrete (= 40).
β Reference time,
α Rate or slope related parameter.

Using this expression, data for each test section can be analyzed to back-calculate the parameters α and β over the curing period when sawcut joints are expected to activate. Greater rates of change in the dielectric constant coincides with greater rates of evaporation as well as slab warping which is a source of stress on the paved concrete towards forming a crack at the tip of the sawcut joint. This is an important observation as not all the sections indicate joint activation in a timely manner. As previously noted, this will likely adversely affect the longevity of the pavement section and limit the total service of life.

Equation 8 can be used to define this change (or slope in the value of dielectric with time) as:

$$\frac{\partial\xi}{\partial t}=-\alpha\left(\tau-\xi\right)\frac{\beta^{\alpha}}{t^{\alpha+1}}=\frac{\alpha\left(\tau-\xi\right)}{t}Ln\left(1+\frac{\xi}{\tau}\right) \qquad \textbf{Equation 9}$$

3.2.4 Shrinkage Measurement

The volumetric shrinkage of concrete can be caused by moisture loss as internal strain, which is the cause of the warping of concrete slabs. During and after hardening, concrete is subjected to shrinkage as water is absorbed and not consumed by cement hydration. The volumetric change due to the loss of capillary water is known mostly as drying shrinkage. The amount of shrinkage of a concrete mixture can be determined using ASTM C 157 (**Figure 22**) test specimens. Concrete mixtures were prepared in the laboratory and tested to evaluate the effects of adding a curing compound on the shrinkage rate. Vibrating

wire (VW) gauges (Geokon Model 4200) were embedded in the specimens to measure the shrinkage strain (**Figure 22**).

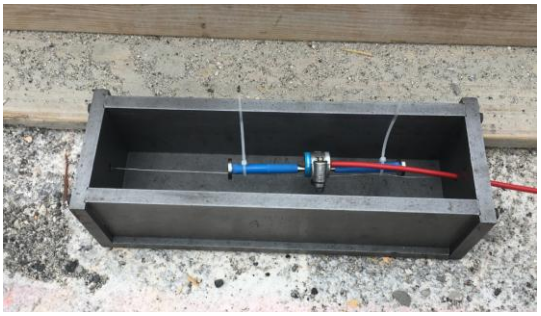

Figure 22. The VW gauge of EM-5 and the Shrinkage Mold

Drying shrinkage specimens were prepared and molded for several of the field test sections set up on STH 15, 29, and 53. Shrinkage data collected using embedded vibrating wire (VW) gauges is illustrated in Appendix F. Measured strains (ε_m) were tracked using a model GK-404 handheld stain gauge reader. The relationship between the measured strain and the drying shrinkage strain is:

$$\varepsilon_m = \left(R_0 - R_i\right)G = \varepsilon_{Temp} + \varepsilon_{Shr} \qquad \textbf{Equation 10}$$

Where:

R_0 = Initial or reference strain gauge reading
R_i = Subsequent strain gauge reading
G = Correction factor ~ 0.98
ε_{Temp} = Induced strain due to temperature change

$= \varepsilon_{pcc} + \varepsilon_{net}$

$\varepsilon_{pcc} = \Delta T_{pcc} \cdot \alpha_{pcc}$

$\varepsilon_{net} = \varepsilon_{pcc} - \varepsilon_g$

$\varepsilon_g = \Delta T_{pcc} \cdot \alpha_g$

ε_{Shr} = Shrinkage strain

$= \varepsilon_m - \varepsilon_{Temp}$

It is important to note two items with respect to the calculation of ε_{Shr}

1. The values of ε_m and ε_{Temp} can be either positive or negative; values of ε_{Shr} are always negative.
2. The VM gauge must always be considered as a fix element within the concrete and cannot move independently of the concrete.
3. The value of α_{pcc} was assumed to be 9.9 με/°C; the value of α_g = 12.2 με/°C

The above expressions were used to calculate or isolate the amount of drying strain occurring in the molded specimens from the measured strain reading data. The calculated values of ε_{Shr} are illustrated in Appendix G. This form can be represented mathematically by the following drying shrinkage strain (ε_i) vs time (t_i) model:

$$\boldsymbol{\varepsilon_i = \varepsilon_u \frac{t_i}{a+t_i}} \qquad \textbf{Equation 11}$$

Where:

ε_u = ultimate drying shrinkage strain

a = constant

$\dot{\varepsilon}_i$ = time derivative of drying shrinkage

These equation forms are useful to ascertain the ultimate amount of drying shrinkage resulting from the various curing conditions monitored at the field sites. A typical drying shrinkage trend with time is shown in **Figure 24**. This specimen was prepared at the STH 15 test site.

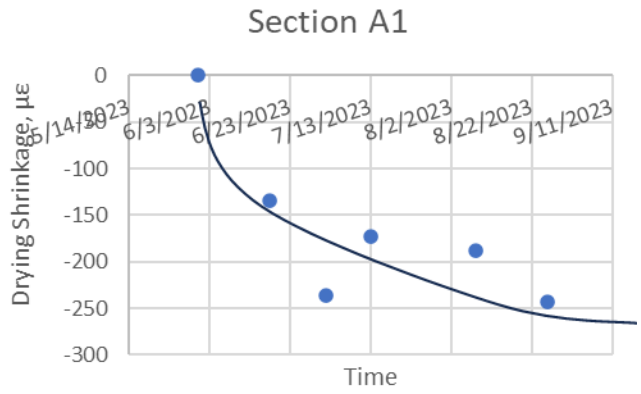

Figure 23. Typical Drying Shrinkage Trend – Uncured

3.2.5 Corner Lift Measurements

Selected activated joints were instrumented with dial gauges to monitor the vertical movement of the slab corner. The dial gauges were mounted on the side of the slab (**Figure 24**) and referenced to an anchor placed along the side of the slab at two locations – one at the corner of the slab and the other offset from the corner 18 inches (**Figure 24**). The reference anchor was a 24-inch portion of rebar hammered into the subgrade. This setup has proven sufficient to measure movement of the slab in previous work performed by team members in TxDOT and USACE testing (Ye et al., 2009; Zollinger et al., 2013). The corner position was to monitor corner movements while the offset position yielded data on the curvature of the slab under warping and curling effects.

Figure 24. STH 15 Dial Gauge Placement (left), Off Set Dial Gauge Setup (right)

The edge gaps are due mainly to the shrinkage gradient developed in the slab but any difference in top and bottom of slab temperature also influences the amount of vertical movement at a slab corner. The amount of the edge gap is of interest since a certain amount of that edge gap is permanent and is built

in or set in the pavement during construction. Climatic conditions during construction are certainly a factor in setting but related factors are the amount of evaporation that takes place during curing as well as the quality of the curing. The amount of set built into the slab during the curing period is also a factor affecting the rate of joint activation since it affects the cracking stresses at the tip of a sawcut. The built-in set is often described or related to a temperature gradient in the slab (that is the difference between the top and bottom of a slab divided by the slab thickness). The set temperature (ΔT_{set}) gradient can be simply defined as:

$$\Delta T_{set} = \Delta T_{cal\ grad} - \Delta T_{\text{meas } grad} \quad \textbf{Equation 12}$$

Where:

$\Delta T_{cal\ grad}$ = Back calculated temperature gradient based on the measured edge gap

$\Delta T_{\text{meas } grad}$ = Equivalent Measured temperature gradient as a function of the induced temperature and moisture strain gradients.

Determination of $\Delta T_{\text{meas } grad}$ is based on the gradient data illustrated in Appendix G. This data was generated from the chilled mirror measurements of the DB and DP temperatures over time. Analysis of this data showed that a negative moisture gradient (i.e. drier at the top than at the bottom of the slab) was prevalent throughout the curing period where the temperature gradient fluctuated between a negative and positive gradient over a 24-hour period. The gradient for the set calculation was taken as the maximum negative values for both temperature and moisture gradient effects. The $\Delta T_{\text{meas } grad}$ was found by fitting the trends shown in Appendix G for both temperature and humidity using the following form:

$$\mathbf{\Delta T}(z), \mathbf{\Delta}(1 - rh^3) = A + Bz + Cz^2 + Dz^3 \quad \textbf{Equation 13}$$

Where:

ΔT = Temperature difference between its value at any point z and the temperature at the slab bottom

$\Delta(1\text{-}rh^2)$ = Relative humidity parameter difference between its value at any point z and the temperature at the slab bottom

The equivalent difference representing the gradient from the slab top to the bottom is computed as:

$$\mathbf{\Delta T}(z)_{eqv}, \mathbf{\Delta}(1 - rh^3)_{eqv} = -12\left(B\frac{h}{12} + D\frac{h^3}{80}\right) \quad \textbf{Equation 134}$$

Using the B and D coefficients from the $\Delta T_{\text{meas } grad}$ model.

The determination of the $\Delta T_{cal\ grad}$ is a bit more involved since it is derived from the measured edge gap data (w_{corner} and w_{offset} shown in Appendix I) but it is defined as:

$$\Delta T_{cal\ grad} = \varepsilon_{grad} / \alpha \quad \textbf{Equation 15}$$

Where:

$$\varepsilon_{grad} = A_0 \frac{h}{1+\nu}$$

h = slab thickness

$A_0 = \frac{1}{\ell^2} \frac{\frac{\rho h}{k} e^s - \sin s \frac{M_{db}}{D}}{\left(0.963\nu \sin s - \frac{\sin s}{2} + \cos s\right)}$

$\ell = \sqrt[4]{\frac{Eh3}{12(1-\nu^2)k}}$

E = Modulus of elasticity of concrete

k = Foundation modulus

ρ = Unit weight of concrete

$s = \frac{S}{\ell}$

$S = \frac{x}{1 - \frac{w_{offset}}{w_{corner}}}$

x = Offset diagonal distance from the corner of the slab to the offset dial gauge location

$= \frac{18}{\sqrt{2}} = 12.728$

M_{db} Dowel bar bending moment

$= K_r \theta_{bar} \left(hb_{spc}\right) = K_r \frac{w_0}{\frac{\ell}{\sqrt{2}} + \frac{K_r}{k\ell^2}} \left(hb_{spc}\right)$

K_r = Joint rotational stiffness = $24\pi \frac{E_{bar} r^4}{L^3}$

θ_{bar} = Dowel bar rotation

b_{spc} = Dowel bar spacing

3.2.6 Surface Sorptivity

Surface sorptivity was measured using a Karsten tube. The tube was placed on the concrete and sealed with plumbers' putty (**Figure 25**). The rate of water absorption into the concrete is measured over various hour periods during the first several days with the absorption decreasing with time. As shown in **Figure 16**, tests were performed on the cured pavement as well as the uncured patches left behind from Caltrans CT535 test.

Figure 25. Karsten tube set-up during I-43 construction

3.3 Observational field visit 1 (I-43 Mequon)

3.3.1 Site description

The first site visit was undertaken on the week of May 8, 2023, near Mequon on southbound I43 just south of County line road (**Figure 26**) with paving performed on May 10th. The test section was a ramp 15 ft. wide and 10 in. depth. During construction it was sunny with temperatures of 60-70°F, 40-50% RH, evaporation rate ranging from 0.03 lbs/in^2/hr during the morning hours to 0.06 lbs/in^2/hr in the afternoon. Four test sections of 100 ft length were observed, placed throughout the morning. Afternoon paving ended early due to forecasted rain. The concrete mixture had 520 pcy of total cementitious material including Type IL cement and 30% Class C fly ash and at w/cm of 0.37 and optimized aggregate gradation using limestone coarse aggregate. The MFCC was Certi-Vex Envio Cure white 1315 from ChemMasters. Construction used dowel baskets and a material transfer device for concrete placement in front of the paver (**Figure 27**).

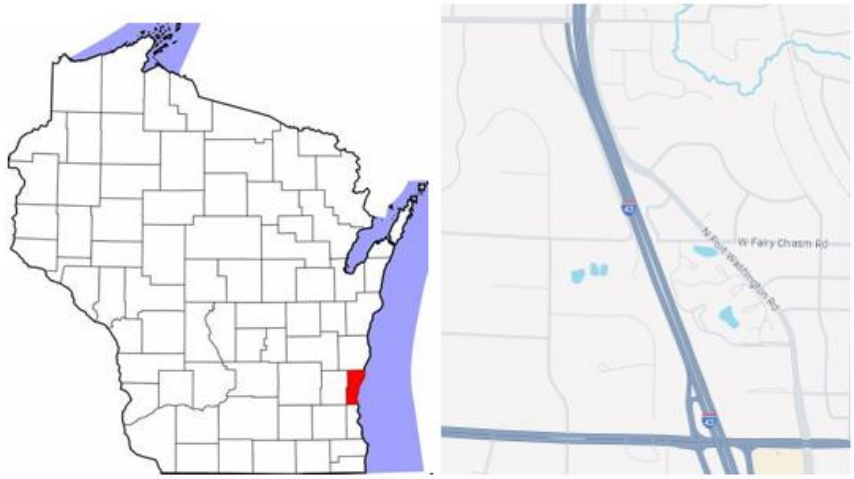

Figure 26. Location of I43 Field Site Near Mequon

Figure 27. I-43 construction

3.3.1 Testing Results and Discussion

The initial and final setting time were 250 min and 425 minutes respectively. The average paving speed was around 7 feet per minute and the average curing cart speed was around 70 feet per minute. **Table 8** shows the construction logistics for the test sections. Section A represents the first 200 feet of paving off the header and Sections B-D steady state paving. The curing cart operator was also a back-of-paver finisher and performed tining and curing operations after about 200 feet of separation was achieved. The curing cart speed was hydrostatic and controlled using a speed dial, but the equipment only began moving after being turned past 50%. When asked about speed control, the operator stated they tried to keep it in the middle unless instructed by the on-site engineer or foreman.

Table 8. I43 Curing Construction Conditions

Section ID	Paving Time	Test Length (ft)	Curing Time	Temperature (F)	Evaporation Rate (lbs/ft^2/hr)
A	7:15	200	9:15	75	0.03
B	9:30	200	10:50	75	0.04
C	10:00	200	11:30	75	0.06
D	10:30	200	12:30	75	0.05

Table 9 shows the area/volume results at the top and CT535 as individual data points. CT535 was not collected for the header Section A and an incorrect tank measurement was presented for Section D. On average the area/volume results are near the desired 150 sf/gal but with a high amount of variability. The effect of wind speed can be clearly seen for Section C where area/volume calculations did not match CT535 results.

Table 9. Caltrans CT 535 results

Sample ID	A (111 ft^2/gal)	B (217 ft^2/gal)	C (149 ft^2/gal)	D (N/A ft^2/gal)
1	N/A	187	240	177
2	N/A	196	231	177
3	N/A	214	330	150
4	N/A	216	340	164
5	N/A	220	181	N/A
Average		207	264	167
STDV		14	61	11
COV (%)		7%	23%	7%

Karsten tube surface absorption results are shown in **Appendix C**. The Day 0 test occurred 4 hours after initial paving and the Day 2 test 48 hours after initial paving. As expected, the uncured portion had higher absorption than the cured portion when tested at 11 hours. Interestingly there were no differences on Day 2.

During Interstate 43 observational field testing, the embedded resistance was measured from section A of the actual concrete pavement as shown in **Figure 27**. Resistance results are illustrated in Appendix D. The section was paved in the morning hours and the curing compound was applied at the application rate of 111 ft^2/gal, 2 hours after paving. Testing was performed on the uncured patch remaining after the CT535 pads were removed. Resistance began to rise rapidly after 50 minutes, which was much earlier than any of the laboratory testing. However, the Karsten tube was tested on the same piece of exposed and the high permeability of the uncured concrete affected saturation at a much farther

distance than expected. As resistance is primarily a measure of moisture content in the first 24 hours, any addition of moisture causes the resistance to drop (**Figure 29**). For subsequent site visits, the Karsten tube test was performed at a different location to not influence resistance testing.

Figure 28. Embedded resistance device set-up during I-43 construction

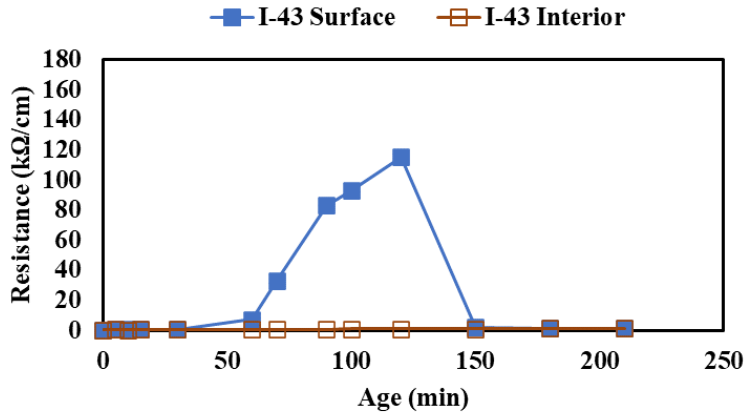

Figure 29. I-43: Embedded Resistance Results

Paving occurred on Wednesday May 10th with sawing overnight. No joints were activated at 8:00am the following day. By 5pm the following day all joints were activated with uniform width and vertical cracking.

3.4 Observational field visit 2 (STH-15 NEW LONDON)

3.4.1 Site description

The second observational field visit took place during the week of May 30, 2023, near New London (**Figure 30**). The research team observed the construction of 2 lanes State Highway 15. The placement was 26 feet wide (14 ft. right lane and 12 ft left lane) and 10 inches thick. During STH-15 field visit the research team collected data during two days of paving May 31st and June 2nd including 8 test sections of 100 ft length, 4 sections on the first day of paving (May 31st, 2023) and the other four sections on the second day of paving (June 2nd, 2023). The weather during day 1 of paving was clear sky with daily

temperature between 78°F and 86°F, relative humidity 40-60%, 2-11 mph wind speed, and evaporation rate ranging from 0.02-0.09 lbs/ft2/hr. The second day of testing took place on June 2nd, 2023, where four working sections were selected by the research team, two in the morning and the other two in the afternoon. The temperature ranged from 74-91°F, relative humidity from 31-65%, wind speed 0-10mph, and evaporation rate 0.02-0.08 lbs/ft2/hr. The concrete mixture had 531 pcy of total cementitious material including Type 1L cement and 15% slag at a w/cm of 0.38 and optimized aggregate gradation using dolomite coarse aggregate. Construction used on-grade delivery with a dowel bar inserter (**Figure 31**).

Figure 30. Location of STH15 Site Near New London/Hortonville

Figure 31. Construction of STH15

3.4.1 Application Rate and Embedded Resistance Results

The initial and final setting time were 180 min and 300 minutes respectively. Sections A-D were placed on the first day of testing and Sections E-H on the second. The delay between paving operations and curing ranged from 60 minutes to over 180 minutes for Sections B and C (**Table 10**).

Table 10. Sections description, paving time, application rates and weather conditions

Section ID	Paving time	Curing time	Temperature (F)	Evaporation Rate (lbs/ft^2/hr)
A	7:30	10:00	77	0.03
B	9:30	12:42	79	0.02
C	14:30	17:34	82	0.09
D	16:00	17:55	82	0.09
F	9:30	10:30	84	0.02
G	13:30	14:50	90	0.04

Six CT535 data sets were collected, four from day one (May 31st, 2023) and two from the second day of testing (June 2nd, 2023). For the Day 1 testing, only CT535 was observed with the application rate highly variability from near the desired application rate of 150 sf/gal to double as shown in **Table 11**. Consequently, for the second day of testing the research team worked with the curing cart operator to calibrate speed for a desired application rate. The high application rate of 167 sf/gal was selected by averaging the highest observed application rates from day one of Sections C and D and the low application rate of 275 sf/gal from the lower observed application rates from day one of Sections A and B. After assisting the curing cart operator to adjust speed, Sections F and G had application rates very close to the desired rate.

Table 11. Caltrans CT535 test results

Sample ID	A	B	C	D	F (167 ft^2/gal)	G (275 ft^2/gal)
1	331	245	235	148	173	244
2	158	202	172	170	172	284
3	193	416	202	114	162	256
4	N/A	374	190	112	143	287
5	N/A	261	190	138	161	280
Average	227	300	198	136	163	268
STDV	75	14	21	25	12	18
COV (%)	33	5%	23%	7%	7%	7%

Absorption using the Karsten tube was measured on Sections A and C in and shown in Appendix C. Like the previous results, the uncured locations had higher absorption than the cured locations and much lower absorption the day after paving as compared with the day of paving. Potentially the effect of higher evaporation rate can be observed by comparing the uncured Day 0 where higher winds during placement of Section C may have caused the higher absorption. Fortunately, the cured sections had similar absorption between sections showing the ability of the MFCC to normalize across different environmental conditions.

Embedded resistance was measured for two sections on the first day and second day. The reported time for all sections started immediately after the curing compound was applied. From the

CT535 data, Section B had a lower application rate than Section C which was observed with an earlier resistance increase from drying (**Figure 32**). The influence of application rate and temperature can be observed more easily in **Figure 33** for the second set of tests where an uncured surface from CT535 is presented along with a high morning application rate (Section F) and a lower afternoon application rate (Section G). The trends from laboratory testing of more rapid resistance increase corresponding with less or no curing compound are similarly observed in the field data.

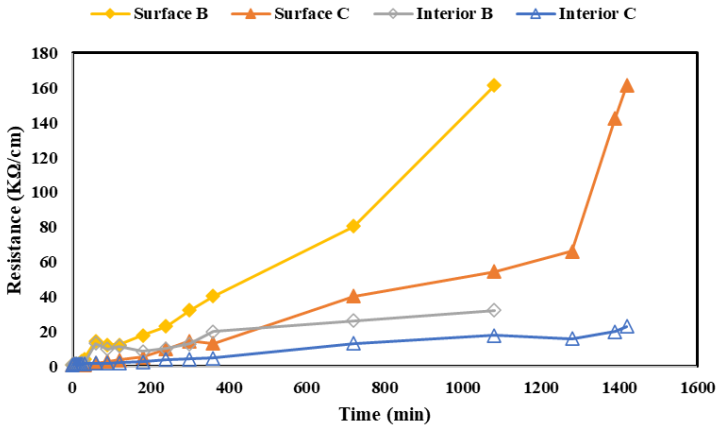

Figure 32. STH 15: Embedded Resistance for Sections B and C

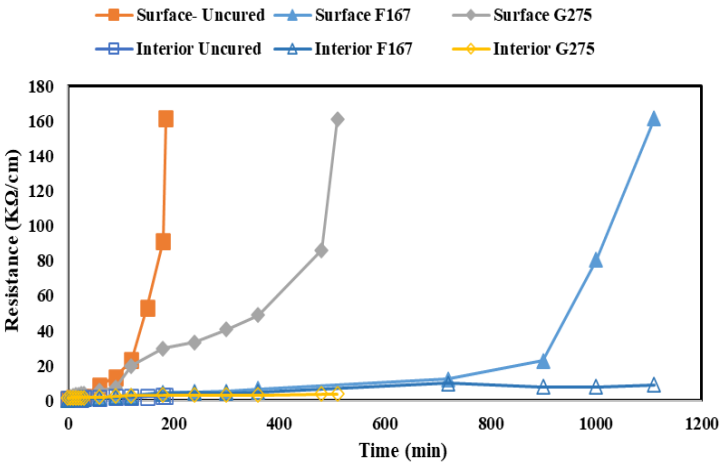

Figure 33. STH 15: Embedded Resistance Data for Sections F and G

3.4.2 Chilled Mirror Temperature and GPR Data

Chilled mirror temperature and GPR data collected from the field are shown in Appendixes D and E. As previously noted, the chilled mirror temperature data is used to calculate the internal relative humidity of the concrete at two positions (referred to as sealed and filtered temperatures). The chilled mirror instrumentation yields dew point (T_{dp}) and dry bulb (T_{db}) temperatures at the two previously noted positions in the concrete slab. The illustrated RH data in **Appendix D** was calculated from T_{dp} and T_{dp} data using the following expression:

$$Rh = exp\left[\frac{17.502T_{dp}}{240.97+T_{dp}} - \left(\frac{17.502T_{db}}{240.97+T_{db}}\right)\right] \qquad \textbf{Equation 16}$$

T_{dp} and T_{dp} measurements were obtained and used to track the curing process and the formation of gradients in the pavement (discussed later in the dial gauge section). The dielectric data shown in Appendix F is directly output by the GPR test instrumentation and is shown with respect to time and a given position on the surface of the pavement.

Of the four sections of paving placed the morning of 31 May 2023, Sections B was instrumented with the chilled mirror device which yielded dew point and dry bulb temperatures as shown in **Figure 34**. Another 4 sections were placed on 2 June 2023 where Section F was instrumented with the chilled mirror device again for dew point and dry bulb temperatures as shown in **Figure 35**. The rate of application (AR) varied from section to section and is shown in **Table 11** to explore its effect on pavement behavior.

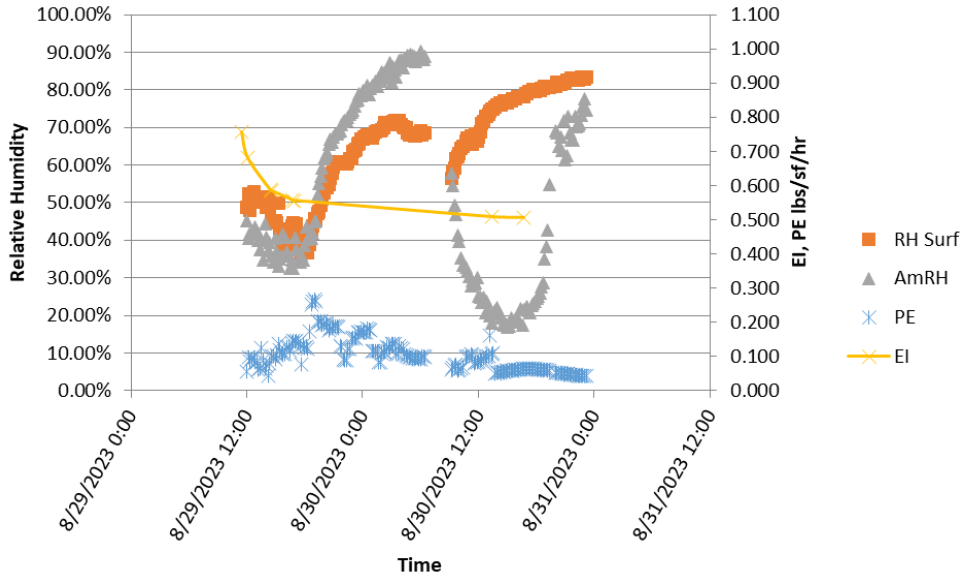

Figure 34. STH 29 Section A – Morning, Aug 29, 2023; No Delay, AR=219 sf/g.

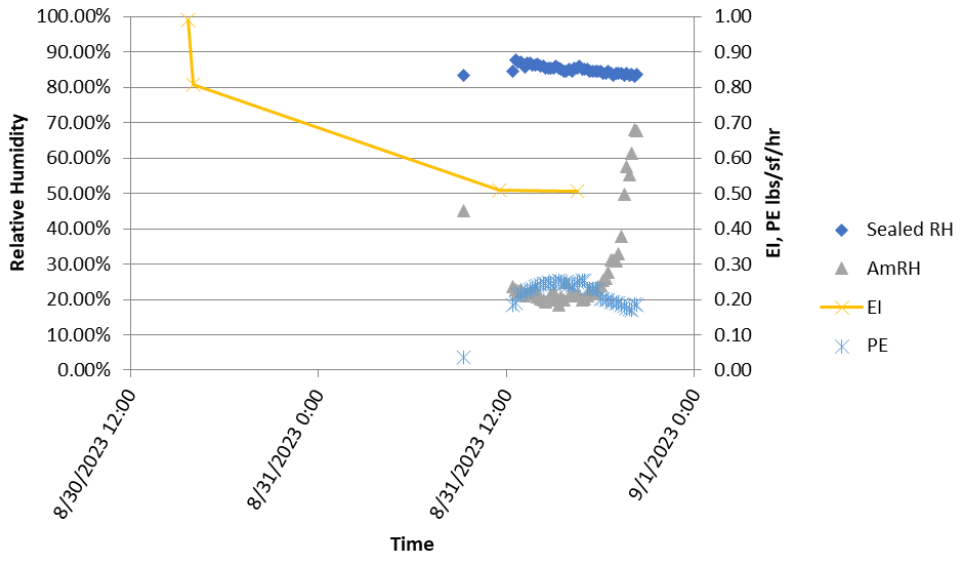

Figure 35. STH 29 Section C – Morning, Aug 31, 2023; 2 hr Delay, AR=219 sf/g.

The data illustrated in **Figure 34** and **Figure 35** shows the filtered and sealed RH values over a 2-day period for Sections B and F. The ambient RH is also shown in the figures. The filtered surface

humidity ranges between 60 and 85% (but was lower the second day) while the sealed humidity peaked between 90 - 92% each day. The ambient Rh ranged between 60% overnight to approximately 45% midafternoon the following day. The PE reached over 0.25 lbs./sf/hr the first day of paving. Note the shift in the surface Rh between the sections placed in the morning hours verses those placed in the afternoon hour likely due to a 2-hour delay in the time of application (ToA) of the curing membrane. Another parameter shown is the Evaluation Index (EI). The EI is based on the moisture-based concrete maturity, as previously noted, which indicates how the curing is progressing based on its relationship to moisture, temperature, age, and strength gain. Accordingly, temperature-based maturity is conventionally an index that depends on only time and the concrete temperature. Since this form of maturity is not an efficient indicator of curing effectiveness, a moisture-modified maturity function is utilized instead. Consequently, the EI can represent the effects of the prevailing evaporative conditions, as represented by the PE parameter, and the quality of the curing application simultaneously which makes it an invaluable index for the assessment of curing quality.

The prevailing conditions during the placements at this site lead to varying rates of activation of the sawcut joints of the morning placements (sections A, B, E, and F) shown in **Figure 36** but none of the sawcuts placed in the afternoon paving (sections C, D, G, and H), generally speaking. The primary reason is due to the lack of sufficient drying time prior to nightfall. The lack of sawcut joint activation is a key performance item and will be enumerated here and in subsequent discussions elaborated under the section on GPR data and other sections of this report. It is pointed out that comparing the trends in EI between those shown in **Figure 34** and **Figure 35**, the effect of delaying the time of application (ToA) of the curing membraned tends to lower the EI (which occurs at a rate of approximately 5 EI points per hour). As previously noted, the key parameter in affecting the EI is the measured internal relative humidity (Rh) of the concrete and delaying the ToA tends to lower the Rh and increase the rate of evaporation.

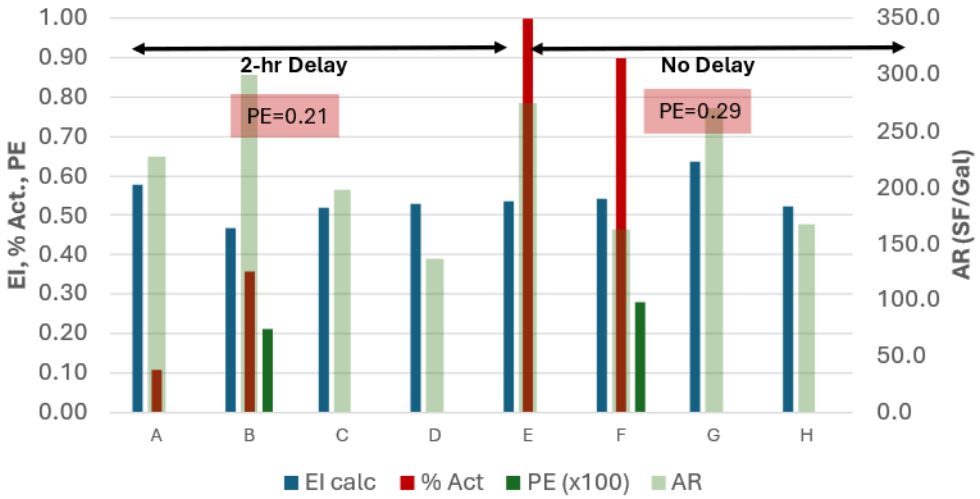

Figure 36. Summary of Curing Effectiveness Testing for STH 15

3.4.3 Analysis of GPR Data

Dielectric data was collected at each site using the GPR equipment previously described. The collected data was a direct output from the GPR equipment and was organized and reformatted as illustrated in Appendix E with respect to time.

Using this expression, the Appendix E data for each test section can be analyzed to back calculate the parameters α and β over the curing period when sawcut joints are expected to activate. The back calculated values for α shown in **Figure E.1** indicate that the rate of change of the dielectric with time (α)

is a key parameter indicating the tendency for the sawcut joints to activate. The data illustrated in **Figure 37** also tends to suggest that the threshold value of α for joint activation to be approximately -0.2. Greater rates of change in the dielectric constant coincides with greater rates of evaporation as well as slab warping which is a source of stress on the paved concrete towards forming a crack at the tip of the sawcut joint. This is an important observation as not all the sections indicate joint activation in a timely manner. As previously noted, this will likely adversely affect the longevity of the pavement section and limit the total service of life.

The instanteous change in ξ with time (t) can be correlated with the EI paramter; Equation 17 can be used to define this change (or slope in the value of dielectric with time) as:

$$\frac{\partial \xi}{\partial t} = -\alpha(\tau - \xi)\frac{\beta^{\alpha}}{t^{\alpha+1}} = \frac{\alpha(\tau - \xi)}{t} Ln\left(1 + \frac{\xi}{\tau}\right)$$

Equation 17

Slope ($\frac{\eth \xi}{\eth t}$) data from selected test sections included in Appendix E and F was compiled and correlated with EI data in a manner to represent the effects of aging through the curing cycle. The resulting relationship is useful to infer the EI based on the measured GPR data. El calculated (EI_c) in this manner is distinguished from measured values of EI using the chilled mirror tempeature data. Values of EI_c are shown in **Figure 37** for all the sections except for B and F.

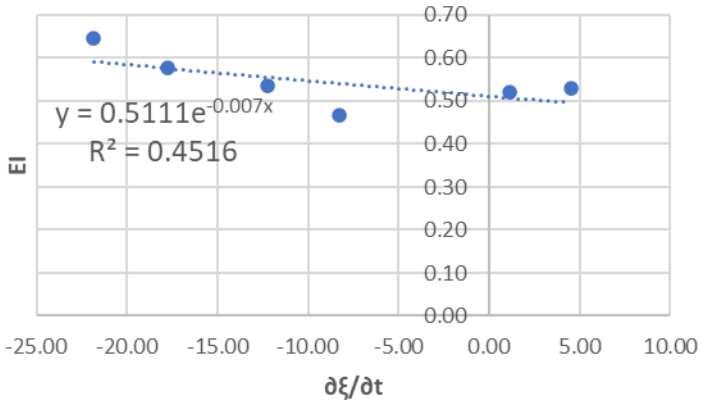

Figure 37. Correlation of Rate of Change in Dielectric with the Measured EI

3.4.4 Drying Shrinkage Data

Drying shrinkage strain behavior as assessed from the analysis of the trends manifest in the collected data are shown in Appendix F. **Figure F.1** illustrates the variation in the ultimate amount of drying shrinkage with the AR. As expected, the shrinkage amount increases with a lower quality of curing irrespective of the time of application (ToA). A similar plot is shown in **Figure F.2** except respect to EI showing that the parameter of EI is as significant as the AR in terms of an indicator of curing quality. **Figure F.3** is again another plot based on STH 15 data showing the effect of the time of placement (ToP) with the AR on ε_u.

3.4.5 Corner Displacement Data

The displacement data is shown in Appendix G. The trends shown in the data helps explain the differences in the joint activation rate manifested in the STH sections shown in **Figure 36**. Measures such as adjustments in the rate of evaporation, the method of curing (ToA, Type of curing), and method of

joint sawing may be to increase the rate of joint activation for afternoon paving. **Figure G.4** summarizes the curing data obtained from STH 29 relative to rate of activation, change in dielectric, EI, and ε_u.

Data in **Figure 38** shows the relationship between the maximum daily measured edge gap (based on Appendix G data) following the formation and activation of the sawcut joint and the average EI during the curing period immediately after construction. This trend is as expected and shows an increase in edge gap with lower EI values. Again, EI decreases with greater amount of evaporation and reduced curing quality; two effects that are necessary to properly activate sawcut joints.

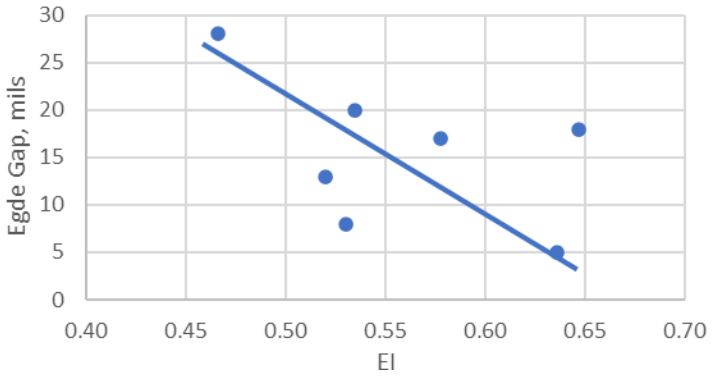

Figure 38. STH 15: Edge Gap vs EI

Modeling in mechanistic-empirical pavement design software has demonstrated the significance of the built-in set (i.e. -10°F) from a pavement design perspective and the trend shown in **Figure 39** demonstrates the role of curing quality on the amount of set that is built into a slab. Furthermore, the trend tends to validate the default value of a -10°F corresponds to the threshold value of α = -0.200 for joint activation to proceed in a timely and complete manner.

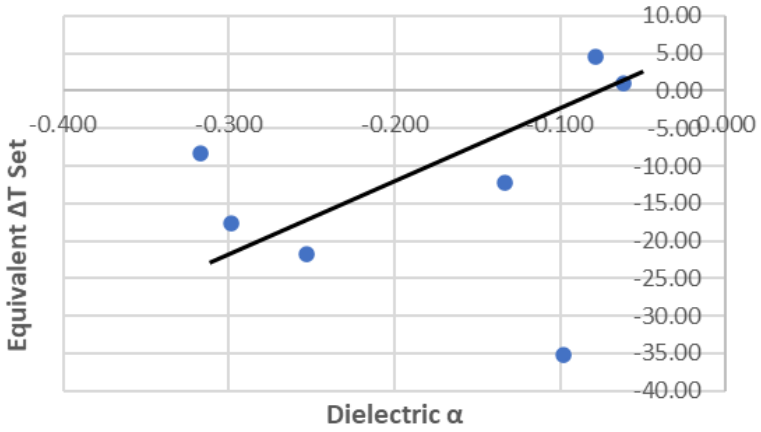

Figure 39. STH 15: ΔT_{set} vs EI

3.5 Observational field visit 3 (STH-29 Wausau)

3.5.1 Site description

The third observational visit took place west of Wausau on State Highway 29 (**Figure 40**) week of August 29th, 2023. The paving section was two lanes 26 feet wide in total and slab thickness of 10 inches.

Three test sections were observed, two on the first test day (August 29) and one on the second (August 30). The temperature ranged from 65°F in the morning to 80°F in the afternoon with 40-65% relative humidity, and evaporation rates from 0.02 to 0.04 lbs/ft^2/hr during paving. Placement was performed by concrete delivery directly on grade with a dowel bar inserter. Tining and curing occurred at the same time (**Figure 41**). The concrete mixture had 565 pcy of total cementitious material including Type 1L cement and 20% Class C fly ash at a w/cm of 0.35 and optimized aggregate gradation using crush granitic gravel coarse aggregate.

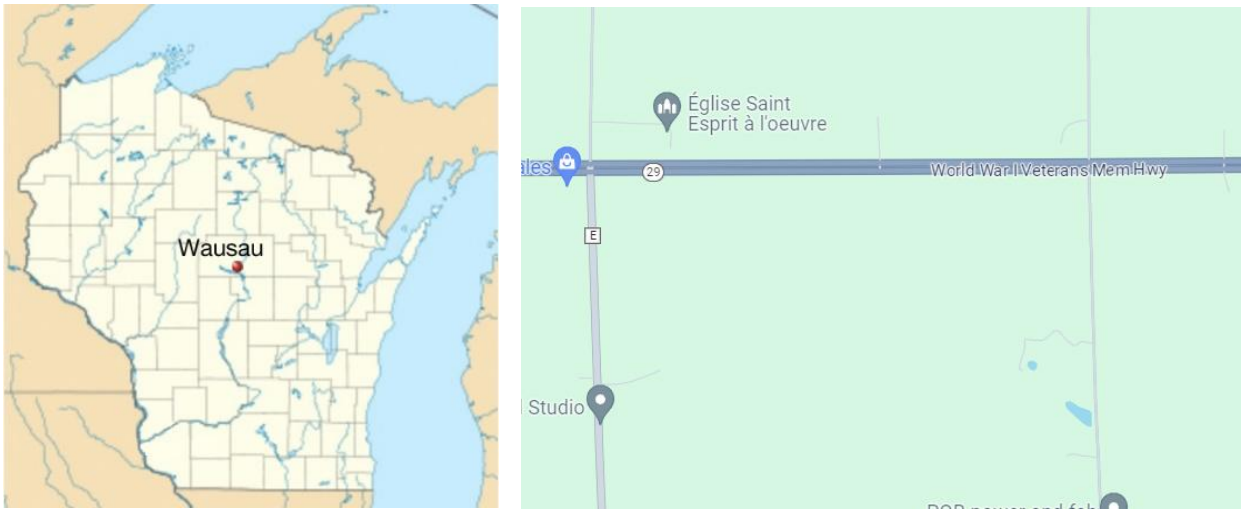

Figure 40. STH 29 Site near Wausau

Figure 41. STH29 Construction

3.5.1 Application Rate and Embedded Resistance Results

The initial setting time was 180 minutes and 280 minutes for final setting time. The time of curing ranged from 15 minutes to 120 minutes within a particular section with bleed water visibly present when MFCC was applied to the concrete closest to the paver. The construction timing is shown in **Table 12**.

Table 12. STH29 Sections description, paving time, application rates and weather conditions

Section ID	Paving time	Curing time	Temperature (F)	Evaporation Rate (lbs/ft^2/hr)
A	8:00	10:00	71	0.02
B	1:30	2:45	80	0.02
C	10:45	11:30	65	0.02

The coverage rate for the three test sections was determined by the equipment parameters and anecdotal range of speeds utilized by the operator. Section A was the maximum speed of the curing cart, Section B was the minimum speed of the cart, and Section C was mid-way between. As shown in **Table 13**, the speed control on the curing cart was not linear with the midpoint more near the application rate at full speed. For lower application rate Sections A and C the amount determined from the area volume method (219 sf/gal and 200 sf/gal respectively) was underpredicted by CT535. While the highest application rate in Section B (85 sf/gal) is close to the CT535 results. The differences in application rate for Sections A and C were likely a result of the wind blowing some off the edge of the pavement. Since none of the sections achieved the desired application rate of 150 sf/gal, an additional calibration section would be needed in practice to ensure proper coverage.

Table 13. STH29 Coverage Results

Sample ID	A (219 ft^2/gal)	B (85 ft^2/gal)	C (200 ft^2/gal)
1	245	95	246
2	257	107	246
3	239	99	249
4	280	93	248
5	239	87	247
Average	252	96	247
STDV	17	7	1
COV (%)	6.8	7.7	0.4

For STH-29 embedded resistance was measured in place for Section A and on a beam for Section C which was placed on the pavement and based on the CT535 and area/volume results, application rates were similar. Although placed on different days, the weather conditions were similar. This set of experiments was performed to determine if embedded resistance for small samples had similar performance as the much larger slab. As shown in **Figure 42**, the embedded resistance results were similar for either the actual pavement or beam indicating that surrogate samples may be allowable or appropriate. Although setting time was similar to the STH 15 test results, the increase in resistance occurred much more rapidly than for the previous field sites. The mixture used for STH29 had a much higher cementitious content and lower w/cm than the previous field sites which likely resulted in faster rise.

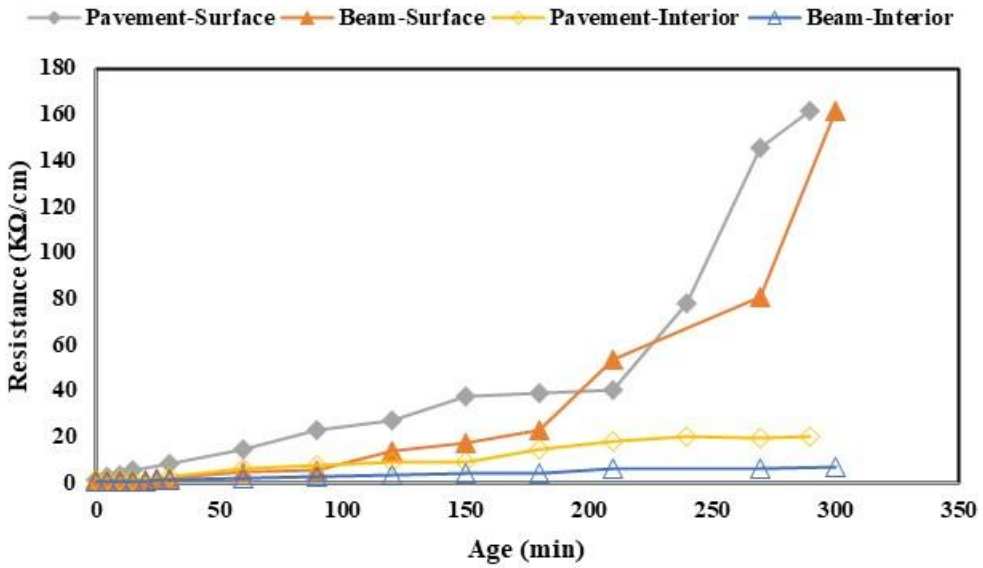

Figure 42. STH29 Embedded Resistance Data

3.5.2 Chilled Mirror and GPR Testing results

Analysis of the Appendix D and E data for STH 29 is summarized in **Figure G.1** all 3 sections that were set up at that site. A revealing data set is the rate of joint activation and the change in dielectric value (α) with time. Clearly, a threshold value of a -0.2 is associated with the tendency for sawcut joints to fully activate.

3.5.3 Shrinkage Testing results

Figure H.4 again shows a revealing trend in the ultimate shrinkage strain vs the rate of joint activation and the AR for each section. Management of the curing process will be key to controlling the amount of evaporation sufficient to activate the joint but not to the extent that the loss of moisture will inhibit the development of impermeability or strength in the surface concrete which is the part of the paved concrete most affected by the quality of the curing.

Joint activation results are shown in **Table 14** with Sections A and C similar application rate and Section B much heavier. The rate of activation was clearly impacted by the application rate of MFCC with Section C activating much more quickly than Section B, even placed a day later.

Table 14. STH 29 Joint Activation

Location	Date	Time	Notes	Joint Activation
A	Tues, Aug 29	8:00am	Paved	N/A
A	Wed, Aug 30	8:00am		1 in 4-5 active of 27
A	Thur, Aug 31	9:00am		19 active of 27
A	Fri, Sep 1	9:00am		24 active of 27
B	Tues, Aug 29	1:30pm	Paved	N/A
B	Wed, Aug 30	4:00pm		0 active of 27
B	Thur, Aug 31	9:00am		7 active of 27
B	Fri, Sep 1	9:00am		13 active of 27
C	Wed, Aug 30	10:00am	Paved	N/A
C	Thur, Aug 31	9:00am		1 in 4-5 active of 27
C	Fri, Sep 1	9:00am		27 activated of 27

3.5.4 Dial Gauge Results

The gauge measurements are shown in Appendix H. The relationship between the maximum edge gap and the slope of the dielectric over time is shown in **Figure 43**. Clearly, the edge gap is a function of the amount of evaporation and drying time the concrete is exposed to. It was shown previously that the greater the edge gap, the greater the built-in set in the slab. This again is further evidence of the effect of curing quality on the behavior of the pavement structure.

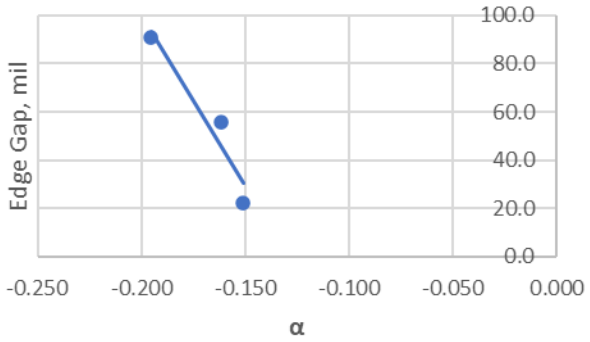

Figure 43. STH 29 Edge Gap vs Dielectric Slope α

3.6 Observational Field Visit 4 (STH-53 Haugen)

3.6.1 Site description

The last observational field visit was undertaken on the week of June 24th, 2024, near Haugen Wisconsin on the northbound lanes of STH53 just north of the 28th Ave. entrance ramp (**Figure 44**). The pavement was two lanes 26 feet wide and 10 inches thick. The temperature ranged from 60-80°F with 50-70% relative humidity, and evaporation rate 0.02-0.05 lbs/ft^2/hr. Five test sections were observed, a control and low/high sections placed each in the morning and afternoon of the first day of paving (Monday June 24, 2024). It rained 0.5 in. around midnight and the end of the first day of paving was covered in plastic to protect. The mixture contained 520 pcy of total cementitious material with Type IL cement and 30% Class C fly ash at a w/cm of 0.38 and optimized gradation of granite coarse aggregate. Constructed was performed by direct discharge on grade and a dowel bar inserter (**Figure 45**). Unlike the previous observational visits, tining and curing operations were performed as two separate steps, albeit with the

same piece of equipment. After a gap of approximately 200 feet was allowed to open between the texture cart and the curing cart, tining was performed, followed by curing. The curing cart was new the previous week and the operator had determined the correct speed by spacing the curing drums at the appropriate location and calibrating for the distance needed to use 55 gallons at an application rate of 150 sf/gal. The research team verified, and the entire placement (other than the research sections) occurred at the DOT-specified rate.

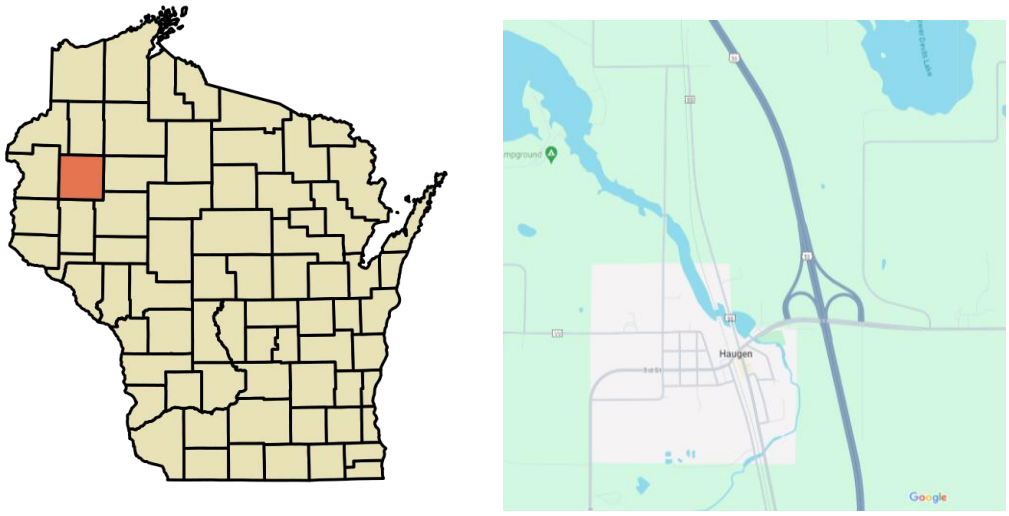

Figure 44. STH 53 Paving Location Near Haugen

Figure 45. STH-53 Construction

3.6.2 Application Rate and Embedded Resistance Results

The initial and final setting times were 220 minutes and 520 minutes, respectively. The calibrated speed on the hydrostatic control dial was at 75 feet per minute. The high/low application rate test sections represented the highest speed the cart could achieve of 100 feet per minute for the low rate and 50 feet per minute for the high rate. The various section parameters are shown in **Table 15**.

Table 15. STH-53 Sections details

Combination	Paving time	Curing time	Application rate (ft^2/Gal)	Temperature (°F)	Evaporation Rate (lbs/ft^2/hr)
A	7:20	9:10	150	63	0.01
B	8:30	9:40	115	69	0.04
C	9:20	10:30	230	72	0.02
D	2:15	3:20	115	81	0.02
E	2:45	3:50	230	80	0.05

The area/volume and CT535 results are shown in **Table 16**. Periodically, on-site engineer verified the best practice of 30% overlap on spray head was achieved. In general, the area volume and the CT535 results matched closely.

Table 16. STH-53 CT535 Test Results

Sample ID	A(150sf/gal)	B(115sf/gal)	C(230sf/gal)	D(115sf/gal)	E(230sf/gal)
1	175	107	212	112	212
2	162	110	214	113	255
3	172	125	194	108	251
4	200	106	197	102	213
5	172	127	224	112	239
Average	170	115	208	109	233
STDV	6	14	11	4	20
COV (%)	3%	12%	23%	7%	7%

The embedded resistance results for Section B are shown in **Figure 46**. The results are significantly different than any of the previous sites with resistance very low due to the rainfall the previous night indicating a small amount of drying from the slab.

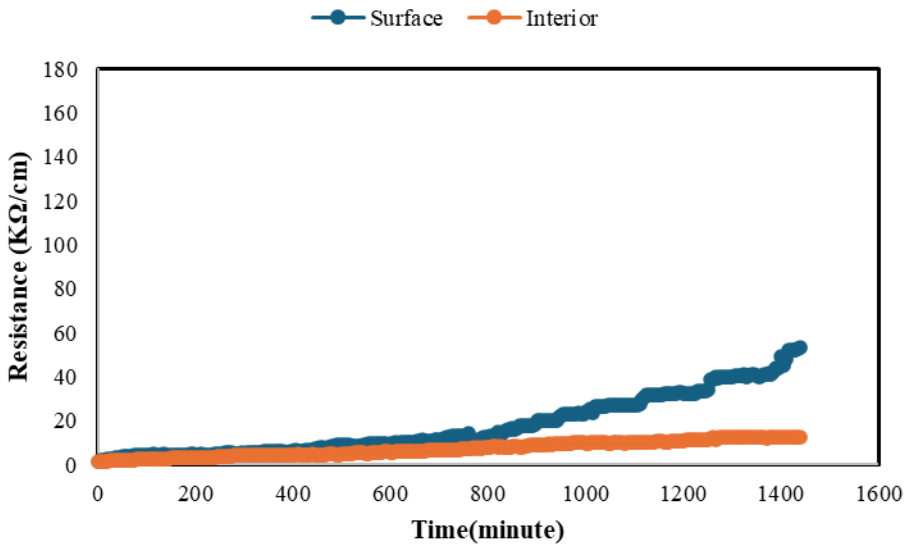

Figure 46. Embedded Resistance Section A

3.6.1 Chilled Mirror and GPR Testing results

Analysis of the Appendix D and E data for STH 53 is summarized in **Figure G.5** and **Figure G.6**. A revealing data set is again the rate of joint activation and the change in dielectric value (α) with time. This contrast between the morning and the afternoon placement is obvious as far as joint activation is obvious. High humidity and low shrinkage levels contributed to the low activation rate.

3.6.2 Shrinkage Testing results

The shrinkage results, shown in **Figure G.5** and **Figure G.6** are inconsistent with respect to the AR and the resulting joint activation likely due to the rainfall before and during construction. Table 17 lists the results of monitoring the pavement joints for activation of the saw-cut joints.

Table 17. STH53 Joint Activation

Location	Date	Time	Notes	Joint Activation
A	Tues 6/25	7:20am	Paved	N/A
	Wed 6/26	11:00am		6 of 8
	Thurs 6/27	10:00am		7 of 8
B	Tues 6/25	8:30am	Paved	N/A
	Wed 6/26	11:00am		4 of 14
	Thurs 6/27	10:00am		12 of 14
C	Tues 6/25	9:20am	Paved	N/A
	Wed 6/26	11:00am		12 of 13
	Thurs 6/27	10:00am		12 of 13
D	Tues 6/25	11:00am	Paved	N/A
	Wed 6/26	11:00am		0 of 14
	Thurs 6/27	10:00am		7 of 14
E	Tues 6/25	2:45pm	Paved	N/A
	Wed 6/26	11:00am		0 of 13
	Thurs 6/27	10:00am		5 of 13

3.7 Summary of Field Observations

The observational field visit took place during the summer of 2023 and 2024. The research team performed a variety of different tests to assess when and how much membrane-forming curing compound (MFCC) was applied to highway pavement and determine how concrete properties were impacted.

Objective 1) Observing and recording when and how uniformly the curing materials are applied by assessing representative concrete pavement projects in Wisconsin.

For the observed construction projects the rate of paving varied between 3 feet per minute up to 8 feet per minute. The curing cart speeds varied from 50 feet per minute to 100 feet per minute with most operational speeds around 75 feet per minute. For three sites tining and curing operations occurred at the same time with the USH53 being the lone site where these operations were performed separately. Since the speed of the curing cart is so much greater than the paving operation, the curing cart operates for short bursts of activity. On average the curing cart operator allowed a gap of 100-200 feet to develop between the texture cart and the curing cart before applying the MFCC, with the texture cart approximately 50 feet behind the paver. So, for the projects, on average the curing compound was applied between 40 and 80 minutes after exiting the back of the paver but up to 120 minutes for the first section of the day.

The application rate was highly variable and dependent on the curing cart operator. The observed variability on the first two sites was too high to produce any reasonable conclusions and the research team began working with the curing cart operator to calibrate application rates. When the speed of the curing cart was calibrated to the application of a known volume of MFCC for the area in question, this was corroborated by the CT535 tests. No significant issues with uniformity were observed on any of the site locations. Clogged nozzles resulting in streaking occurred twice during the observational visits and were identified quickly by the curing cart operator and cleared. The current practice of visual assessment appears sufficient, further supported by the laboratory research showing the rate is much more of a significant factor than uniformity for most environmental conditions.

Objective 2) Documenting how curing compound application times and coverage relate the development of distress (such as: shrinkage, cracks, scaling, or delamination) on concrete pavement

The rate of application was highly correlated with early-age joint activation with higher application rates delaying joint activation. Within the timeframe of the study, no distresses were observed on any of the sites. The benefit of a more actively managed curing process and the timely initiation of the sawcut joints, will be greater uniformity in the distribution of joint movement across an entire paved area, and an improvement in long-term pavement performance. Based on the finding of this study, only a small portion of the sawcuts placed in concrete paving cured according to the present curing standard used by the Wisconsin DOT activate consistently in the first 24-48 hours. The sawcuts that do activate are widely spaced. This is especially the case for afternoon paving. Proper activation, on the other hand, can significantly reduce the incidence of pavement blow-ups, dominant and failed joints, and uncontrolled, isolated slab cracking. The rate of application is one factor that was highly correlated with early-age joint activation where higher application rates delayed or simply prevented joint activation. Within the timeframe of the study, no immediate distress was observed on any of the sites. The results of the field testing clearly indicated two ways of promoting timely activation of the sawcut joints.

Objective 3) Developing a measurable methodology to establish optimal times and assess uniform application.

The research team identified 3 key items related to the optimal time of application (ToA): prevailing climatic conditions as indicated by the potential evaporation (PE); the evaluation index (EI), and the rate of change in the measured dielectric or resistance with time. The test equipment used by the research team to collect the field data is the same type of equipment to constitute a measurable methodology to establish an optimal ToA. **Figure 47** shows an example of this type of data where PE could be used to actively manage application rate for a known mixture and MFCC type.

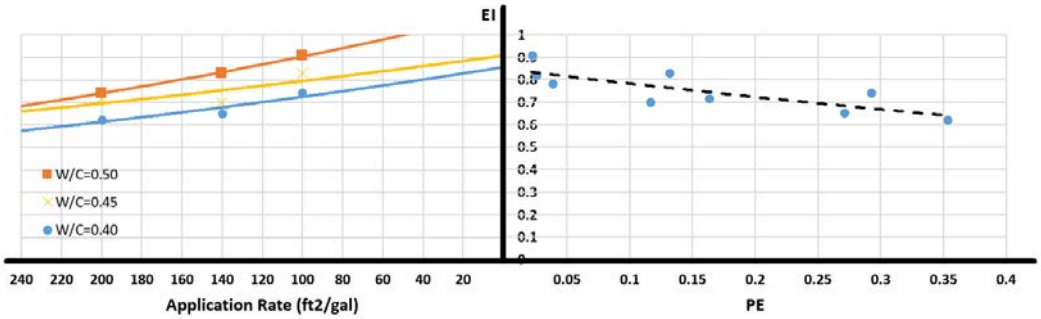

Figure 47. Curing Reference Chart

Verification of the application rate could then be determined at the early age at discrete locations along the pavement using resistance. **Figure 48** shows the acceptable performance for the desired MFCC application rate across a range of evaporative conditions. If readings climbed at too fast of a rate, additional MFCC could be applied. Then the GPR could be used to assess the conditions more broadly (**Figure 49**).

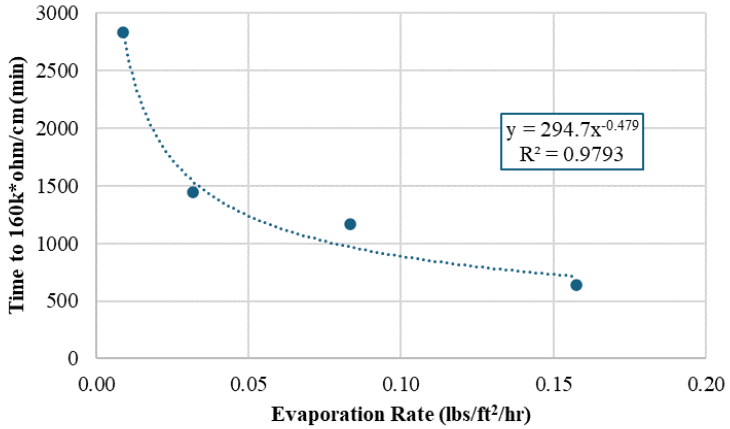

Figure 48. Acceptable Drying Time Equivalent to Desired Curing Rate

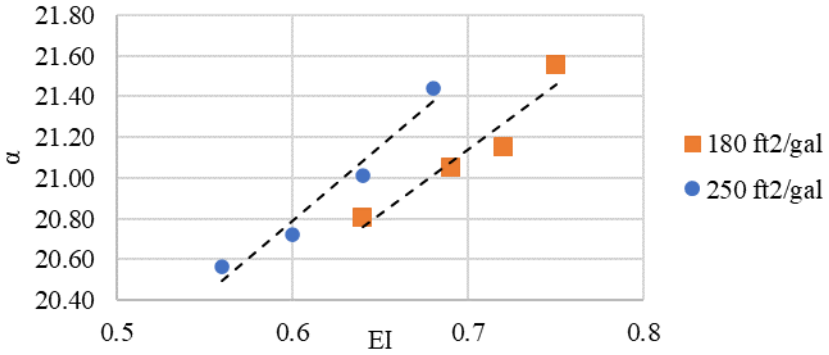

Figure 49. GPR calibration curve

The measurable methodology to establish the optimal ToA consists of the following steps:

1) Establish a curing reference as a function of the PE, AR, embedded resistance, EI and/or the α from dielectric readings for a given curing compound.
    a. An example reference chart is shown in **Figure 49**. This information is derived in the laboratory for a given method of curing and establishes the relationship between the slope of the surface dielectric (α) and the measured EI. The same can be done using resistivity measurements.
2) Monitor the PE and EI during morning placement to adjust the AR to insure EI below 0.75 and an α of -0.2 or greater during the afternoon placement.
    a. To facilitate management of the curing process, a curing chart should be prepared

Table 18. Example Curing Chart

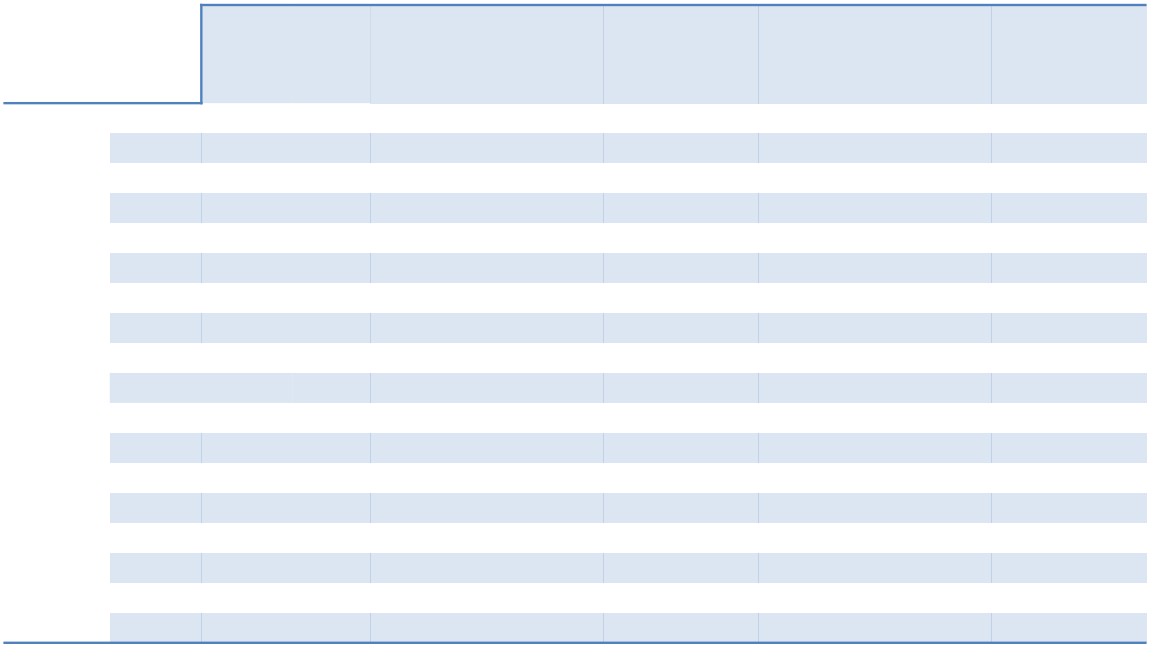

b. (**Table 18**) based on expected weather trends (temperature, humidity, and wind speed) as a specification item to assist the contractor in controlling and anticipating the speed of the spraying cart at critical times during the paving day. A provision should be provided in the curing specification to require a 300-foot test run with the spray cart for the purpose of calibration of the AR and the speed of travel of the spray cart.
c. The chilled mirror test equipment used during and to carry out the research will soon be available commercially in an upgraded format to better facilitate adoption and training of construction personnel to make use and implement the technology.
d. It is anticipated that once the climatic trends are understood and appropriately reacted to for a given project, the construction process will be able to successfully proceed with improved joint activation without the aid of monitoring technology.

3) Continue monitoring for 24 hrs to update the EI/AR relationship as needed.

4 Observations and Recommendations

The following are specific observations and recommendations from this study:

- The application rate of MFCC is highly variable and operator dependent. In the best case, the cart speed had been calibrated to the rate of application as determined by the placement of the MFCC barrels. In the worst case, cart speed was determined by the amount of time the operator could be away from back of paver activities. It is clear that attention is needed to ensure operational speed produces the desired application rate.
- For the observed construction projects, the rate of paving varied between 3 feet per minute up to 8 feet per minute. The curing cart speeds varied from 50 feet per minute to 100 feet per minute with most operational speeds around 75 feet per minute. For three of the sites, tining and curing operations occurred at the same time with the USH53 being the lone site where these operations were performed separately. Since the speed of the curing cart is so much greater than the paving operation, the curing cart operates for short bursts of activity. On average the curing cart operator allowed a gap of 100-200 feet to develop between the texture cart and the curing cart before applying the MFCC, with the texture cart approximately 50 feet behind the paver. So, for the projects, on average the curing compound was applied between 40 and 80 minutes after exiting the back of the paver but up to 120 minutes for the first section of the day. Timing was not adjusted for environmental conditions nor was it monitored, and some degree of timing control is needed.
- CT535 is not a practical test for actual field quality control or assurance and has several significant drawbacks. First, on three of the observational visits tining and curing were performed at the same time. To obtain the CE535 information the operator was required to perform two passes slowing productivity. Second, the pads were located only near the pavement edge and captured one to one and a half nozzles of spray area. Any variability in the selected location would then be represented for the entire pavement width. Also, for several sites the bar height was not level and placing the pads only at the pavement edge meant they were either at the closest or farthest point from the spray bar. Third, the test requires the pad mass to be measured very quickly after spraying with a high-precision scale. High-precision scales are highly sensitive and on the side of the road, even with a windbreak, obtaining accurate readings was challenging. Lastly, when a moderate level of wind was present the pads would move or fold over, reducing the number of tests.
- Embedded resistance is highly influenced by environmental conditions and the rate and quality of MFCC application. It is highly likely that an acceptable time to a desired resistance threshold, calibrated against moisture loss, for actual environmental conditions could provide actionable quality control and assurance information for approval of MFCC effectiveness.

4.1 Immediately Implementable Actions

It is clear from this research that the time of application and rate of application of MFCC influence concrete properties as well as the long-term performance of the pavement section. In practice both were highly variable initially but simple intervention by the research team significantly improved coverage consistency. We recommend taking the first 300 feet of the day to calibrate the speed to the application rate and adjust bar height to ensure proper overlap.

a) Improved uniformity of the curing application; record/measure how much MFCC was used.
b) Improve integration of the curing (time of application (ToA)) and sawcutting (time of cutting (ToC)) operations; consider the use of curing methods to make greater use of the advantage that

green cutting offers coupled with the curing operation to insure successful activation of the sawcut joints.

c) Consider the use of a broader range of curing compound efficiencies to facilitate management of the curing process. Several new surface treatments are coming on the market that should facilitate controlling the rate of evaporation and setting especially with the advent of low carbon cements.

4.2 Near Future Actions

The research recommends funding an implementation project or initiative to assess the feasibility of adopting a revised curing specification to include curing monitoring technologies such as:

- Chilled mirror-based technology for the purposes of monitoring internal humidity, rates of evaporation, and moisture levels for the first 30 hours of paving. The research has substantiated the utility of an EI-type parameter that can be used as a curing effectiveness indicator to assist in management decisions to between activate sawcut joints and improve long-term performance. Other sensor technologies such as the use of resistance and time domain reflectometry (TDR) also have potential for use in this application.
- Use of GPR and GPS technologies in and around the paving operation. This type of instrumentation will facilitate the establishment of a fixed time window for texturing and curing operations based on data collected covering the full paved area. Critical threshold rates associated with evaporation and setting will serve as indicator on the ToA and when the curing cart operator should proceed.
- Improved instrumentation the curing cart with vehicle speed (if not already present), pumping pressure, along with a curing compound flow and spray monitoring.
- Development specification items to incentivize the paving industry to facilitate improved joint activation and pavement performance.

4.3 Actions Required for Fully Managed Performance Engineered Curing

First and foremost, would be to fund an implementation project to assess the feasibility and impact of managed curing for concrete pavement construction in Wisconsin. This effort could prequalify methods of curing with evaporation rates for the range of potential environmental conditions including actual MFCCs (Low, Medium, High), curing cart or weather station monitors current weather and forecast, monitor concrete via selected sensors, and adjusts in real-time. Figure 50 shows an example of the process highlighted by the observations and research results. First, an evaporation reference curve can be established for a particular mixture, MFCC, and range of environmental conditions. Various on-site monitoring can be used to assess the behavior of the concrete along with actual weather conditions. Based on the concrete behavior, recent weather conditions, and forecasted future weather conditions, curing timing and rate can be adjusted to ensure consistent joint activation behavior.

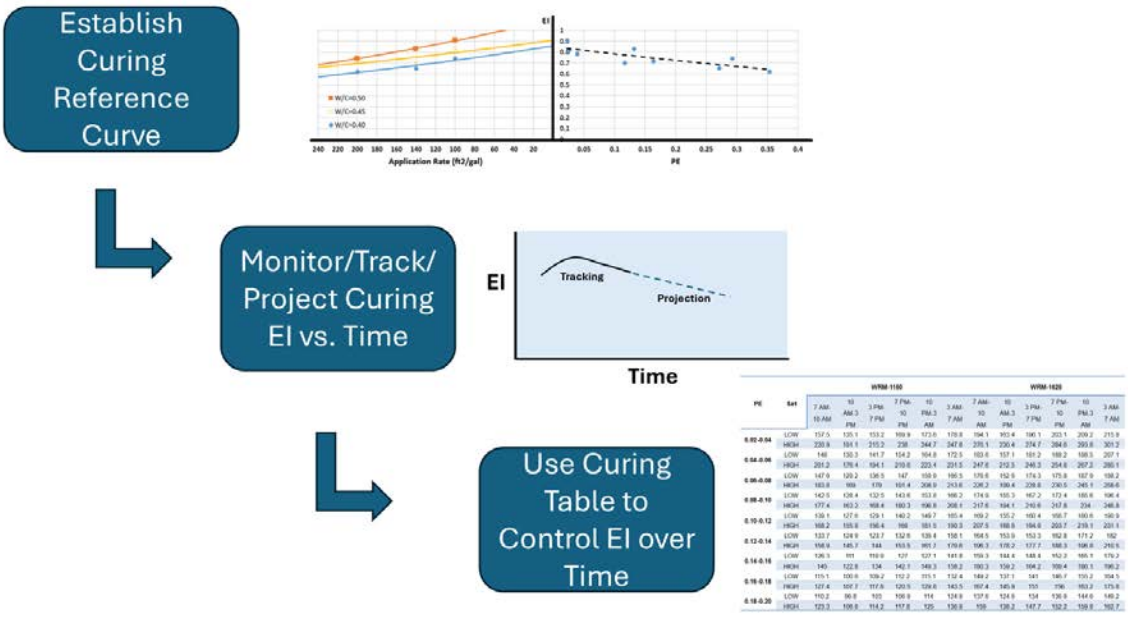

Figure 50. Process for Fully Managed Curing Operations

5 References

ACI Committee 238, (2008). ACI PRC 238.1 Report on Measurements of Workability and Rheology of Fresh Concrete. American Concrete Institute, Farmington Hills, MI, 70 pgs.

ACI Committee 308R-16 (2016). Guide to External Curing of Concrete. Farmington Hills, Mich: American Concrete Institute, 1st Printing, 6 pgs.

American Concrete Pavement Association (ACPA) (2010). Concrete Pavement Field Reference Paving, American Concrete Pavement Association (ACPA), EB238P, Rosemount, IL, 150pgs.

Artioli, G. and Bullard, J.W. (2013). Cement hydration: the role of adsorption and crystal growth. Crystal Research and Technology, 48(10), pp.903-918.

ASTM C150 (2005) Standard Specification for Portland Cement, C150-05, West Conshohocken, PA: ASTM International.

ASTM C156. 2020a. "Standard Test Method for Water Loss [from a Mortar Specimen] Through Liquid Membrane-Forming Curing Compounds for Concrete", ASTM International: West Conshohocken, PA.

ASTM C232 (2010). "Standard Test Methods for Bleeding of Concrete," ASTM International: West Conshohocken, PA. 4.02, 5 pgs.

ASTM C 309 (2019). Standard Specification for Liquid Membrane-forming Compounds for Curing Concrete. Annual Book of ASTM Standards. West Conshohocken, Pennsylvania, 4.02, 3 pgs.

ASTM C1202 (2019a). "Standard Test Method for Electrical Indication of Concrete's Ability to Resist Chloride Ion Penetration," ASTM International: West Conshohocken, PA. 4.02, 8 pgs.

ASTM C1876 (2019b). "Standard Test Method for Bulk Electrical Resistivity or Bulk Conductivity of Concrete," ASTM International: West Conshohocken, PA. 4.02, 7 pgs.

ASTM E1347 (2020b). "Standard Test Method for Color and Color-Difference Measurement by Tristimulus Colorimetry," ASTM International: West Conshohocken, PA. 6.01, 5 pgs.

Bye, G.C., 1999. Portland cement: composition, production, and properties. Thomas Telford, 225 pgs.

California Department of Transportation (CalTrans). (2014). Method of Test for the Application Rate of Concrete Curing Compound In the Field, California Test 535, January, 5 pgs.

Chen, Z., Derakhshani, R.R., Halmen, C. and Kevern, J.T., 2011, July. A texture-based method for classifying cracked concrete surfaces from digital images using neural networks. In The 2011 International Joint Conference on Neural Networks (pp. 2632-2637). IEEE.

Choi, S. and Shah, S.P., 1997. Measurement of deformations on concrete subjected to compression using image correlation. Experimental mechanics, 37(3), pp.307-313.

Choi, S. and Won, M. (2008). Identification of compliance testing method for curing effectiveness, Texas Department of Transportation Report 0-5106-2, 53 pgs.

Choi, S., Yeon, J. H., and Won, M. C. (2012). Improvements of curing operations for Portland cement concrete pavement. Construction and Building Materials, 35(0), 597–604. doi:10.1016/j.conbuildmat.2012.04.065

Crovetti, J. and Kevern, J.T. (2018). "Joint Sawing Practices and Effects on Durability," Final Report for Wisconsin Highway Research Program, Project WHRP 0091-16-01, August, 265 pgs.

Dewangan, A.K., Singh, L., Kantode, V., and Verma, P. (2019). Critical Review on Curing in Concrete, International Journal of Innovations in Engineering and Science, Vol. 4, No. 12, 8 pgs.

Fagerlund, G. (2009). Chemically bound water as a measure of the degree of hydration: method and potential errors. (Report TVBM; Vol. 3150). Division of Building Materials, LTH, Lund University.

Gartner, E.M., Young, J.F., Damidot, D.A. and Jawed, I. (2008). Hydration of Portland cement. In: Gartner, P. and Bensted, J., Eds., Structure and Performance of Cements, Taylor & Francis Group, London, 107-113

Gowsika, D., Balamurugan, P. and Kamalambigai, R. (2017). Experimental study on curing methods of concrete. Int. J. Eng. Dev. Res, 5(1), pp.2321-9939.

Grasley, Z. C., Lange, D. A., and D'Ambrosia, M. D. (2006a). Internal relative humidity and drying stress gradients in concrete. Materials and Structures, 39(9), 901-909. https://doi.org/10.1617/s11527-006-9090-3

Grasley Z.C., Lange D.A., D' Ambrosia M.D, and Villalobos-Chapa S. (2006b). Relative Humidity in Concrete, Concrete International, pp. 51-57, Oct.

Hajibabaee, A., Khanzadeh Moradllo, M. and Ley, M.T. (2018). Comparison of curing compounds to reduce volume change from differential drying in concrete pavement. International Journal of Pavement Engineering, 19(9), pp.815-824.

Hansen, R.S., Waldram, D.W., Thai, T.Q. and Berke, R.B. (2021). Super Resolution Digital Image Correlation (SR-DIC): An Alternative to Image Stitching at High Magnifications. Experimental Mechanics, 61(9), pp.1351-1368.

Helgeson, S.R. (2014). Evaluation of Curing Compound Application Time on the Surface Durability of Concrete, MS Thesis, University of Wisconsin-Madison, Madison, WI, 145 pgs.

Henkensiefken, R., Bentz, D., Nantung, T., Weiss, J. (2009). Volume change and cracking in internally cured mixtures made with saturated lightweight aggregate under sealed and unsealed conditions, Cement and Concrete Composites, Volume 31, Issue 7, Pgs 427-437, ISSN 0958-9465.

Joshaghani, A., and D. G. Zollinger (2017). Concrete Pavements Curing Evaluation with Non-Destructive Tests. Construction and Building Materials, Vol. 154, 2017, pp. 1250–1262.

Joshaghani, A. (2019). Identifying the Problematic Areas with Structural Deficiencies of Pavements Using Non-Destructive Tests (NDT). International Journal of Pavement Engineering, Vol. 20, No. 11, 2019, pp. 1359–1369.

Joshaghani, A. and Zollinger, D.G. (2021). Evaluating the Quality of Curing Applications on Concrete Pavements with Ground-Penetrating Radar. Transportation Research Record, Vol 2675, No. 8.

Josserand, L. (2004). A method for concrete bleeding measurement. Materials and Structures, 37(274), 666–670. doi:10.1617/14052

Kevern, J.T. "Using Soybean Oil to Improve the Durability of Concrete Pavements," International Journal of Pavement Research and Technology, Sustainable Concrete Pavements Special Edition, V.3, No. 5, Sept. 2010.

Kevern, J.T., Halmen, C., Hudson, D. and Trautman, B. "Evaluation of Surface Resistivity for Concrete Quality Assurance in Missouri," Transportation Research Record: Journal of the Transportation Research Board, No. 2577, Transportation Research Board of the National Academies Washington D.C., pp. 53-59, 2016. DOI: 10.3141/2577-07.

Kewalramani, M.A. and Gupta, R. (2006). Concrete compressive strength prediction using ultrasonic pulse velocity through artificial neural networks. Automation in Construction, Vol. 15, No. 3, pp.374-379.

Khayat, Kamal & Sadati, Seyedhamed. (2014). Recycled Concrete Aggregate: Field Implementation at the Stan Musial Veterans Memorial Bridge. Center for Transportation Infrastructure and Safety/NUTC program, DTRT06-G-0014, 180 pgs.

Kroop, R., Cramer, S.M., and Anderson, M. A. (2012). Laboratory study of high performance curing compounds for concrete pavements: phase I, Wisconsin Highway Research Program Final Report #0092-1105, June 2012, 53 pgs.

Li, Y., Dong, W., Li, H. and Li, Z., 2015. Method of vacuum water absorption to determine the porosity of hardened concrete. International Journal of Structural and Civil Engineering Research, 4, pp.282-286.
Maierhofer, C., (2003). Nondestructive evaluation of concrete infrastructure with ground penetrating radar. ASCE Journal of materials in civil engineering, 15(3), pp.287-297.
Meadows W.R., (2020). 1610-white water-based, wax-based concrete curing compound. Available at: https://www.wrmeadows.com/1610-white-water-based-wax-based-concrete-curing-compound/ Accessed on 15/10/2022
Nahata, Y., Kholia, N., and Tank, T.G. (2014). Effect of curing methods on efficiency of curing of cement mortar. APCBEE Procedia, Vol. 9, pp.222-229.
Naik, T.R. and Moriconi, G. (2005). October. Environmental-friendly durable concrete made with recycled materials for sustainable concrete construction. In International Symposium on Sustainable Development of Cement, Concrete and Concrete Structures, Toronto, Ontario, October (Vol. 5, No. 7).
Neville, A.M., 1995. Properties of concrete (Vol. 4). London: Longman Group UK Limited, 844pgs.
Poole, T.S. (2006). Guide for Curing of Portland Cement Concrete Pavements 2006: Turner-Fairbank Highway Research Center, Research, Development, and Technology. FHWA-HRT-05-038,
Powers, T. C. (1947). "A Discussion of Cement Hydration in Relation to the Curing of Concrete," Proceedings, Highway Research Board, V. 27, pp. 178-188.
Rao, C. and M.I. Darter, (2013). Evaluation of Internally Cured Concrete for Paving Applications, Report.
Rupnow, T. and Icenogle, P. (2012) “Evaluation of Surface Resistivity Measurements as an Alternative to the Rapid Chloride Permeability Test for Quality Assurance and Acceptance.” Transportation Research Record: Journal of the Transportation Research Board, Vol. 2290/2012 Concrete Materials, 8 pgs.
Santos M., (2013). 554th red horse airmen pave the way for silver flag. Available at: https://www.andersen.af.mil/News/Features/Article/638635/554th-red-horse-airmen-pave-the-way-for-silver-flag/ Accessed on 05/11/2022
Sayahi, F., Emborg, M., Hedlund, H., and Cwiren, A. (2019) Plastic Shrinkage Cracking of Self-Compacting Concrete: Influence of Capillary Pressure and Dorman Period, Nordic Concrete Research, Vol. 60, I. 1, pp. 67-88.
Siddique, Z.Q., Hossain, M. and Meggers, D., 2005, August. Temperature and curling measurements on concrete pavement. In Proceedings of the 2005 Mid-Continent Transportation Research Symposium, Iowa State University, Ames, IA, 10 pgs. ISBN:9780965231084
Slowik, V., Schmidt, M., Kässler, D. and Eiserbeck, M. (2014) Capillary pressure monitoring in plastic concrete for controlling early-age shrinkage cracking. Transportation Research Record, 2441(1), pp.1-5.
Sun, P. (2013). A new protocol for evaluating concrete curing effectiveness, MS Thesis, Texas A&M University, College Station, TX, August, 101 pgs.
Suprenant, B.A. (1999). Repairing curled slabs. Concrete Construction Magazine, Vol. 9, pp.58-65.
Tafheem, Z., Khusru, S. and Nasrin, S., 2011, December. Environmental impact of green concrete in practice. International Conference on Mechanical Engineering and Renewable Energy, Vol. 22, 24 pgs.
Taylor, P. C. (2014). Curing Concrete, 1st Ed., CRC Press, Taylor & Francis Group, 191 pgs.
Taylor, P.C., Kosmatka, S.H. and Voigt, G.F. (2007). Integrated materials and construction practices for concrete pavement: a state-of-the-practice manual, FHWA Publication No. HIF-07–004.

Taylor, P.C., Van Dam, T., Sutter, L., and Fick, G. (2019). Integrated materials and construction practices for concrete pavement: a state-of-the-practice manual, InTrans project 13-482, May 2019, 333 pgs.

Topçu, İ. B., and Elgün, V. B. (2004). Influence of concrete properties on bleeding and evaporation, Cement and Concrete Research, Vol. 34, No. 2, pp 275–281.

Tikalsky, P., Taylor, P., Hanson, S. and Ghosh, P. (2011). Development of performance properties of ternary mixtures: laboratory study on concrete (No. DTFH61-06-H-00011 Work Plan 12 Pooled Fund Study TPF-5 (117)). Iowa State University. National Concrete Pavement Technology Center.

Vandenbossche, J. M. (1999). A Review of the Curing Compounds and Application Techniques Minnesota Department of Transportation Final Report 2001-06, St. Paul, MN, 35 pgs.

Vosoughi, P., Ceylan, H., and Taylor, P. (2017). Impacts of Internal Curing on the Performance of Concrete Materials in the Laboratory and the Field, National Concrete Pavement Technology Center, Final Report IHRB Project TR-676, Ames, IA, 56pgs.

Wang, K., Cable, J.K., and Ge, Z. (2006). Evaluation of Pavement Curing Effectiveness and Curing Effects on Concrete Properties, ASCE Journal of Materials in Civil Engineering, Vol. 18, No. 3, pp 377-389.

Wei, Y. and W. Hansen, 2011. "Characterization of Moisture Transport and Its Effect on Deformations in Jointed Plain Concrete Pavements," Transportation Research Board.

Whiting NM and Snyder MB. (2003). Effectiveness of Portland Cement Concrete Curing Compounds. Transportation Research Record. 1834(1): 59-68. doi:10.3141/1834-08

Sayahi, F. (2019). Plastic Shrinkage Cracking in Concrete: Mitigation and Modelling, Doctoral dissertation, Luleå University of Technology, Lulea, Sweden, 200pgs.

Sun, P. and Zollinger, D.G. Concepts to Enhance Specification and Inspection of Curing Effectiveness in Concrete Pavement Design and Construction, Transportation Research Record: Journal of the Transportation Research Board, National Academies, V. 2504, Issue 1, 2015.

Wittmann, F.H., 1976. On the action of capillary pressure in fresh concrete. Cement and concrete research, 6(1), pp.49-56.

Ye, D., Mukhopadhyay, A., and Zollinger, D.G. Laboratory and Field Evaluation of Concrete Paving Curing Effectiveness, Texas Department of Transportation, Report 0-5106-3, 196 pgs, December 2009.

Zemajtis, J.Z. Role of Concrete Curing, website, last accessed 5/10/22. https://www.cement.org/learn/concrete-technology/concrete-construction/curing-in-construction#:~:text=Curing%20plays%20an%20important%20role,for%20extended%20periods%20of%20time.

Zollinger, D., Moon, W., Ley, T., Riding, K., Wimsatt, A., Wujun, Z., Ryo, S., and Choi, P. Implementation of Curing, Texturing, Subbase, and Compaction Measurement Alternatives for Continuously Reinforced Concrete Pavement, Texas Department of Transportation, Report 5-6037-01-1, 136 pgs, February 2013.

6 Appendix

6.1 Appendix A- Literature Review

INTRODUCTION

Curing of concrete is a process to maintain an appropriate temperature and the moisture content in the concrete for a defined period so the concrete develops the desired material properties (Vandenbossche,1999; ACI, 2016). Most simply, curing of concrete promotes increased hydration of portland cement (Powers, 1947). Curing of concrete occurs immediately after concrete is placed and finished and requires the maintenance of favorable conditions both at depth and near the surface for an extended period with the early age moisture and temperature control the most strongly correlated to long-term performance (Dewangan et al., 2019).

Curing of concrete is a crucial step for concrete performance and durability. ASTM C156-20 the Standard Test Method for Water Loss [from a Mortar Specimen] Through Liquid Membrane-Forming Curing Compounds for Concrete is the most common test method for evaluating the performance of curing compounds where mass of water lost by the specimens under hot (38°C) and dry (32% RH) laboratory conditions is determined (ASTM, 2020a). The purpose of the test is to limit moisture loss to help promote good curing. However, many practioners and researchers have pointed out the inherent limitations such as the difference in evaporation between laboratory and field conditions and question the applicability of using small mortar specimens to represent field concrete (Sun, 2013; ASTM, 2020). While measuring moisture loss is an important step, moisture loss by itself does not provide any prediction of future concrete properties of concern. For modern pavements, a practical quantification of curing compound application in the field to concrete is crucial to ensure long-term performance. Currently field quantification, when performed, is rudimentary. Some States Highway Agencies (SHAs) such as the Texas DOT (TXDOT) use the “calibrated” white paper sheet examination or rely on number of empty barrels that have been used for the given area. While these techniques provide a broad indication of the field application they are either 1) qualitative or 2) too slow for real-time remediation. The results of inadequate curing can lead to reduced concrete strength and increased surface permeability while decreasing wearing resistance and increasing the risk for plastic shrinkage cracking as shown in Figure A.1 (Helgeson, 2014).


Figure A.1: Pavement plastic shrinkage cracks (Sayahi, 2019)

Proper curing allows continuous hydration of cementitious materials and consequently continuous gain in strength and pore refinement. Once curing stops, the strength gain of concrete also stops as well as microstructure development. Practically, hydration ceases when relative humidity within the capillaries drops below 80% (Nahata et al., 2014). Curing preserves water for hydration, maximizing pavement strength and durability and also helps prevent the surface from drying out more quickly than the rest of the slab, reducing the possibility of surface damage due to differential shrinkage (Powers, 1947). Curing compounds help prevent shrinkage cracking by reducing the evaporation of water from the concrete (Jerzy, 2010).

CONCRETE

Concrete is an abundant and versatile construction material and ubiquitous world-wide (Tafheem et al., 2011) and most simply is comprised of a mixture of cement, aggregates, and water. The handling, placing, and curing conditions strongly influence the final product (ACPA, 2010).

Cement Production and Hydration

Cement is a finely ground powder which binds substances such as aggregates, sand, and gravel, among others, through the reaction called hydration, into an aggregated concretion (Bye, 1999). Cement production involves the conversion of various chemical constituents into new hydraulic mineral phases. Cement production is subdivided into four main stages: (1) crushing and grinding of raw material, mainly finely ground siliceous materials (shale) and calcareous materials (limestone), (2) blending the materials in the correct proportions, (3) burning of the prepared mixture in a kiln, and (4) grinding the fused product, known as clinked, together with gypsum to control setting (Bye, 1999). A cement and water mixture containing fine aggregate is called mortar and when mixed with coarse aggregate, concrete (Naik and Moriconi, 2005).

The chemical composition of portland cement includes tricalcium aluminate (3CaO. Al2O3), dicalcium silicate (2CaO · SiO2), tricalcium silicate (3CaO · SiO2), and tetra-calcium aluminoferrite (4CaO · Al2O3Fe2O3). Cement compounds react with water to produce various hydration products including: calcium silicate hydrate, calcium hydroxide, ettringite, monosulfate, and calcium aluminate hydrate (Bye, 1999). The chemical composition of cement influences the behavior and durability of concrete, which guides the selection according to ASTM C150 (ASTM, 2005).

When portland cement meets water the cement particles partially dissolve, and the various dissolved components start to react at different rates to produce hydration products (Gartener et al., 2008). During hydration the chemical reactions occurring are generally more complex than simple conversions of anhydrous compounds into hydrates and are controlled by the exact mineral composition, combination, and reaction conditions creating a plethora of various potential hydration products at any given concrete age. The new hydration compounds produced causes the cement paste to harden, bond to the aggregate in the concrete mixture, and become strong and dense (Artioli and Bullard, 2013). Additionally, the hydration products will occupy some of the original space previously occupied by mixing and water that did not take place in hydration reactions will either remain in the concrete in the capillary pore system or evaporate out once the concrete dries which leads to change in volume of concrete (Taylor et al., 2007). Cement hydration is an exothermic reaction consistent with a large thermodynamic driving force for dissolution. The hydration of cement paste is responsible for the development of concrete properties. Therefore, controlling hydration and providing a longer hydration process will result in concrete developing desirable properties. As available moisture and the hydration reaction are intrinsically linked, measurement of hydration using isothermal calorimetry is one technique suitable in the laboratory of assessing the degree of hydration. Figure A.2 presents the five stages of strength development as assessed by isothermal calorimetry. Stage 1 represents a rapid initial heat generation and drop as gypsum controls the initial aluminate reactions. In Stage 2 the concrete is dormant which allows transportation and placement but with a continued rise in pH as calcium dissolves into the mixing water. The transition from Stage 2 to Stage 3 is termed initial set, where sufficient hydration products have formed that the external volume has been fixed and the concrete can no longer be moved. In stage 3 the pH exceeds 13 SU and hydration products are rapidly formed and strength gain accelerates. Strength at initial set is typically less than 250 psi. Between initial and final set the concrete surface can be finished and curing commences. Near the end of stage 3 the concrete will pass through final set, where concrete is sufficiently hard that all finishing activities cease. Stage 4 represents continued hydration, strength gain, and maximum calorimetric heat generation. Concrete sawing activities occur late in stage 3 and throughout stage 4. Stage 5 represents all densification and strength gain after about 24 hours where a majority of pore refinement and permeability reduction occurs. Calorimetry is a useful tool for assessing activity timing for particular concrete mixtures and can help evaluate setting and sawing behavior under a range of anticipated construction temperatures.

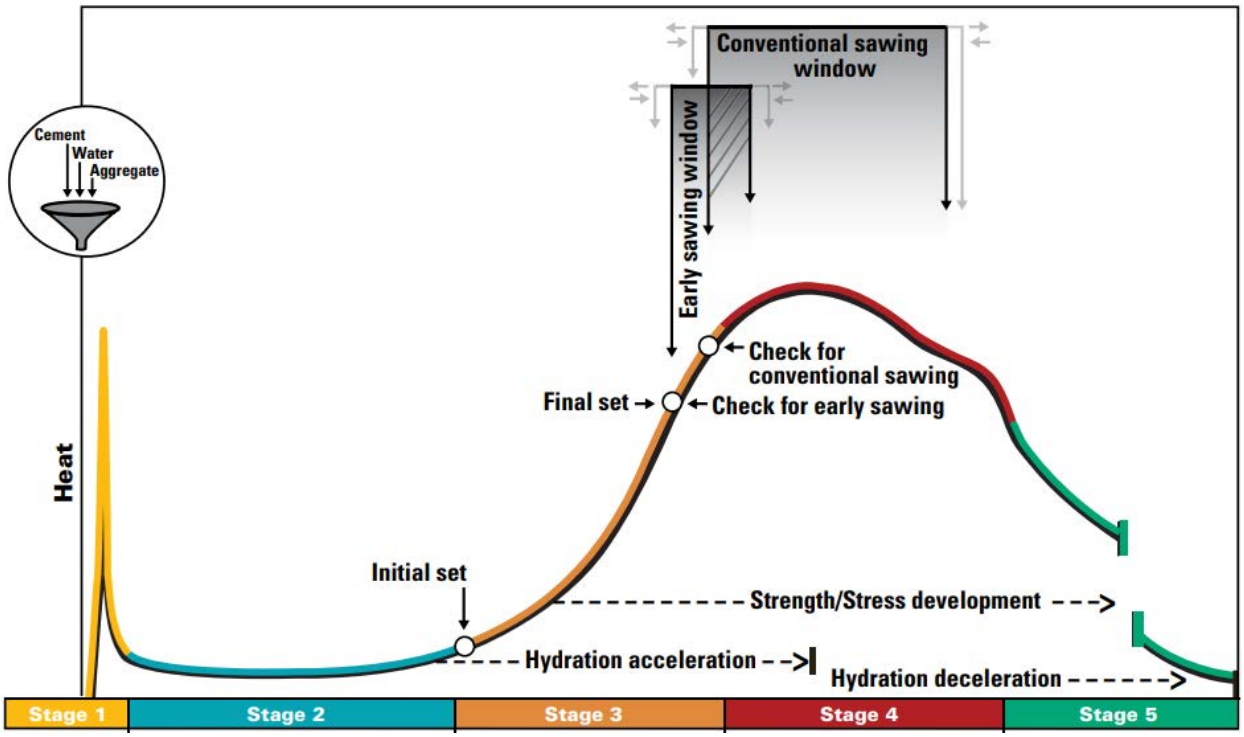

Figure A.2: Stages of Concrete Hydration Assessed Using Isothermal Calorimetry (Taylor et al., 2019)

Concrete pavement construction.
While proper mixture proportions and batching are fundamental to concrete durability, construction in the field is just as important for long-term performance and since it is influenced by many uncontrollable factors such as weather, proper site construction practices as especially important. Concrete pavement construction includes everything from initial field verification of project materials and site conditions to opening to service. The following sections will detail some stages of concrete pavement construction important to moisture management and could influence curing.

On site concrete pavement construction starts by preparing a rigid pavement subgrade/base to provide uniform support between the concrete slab and the soil foundation. Field verification is an important stage of concrete pavement construction prior of concrete transportation process, as it ensures subbase is maintained in good condition and will not draw water from the hydrating cement paste. During concrete production the mixing of cementitious materials should maintain the desired water-to-cementitious materials (w/cm) ratio. During transport the concrete mix should be covered, when needed, to avoid change of water content and temperature of the concrete prior to placement.

Once the concrete passes through the paver, the surface usually is finished to close holes and create a tight surface. If the concrete is not workable, crews may overwork the surface and reduce air content or be tempted add water to complete finishing. Both over finishing and adding water can lead to surface scaling caused by freeze-thaw and deicer damage. After finishing, two operations are used to create microtextured and macro-texture. Micro-texture is created by dragging turf, burlap, or coarse carpet along the pavement surface. Finally, macrotexture is created with a tining device or rake that makes transverse or longitudinal grooves in the wet pavement surface. The orientation, depth, and spacing of the grooves should be specified for each job (ACPA, 2010). The texture, both micro and macro, influence the exposed

surface area and curing compound application rate for complete coverage with rougher sections requiring a higher application rate.

Once texture has been applied, curing compounds are applied and the significance of controlling moisture in concrete shortly after installation cannot be overstated. Concrete internal relative humidity is primarily regulated by proper curing with the zone nearest the surface (1/4 in.) directly affected. Curing compounds slow surface drying and maintain a relative humidity near the surface more similar to the remainder of the slab, lowering the risk of surface damage from differential shrinkage (Taylor et al., 2007). Shortly after curing (6-24 hours), control joints are sawn to allow concrete to crack at predefined locations and preventing random. While numerous additional variables specific to sawing exist such as timing, type of sawing equipment, and condition of sawing equipment, significant distresses related to moisture loss or curing compound damage during sawing have not been observed or able to be directly attributed (Crovetti and Kevern, 2018).

The last stage of concrete pavement construction is the opening to traffic. The opening to traffic takes place once the concrete has gained enough strength to prevent unwanted distress before applying loads. Instead of using the strength of a cylinder or beam that cured and acquired strength under different conditions than the pavement, the strength utilized to calculate opening time should be the real strength of the concrete pavement. As a result, the maturity approach is recommended for determining in-place strength before traffic opening. (Taylor et al., 2007). Maturity is a function of time and temperature with curing and hydration a significant contributor to temperature and degree of hydration, curing is fundamentally linked to traffic opening performance.

Concrete bleeding

In the construction and finishing operations there are several steps of specific importance to appropriate and correct application of curing materials. Since cement only requires around 0.25g of water to theoretically hydrate each 1g of cement, but additional water is needed to create pores and channels to allow the water to access the unhydrated cement, typical concrete paving mixtures possess more water than is needed for complete hydration. Immediately after placement the concrete settles and the extra water migrates to the surface, termed bleeding (Sun, 2013; Topcu and Elgun, 2004; Helgeson, 2014). Bleeding can be reduced by limiting extra water of convenience, improving the aggregate gradation, increasing the amount of powder or fine aggregate in the mixture, and limiting workability. Excessive bleeding will cause the finishing and curing process to be delayed.

The finishing and curing process should not begin until the bleed water has evaporated from the surface or been reabsorbed into the hydrating matrix. A small amount of bleeding in most concrete pavements is typical and expected. Bleeding usually takes place 30 minutes after placement, followed by a steady decline in the rate over the following hours as the concrete enters the hardening process (Joserand, 2004). Bleeding plays an important role in construction practices. Some bleeding helps control the development of plastic shrinkage cracking by maintaining a high relative humidity near the concrete surface (Neville, 1995). However, excessive bleeding affects the strength and durability of concrete at the surface by increasing the near-surface w/cm and in severe cases, creating channels in the matrix, increasing permeability dramatically. Early finishing can trap bleed water at the surface resulting in scaling.
The standardized test for evaluating the amount of mixed water bleed is given by ASTM C232/AASHTO T 158 (ASTM, 2010). The ASTM test for bleeding involves consolidating a sample of concrete and covering to prevent evaporation. Bleed water is pipetted off at prescribed time intervals with bleeding reported as mass collected divided by the mass of available water in the specimen. Nevertheless, the

standard test has been criticized by different researchers as it does not correlate with the actual bleeding behavior of concrete and does not consider the evaporative conditions of the environment (Choi et al., 2012). Figure A.3 shows the presence of significant bleed water present on a vibrated concrete pavement.

Figure A.3: Bleed water concrete (Santos, 2013)

Hardened concrete properties

The curing of concrete strongly influences the properties of hardened concrete (Taylor, 2014). The hardened properties influenced by curing are strength, porosity, resistance freezing and thawing, and volume change.

Strength

Concrete compressive strength is the most commonly measured property because compressive strength is relatively easy to assess and provides a fair analog with other properties such as tensile and flexural strength. Strength development is a factor of the amount and chemistry of the cementitious materials, curing temperature, and the availability of moisture. Well-cured concrete has higher strength (Taylor et al., 2019).

Porosity and Permeability

Besides compressive strength, the property of most concern is porosity. The porosity of the concrete influences strength, permeability, durability, and volume change behavior. Porosity is the ratio of void volume to the total volume. The decrease in capillary porosity increases the compressive strength of the concrete. Porosity measurement techniques include Mercury intrusion porosimetry (MIP), helium or nitrogen absorption, and calculations from measurements of weight loss or by the methods of vacuum water absorption (Li et al., 2015). While various techniques exist to measure porosity, of more immediate concern for concrete pavements are the actual properties controlled by porosity, with permeability directly correlated with durability.

Permeability is defined as the ease with which fluids can penetrate the concrete, namely water, deicer solutions, and carbon dioxide of importance for DOT structures. Reducing the permeability properties of the concrete can slow or stop the durability-related distresses. Permeability of concrete can be measured directly, although not easily, and surrogate electrical measures are the most common. ASTM C1202 the Rapid Determination of the Chloride Permeability of Concrete (RCP) test is based on the assumption that when an electrical change is applied to concrete, the high ionic fluids in the pore system transmit changer much faster than in the solids of the hydrated cement paste (ASTM, 2019a; Tikalsky, 2011). So for the RCP test a low charged passed is a good indicator of a low number of pores and correlated with good durability. Another common test and ancillary to electrical conductivity is electrical resistivity where the assumption is the solid phase resists electrical charge and a high resistivity is a good indicator of a low number of pores and correlated with good durability (ASTM 2019b; Rupnow and Icenogle, 2012; Kevern et al., 2016). While typically laboratory-based tests, variants of both could be utilized in the field to quantify porosity development related to curing.

Resistance to Freezing and Thawing

Freeze-thaw durability is a multi-faceted problem faced by concrete exposed to cold weather in moist conditions. Damage occurs by the expansion of water during freezing and the osmotic pressures exerted as pure water is attracted to the freezing front. While saturation may be limited to a short depth, cracking at the surface can open the system, allowing further damage to occur, making the freeze-thaw damage cyclic (Kropp et al., 2012; Taylor, 2014)

Deicer salts are often present for concrete pavements and exasperate freeze-thaw distress. Salt solutions depress the freezing point of water in concrete and can increase osmotic pressures. Deicer salts also change the drying behavior and allow concrete to remain more saturated over a larger climate window, effectively increasing the number of potential freeze-thaw cycles in a saturated stated. Once concrete dries, salt crystallization in the pores causes increased internal tensile stress and can lead to scaling. Since all freeze-thaw distress can be reduced or mitigated by minimizing pores, good curing is linked to good durability.

Volume change

Concrete is a heterogeneous material with an ever-changing combination of hydration products linking aggregates. In general the aggregates have little volume change and all of the significant volume change can be attributed to the cement paste phase. The initial volume change occurs as the combination of cement and water is larger than the hydrated cement phase, which includes autogenous and chemical shrinkage. Components of very early age shrinkage also include drying as the water not being utilized by hydration evaporates. Volume change at later ages is a function of moisture movement into or out of the concrete and temperature, termed curling and warping.

Concrete curling is when the edges of concrete pavement or slab deflect compared to the middle (Figure A.4). Curling is caused by a difference in volume change between the slab's top and bottom caused by temperature. Warping is caused by a difference in volume change between the top and bottom caused by moisture. If the pavement dries out faster on the surface than the bottom of the slab, it will deflect upwards and could result in a loss of contact between the slab and subbase. Curling is most noticeable at the construction joints or areas of poor load transfer (Suprenant ,1999). To minimize building in a hardened curling and warping mixtures should contain the lowest practical amount of water, contain well-graded aggregates, and utilize membrane-forming curing compounds (Siddique et al., 2005).

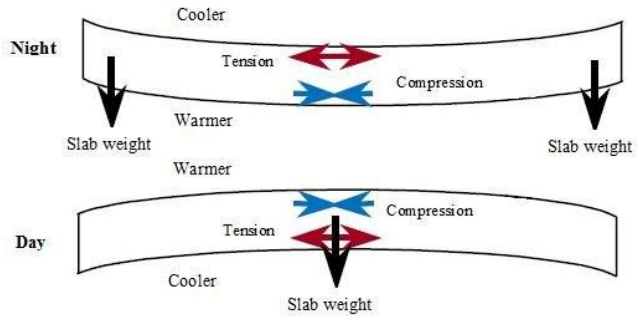

Figure A.4: Curling of concrete slabs (Khayat and Sadati, 2014)

CONCRETE CURING TECHNIQUES

Moisture control is of fundamental importance to ensure continued hydration and allow concrete to develop the necessary properties for good long-term performance. The two broad categories of curing concrete include external curing and internal curing.

External curing

The concrete curing process aims to support continued hydration and property development. Since freshly mixed concrete pavement always has more water than is needed for cement hydration, attention is required to control the evaporative water from the concrete. Bridge decks may possess much lower w/cm to promote additional reinforcing steel protection and include external curing via ponding while applying membrane-forming curing compounds (MFCC) are more common for pavements.

Ponding

Bridge decks and other reinforced structural elements many be produced with low w/cm and susceptible to significant autogenous shrinkage. Bridge decks are commonly covered with wet burlap (Amit and al., 2019, Gowsika et al., 2018). Historically wet sand or sand dikes have been used to pond water on concrete pavement, however as concrete construction has become faster and more wide-spread, the industry has progressed to MFCC for concrete pavement construction.

Membrane forming curing compounds (MFCC)

MFCC are applied to the surface of fresh concrete immediately after the bleed water is no longer present. MFCC are use water, alcohol, petroleum fractions, or a combination as a solvent and carrier for the membrane chemistry (Whiting and Synder, 2003). Once applied the solution breaks and the carrier evaporates, leaving behind a low permeability membrane. Common MFCC chemistries consist of waxes, resins, chlorinated rubber, and acrylics. Evaporation retarding performance is directly related to the chemistry and solids content of the MFCC. The most common curing materials used for DOT concrete pavement construction include white-tinted wax or poly alpha-methyl styrene (PAMS). Wax curing compounds, while low-cost, can negatively influence the surface friction until effectively worn away. Hajlbabee et al. (2016) state that a solvent-based curing compound such as poly alpha-methyl styrene (PAMS) was more effective than two water-based curing compounds in providing water retention due to a better surface wetting that produces fewer imperfections. More than one coat may be necessary for a successful surface seal to prevent water from evaporating and DOT specifications such as employed by TXDOT require two coats.

In addition to chemistry, color is an important factor controlling MFCC performance. While quite effective limiting evaporation, bituminous compound absorbs heat because of the dark color and as a result, the temperature in the concrete body rises, which is undesirable. A limewash may be recommended to be applied to the black coating to reduce heat absorption. Because of the temperature considerations, many MFCC are white pigmented or contain a dye to help ensure uniform coverage. According to ASTM C 309-19 Standard Specifications for Liquid Membrane Forming Curing Compounds and Curing and Sealing Compounds specifies the allowable evaporation rate, reflectivity, and basic carrier/solvent solution as shown in Table A.1.

Table A.1: Curing compound classification

Color		Solid constituent	
Types	Description	Class	Description
1	Clear or Translucent w/out Dye	A	No Restriction
1-D	Clear or translucent w/Fugitive dye	B	Resin
2	White pigmented		

MFCC was created to develop an evaporative barrier sprayed quickly over large swaths of exposed surface, reducing labor and time required by other curing methods. MFCC are applied using a spraying machine or hand-held sprayer. Shobber (1974) conducted a study on the evaluation of curing continuously reinforced concrete pavement using white-pigmented liquid membrane and white translucent polyethylene paper film curing. For these two methods, tensile and compressive strength were similar. Both the MFCC and film curing produced acceptable crack-spacing distributions when climatological conditions were favorable, although neither produced acceptable crack-spacing distributions during hot weather paving conditions.

Cramer and Anderson (2012) performed a study investigating the performance and durability of various concretes with five different types of MFCC. The MFCC used included: white pigmented wax emsulsion, white pigmented linseed oil emulsion, white pigmented PAMS, acylic, and chloride rubber epoxy. Testing included chloride ion penetration, water evaporation, and resistance to carbonation. Final finishing and curing compound application occurred at two hours after casting. Results showed type of coarse aggregate (limestone or igneous gravel) had little or no effect while different performance was related to cementitious material combination. Scaling was much higher in the slag and fly ash combinations than the conventional portland cement mix. MFCC moisture loss did not correlate with scaling. Overall, the best protection was offered by the acrylic sealing compound. Therefore, effective concrete curing guidelines should consider the mix type and the state of the concrete surface at the time of MFCC application and not only rely on moisture loss. Table A.2 presents a summary for the most common MFCC.

Table A.2: Summary of Membrane Forming Curing Compounds

Types	Advantages	Disadvantages
Wax	Low VOCs No special handling Can be used as a debonding agent. Easily sprayed with most used spraying equipment Can be removed with hot water	Soft Loses efficiency with time Hampers adhesion of paint Concern with surface friction
Resin	Dissipates Less prone to abrasion than wax Variable VOCs, can be low Can be removed with hot water	Comparatively short shelf life
Chlorinated rubber	High degree of moisture retention. Can act as a barrier against ion ingress Forms a thick layer Dissipates quickly Long shelf life	Expensive Dissipates quickly High VOCs are flammable and can be hazardous Runoff can be harmful to the environment
Acrylic	Environmentally friendly Increases surface hardness Deeper penetration Film does not dissipate and can act as a sealer Water or solvent carried	Can peal from surface Does not dissipate

Internal curing of concrete.

While not a specific focus of the current research, in the past few years the discussion of curing now can include the concept of Internal Curing (IC) as well. Whereas conventional curing focuses on maintaining sufficient surface moisture to reduce drying shrinkage, lightweight fine aggregate or super absorbent polymers provide additional moisture within the concrete to reduce self-desiccation. IC is maximized by replacing fine aggregates in a mixture with saturated lightweight fine aggregate. Internal moisture curing must be accompanied by external curing methods for proper concrete curing.

In addition to better hydration of cement, IC has other additional benefits. IC can reduce autogenous shrinkage, the rate of drying shrinkage, and restrained shrinkage cracking. IC can also reduce transport properties (permeability, diffusion, and sorption) (Peled and al., 2010). IC is beneficial for mixtures containing high volumes of supplementary materials, which may require longer to hydrate. IC can also make concrete less susceptible to thermal cracking as the built-in stress caused by autogenous shrinkage is substantially reduced. Additional benefits are being investigated, like reduced curling (Wei and Hansen, 2011). It is also frequently observed that resistance to flexure cracking is increased for internally cured concrete, hence improving pavement performance life (Rao and Darter, 2013).

Curing specification in the United States

In the United States each SHA is allowed to control their individual specifications. A selection of MFCC specifications is shown in Table A.3, with the National Concrete Consortium (NCC) 2015 state report on

curing included as an appendix. The majority of SHAs use ASTM C309 Type 1 compounds, but several utilized different application rates (ASTM, 2006). Application rate Moreover, each SHA has its own test methods and requirements to meet prior to the application of the curing materials. Some SHAs prefer the curing compound to be applied twice to obtain a better curing of the concrete.

Table A.3: Selected DOTs curing compound specification

STATES	ALLOWABLE MFCCs	RATE OF APPLICATION	APPROVAL/TESTING
CALIFORNIA	Type 1, Class B	1 gallon/ 150 ft^2	ASTM C309; Material should be tested under California Test 534
FLORIDA	Liquid membrane curing compound	1 gallon/ 200 ft^2 maintained for a period of 72 hours	ASTM C309
ILLINOIS	Type 1 class A, Type 1-D Class B, Type 2, Class A	1 gallon per 250ft^2	ASTM C309
INDIANA	White pigmented and Wax Resin	1 gallon/ 150ft^2	N/A
KANSAS	Type-2 Liquid membrane-forming compounds	1 gallon/ 150ft^2	ASTM C309
MICHIGAN	White Type 2, Type 1-D, class B	1 gallon per 144 ft^2 for non-grooved surfaces; 1-gallon per 225 ft^2 for grooved surface	ASTM C309
MINNESOTA	Type 1-D curing compound (PAMS and Linseed oil)	Application rate of 1 gallon per 200 ft^2	ASTM C309, <0.15kg/m^2 @ 24 hrs, <0.40 kg/m^2 @ 72 hrs.
MISSOURI	Types 1-D, Types 2A	1 gallon/ 200 ft^2	ASTM C309
NEW YORK	White pigmented	1 gallon per 150 ft^2	Materials Bureau testing: Drying,4hrs, Permeability,0.04g/cm2, Reflectivity>60%, Durability>7 days
OHIO	Wax based, water based and resin-based membrane curing compound. Type 1D and Type 2 for pavement.	Minimum Application rate 1 gallon/200 ft^2 for structural concrete and 1 gallon/ 150 ft^2 for concrete pavement.	ASTM C309, solids >25%, MnDOT moisture loss, reflectance>65%
OKLAHOMA	Impervious membrane (white pigmented CC)	Min. rate of 1 gal/200 ft^2 at 100F or at 1 gal/ 150 ft^2 for temperature higher than 100F	ASTM C 309
TEXAS	Types 2 membrane curing compound and Type 1-D	Not more than 1 gal/180 ft^2	ASTM C 309
WISCONSIN	PAMS-BASED (C309 Type 2 Class B), WAX-BASED WHITE-PIGMENTED (C309 Type 2 Class A)	1 gallon per 150 ft^2/gal, or two applications at 300ft^2/gal,	ASTM C 309, MnDOT moisture loss
WASHINGTON	Type 1 or 2; Class A or B	Minimum application rate of 1 gallon/150 ft^2	ASTM C 309 and WSDOT T 814

Wisconsin Department of Transportation (WisDOT)

According to WisDOT Standard Specification 415/3/12, the goal of curing concrete is to maintain adequate moisture throughout the concrete mass to support hydration until the concrete develops sufficient strength to open it to service. MFCC should be applied right after finishing and as soon as the bleed water disappears. A uniform coating of curing compounds should be sprayed on concrete. Sufficient agitation should be provided while spraying the curing compound to ensure uniform consistency and dispersion of pigment within the curing compound during application. WisDOT accepts two types of curing compounds Poly-alpha-methyl styrene (PAMS) and water-based wax. PAMS have excellent water retention and can be used for concrete pavement on rural highways and expressways and high-performance concrete (HPC) in urban areas and are preferred. Wax curing compounds provide adequate water retention for miscellaneous items.

The specified application rate is one gallon per 150 square feet for the higher surface area tined surfaces and one gallon per 200 square feet for other surface finishes. WisDOT has adopted the more stringent evaporation requirements of 0.15 kg/m2 at 24 hours and 0.40 kg/m2 at 72 hours with reflectance greater than 65% and volatile organic compounds (VOCs) less than 350g/L. Additionally, curing compounds should be applied using an engineer-approved self-propelled mechanical power sprayer or hand-operated spraying equipment on irregular, narrow, or variable width sections; for re-coating applications or some specials applications approved by the engineer.

The compressive strength required by WisDOT is 3000 psi of the concrete before its opening to traffic unless otherwise approved by the engineer. Thermal stress must be avoided until newly laid concrete has established sufficient tensile strength to resist thermal cracking. Even in warm weather, covering should be considered when dusk or coming storms may result in quickly lowering temperatures that could cause surface damage.

CURING COMPOUND APPLICATION EVALUATION METHODS

The effectiveness of a curing compound depends on the surface condition of the concrete. The concrete curing method effectiveness is impacted by the type of material utilized, the construction process, and the intended use of the hardened concrete (Amit et al., 2019). Moreover, the ambient condition such as wind velocity, relative humidity, atmospheric temperature, water to cement ratio of the mix, and types of cement used in the combination can affect the concrete pavement curing quality. The following section contains a summary of currently utilized and potential tests to assess the effectiveness of the curing process.

Visual evaluation

Visual inspection of concrete is one of the most useful non-destructive techniques and methods used to evaluate a concrete structure (ACI, 2008), however possess little quantifiable data to make actional decisions on curing effectiveness. Inspection should be conducted by someone who has a good understanding and knowledge of concrete to document areas with too much or too little MFCC to help relate the visual assessment to future durability and performance (ACI, 2008). Visual inspection of curing compound application is essential as it can detect if the curing compound was uniformly applied or if there is any defect. However, the effectiveness of the visual evaluation depends on the knowledge and experience of the investigator. The limitation faced when dealing with visual evaluation or inspection is that internal detects are not noticed and human assessment does not have the nuance to determine slight differences between application rate, including between 150sf/gal and 200 sf/gal. Moreover, no

quantitative information about the properties of the concrete is obtained. Therefore, associating the visual evaluation with other non-destructive techniques could be the best option to maximize all the information.

Reflectance

Reflectance is commonly used in the paint industry to measure the degree of whiteness (ASTM E 1347) and for performance of pavement markings for nighttime headlight performance (ASTM, 2020b). Reflectance is the ratio of incident light intensity on a sample surface to reflected intensity from the surface (Figure A.5). As a quantifiable methodology, reflectance may be a useful comparison of application rate if reflectance is proportional to the application rate of the curing compound. TxDOT investigated the curing effectiveness using reflectivity and showed good correlation of application rate under both laboratory and field conditions (Choi and Won, 2008). Reflectance was calculated using Equation A.1.

$$R=I_L/I_R \quad \text{(A.1)}$$

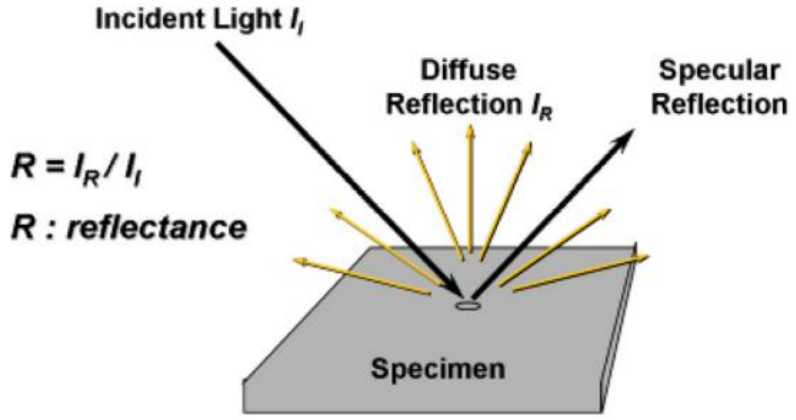

Figure A.5: Illustration on how reflectance data can be collected (Choi and Won, 2008)

In the TxDOT study by Choi and Won (2008) field testing was performed one day after application. Reflectance showed a good agreement with visual estimation and higher application rates produced higher reflectance (Figure A.6).

Figure A.6: On Field Reflection test (Choi and Won, 2008)

Image analysis

Image analysis further extends potential visual assessment techniques. Camera-based image analysis is a non-destructive technology used to study micro-crack propagation in asphalt concrete and concrete (Choi and Shah, 1997; Chen et al., 2011). Digital Image Correlation (DIC) compares images of damaged specimens with that of an initial or undamaged specimen (Hansen et al., 2021). The equipment used for the digital image correlation test is a digital camera with appropriate lighting combined with Artificial Intelligence to assess defects. DIC analysis essentially involves measuring the grayscale level at each pixel location, thus creating a map within the area of interest. Each spot on this map is compared with the initial, undeformed image, and the movement of each pixel in the horizontal and vertical directions is determined, from which displacements and strains are calculated using advanced mathematical techniques (Choi and Shah, 1997). Chen et al. (2011) used a novel combination of standard multi-light source photography and texture-based feature extraction in conjunction with neutral network analysis to identify and classify the extent of concrete cracks (Figure A.7). The results of this study show that digital image processing and data-driven feature extraction methods can be used to distinguish between good quality and damaged concrete surfaces. The advantages of using DIC techniques are it is non-destructive technology and a non-contact system. When already trained on previous data sets, assessment of infrastructure performance is rapid.


Figure A.7: Camera set-up for digital image correlation (Chen et al. 2011)

Rate and application time.
In addition to visual inspection, quantification of application rate and timing is relatively low cost and can be a useful tool assuming uniform application of curing materials. Different equipment, such as a hand-held sprayers, vehicle-mounted sprayers, and curing carts (Figure A.8) can all be utilized during a single construction project and need to be individually-assessed. All can be effectively assessed if functioning correctly and appropriate time, area, and volume data is recorded which can be a challenge during construction.

Figure A.8: Curing compound spraying cart (Meadows, 2020)

MFCC should be applied homogeneously for best performance. Uniform applications provide a solid, white opaque coverage on all exposed concrete surfaces compared to a white sheet of typing paper. The uniformity of the curing compound is obtained when the equipment to be used for the specific work functions correctly. Nozzle, nozzle spacing, boom height, nozzle orientation, and spraying machine speed should be cleaned and fixed before the operation. Additionally, the curing cart speed, theoretically, can be adjusted or measured once a nozzle has been chosen. Equation A.2 shows how the cart speed could be adjusted if the sprayer parameters are known (Vandenbossche, 1999).

$$v=(Coeff.*F)/(C*W) \quad (A.2)$$

Where: V = Cart speed, (km/hr); Coeff. = 6 when using SI unit (0.13636); F= Flow rate (litters per minutes per nozzle or gallons per minutes per nozzle); C= desired coverage, liters per square meter (gallons per square foot) ; W= Nozzle spacing, cm (inches)

A study performed by (Helgeson, 2014) examined the effect of curing compound application time after concrete finishing. Different times (30 minutes, 2 hours, and 4 hours) were considered, and repeatability was evaluated. According to the findings, scaling differed depending on the mix type and curing ingredient type and none of the MFCC had the same level of scaling resistance as wet curing. The efficiency of most MFCCs depended on the concrete surface condition and the presence of bleed water varied by mix type. When bleed water was present when curing was applied, scaling increased. Within the study parameters, PAMS were the least sensitive to application time and coverage rate, wax-based, linseed oil, and acrylic curing compounds were sensitive to timing and coverage rate.

CalTrans utilizes CT535 Method of Test for the Application Rate of Concrete Curing Compound in the Field which is unique nationally (CalTrans, 2014). The test method utilizes an absorbent pad placed on the concrete surface prior to curing (Figure A.9). Pads are weighed before and after curing and application rate determined by mass gained. Five pads are placed at random intervals 6 to 12 feet apart over a 50 ft section. The placement location is not fixed other than instructing as far from the edge without stepping on the fresh concrete. While this test method is relatively straightforward and simple for testing near the edge of concrete, it becomes more logistically challenging if variability across the width of the pavement is desired.

Figure A.9: CT535 Absorbent Pad Placement (CalTrans 2014).

Moisture retention

The moisture retention test is among the standard test described by ASTM C156 (ASTM, 2020a) and commonly used to approve curing materials. Each specimen must be placed in a test chamber which keeps a specific temperature (73°C), relative humidity (50%), and evaporation rate (2.0-3.4 g/hr). The mass loss is determined after 72 h and total evaporation less than 0.55kg/m2 at 72 hrs is acceptable. Since early-age moisture loss is most correlated to drying shrinkage cracking, MnDOT set more stringent requirements of <0.15 kg/m2 in 24 hrs and <0.40 kg/m2 in 72 hrs. Since moisture retention is performed on mortar and not paving concrete, reducing the moisture loss requirement is important and if translated to paving concrete which contains significantly less moisture than mortar, a loss of 0.33kg/m2 would be equivalent if ASTM C156 testing is performed on actual concrete.

Even when performed on the small samples used in ASTM C156, visual differences in application can be observed as shown in Figure A.10. Sun (2013) stated the moisture retention test is straightforward, but the precision is not reliable. A high level of variability of standard deviation between laboratories makes it difficult to confirm whether a curing compound has met the standard or not. Several factors, such as the precision of controlled temperatures, wind speed, time of application, and rate of application of curing compounds, contribute to the poor accuracy between laboratories (Poole et al., 2006). Moreover, moisture retention is limited to fixed ambient conditions and a single application rate of curing compounds under a laboratory environment, making it difficult to set standards for all field tests as the field environment is exposed to various conditions. Nevertheless, the inapplicability of the moisture retention test under a field environment prevents its direct application as a quality assurance tool.


Figure A.10: Intersample variability of ASTM C156 (Kevern, 2010)

Related to moisture retention is moisture content. Wang et al. (2006) evaluated the moisture content across a series of lab specimens cured under over, air, or wet curing conditions. The oven and air conditions had lower moisture contents than the wet-cured specimens at the early ages of 1 and 3 days evaluated.

Relative humidity test

Further extending the consideration of moisture retention to a test more conducive to field construction is a consideration of relative humidity test to determine the effectiveness of MFCC. Higher rates of evaporation indicate more significant moisture variations within the concrete immediately below the surface (Grasley et al., 2006b). Since MFCC evaporation, relative humidity below the surface should be maintained and a potential indicator for curing operation and curing effectiveness.

A relative humidity test can be used in the laboratory or field through capacitive sensors embedded in the concrete. Relative humidity sensors measure changes in the capacitance of a thin hygroscopic polymer film as it absorbs moisture (Grasley et al., 2006a). Relative humidity values are estimated from the calibrated reference curve developed in a controlled humidity chamber with a chilled mirror hygrometer. Typical concrete relative humidity probes are used to assess the dryness of concrete prior to application of moisture-sensitive flooring materials. Unfortunately the operational range and depth precision of the available low-cost probes are not suitable for determining nuanced very high relative humidity changes near the surface of fresh concrete. The technology on the internal RH of early age concrete is still in progress, with various humidity types and field investigation needs to rely on the more conventional chilled mirror installation.

Degree of Hydration, Sorption, and Electrical Properties

Since the retention of moisture is desired to ultimately increase the amount of hydrated cement and pore refinement, measurement of each may prove important to actual properties of concern in the field. A 2006 study by Wang et al. evaluated all three measures were evaluated on concrete cured under a range of conditions and single and double applications of Type 2 Class A MFCCs. The degree of hydration was increased at the surface when single and double applications of curing were applied. For the lower efficiency (<90%) curing compound, two applications were needed, while the higher efficiency compounds (<95%) no difference was observed between single and double coats with respect to degree of hydration. Surface water sorptivity was highly influence by curing condition for the uncoated specimens, however no difference was observed when the curing compounds were present. When the curing compounds were removed via light abrasion, slight differences in water absorbed were observed. Under laboratory conditions, they did observe differences in electrical conductivity with the more favorable

curing conditions producing higher conductivity, which is most likely caused by the differences in moisture content. No significant differences were observed between single or double application of the various curing compounds or timing of application. Unfortunately, when these techniques, other than conductivity, were applied to concrete in the field, there was not sufficient precision to yield useful results. Although a single snapshot, conductivity did show differences between uncured and wet cured concrete and may be a candidate for further exploration.

Penetration resistance

The effectiveness of a curing compound is governed by the integrity of the formed membrane. Several factors can impact the integrity of the membrane, especially the quality of the curing compound material (Choi et al., 2012). The strength of concrete is correlated to curing effectiveness, and mainly near the surface exposed to environmental conditions.

Penetration resistance is one such test to determine surface strength and commonly performed using the Windsor probe (Figure A.11 and Figure A.12). An explosive charge is used to fire a steel probe into the concrete. The compressive strength is correlated to the penetrated or exposed length of the probe where deeper penetration equates to weaker concrete (ACI 228, 2003).

Figure A.11: Windsor probe, equipment used during penetration resistance test (Choi and Won, 2008)

Texas Department of Transportation (TxDOT) investigated the Windsor probe across five different curing conditions on the surface of pavement at construction (Choi and Won, 2008). The application rate of the curing compound was controlled by placing a plastic sheet when the paver passed the testing section. A white pigmented wax was used in the test and applied at one coat, two coats, and three coats at 180 feet square per gallon. Based on the results penetration depth did not provide a good correlation with the curing methods. The lack of signal in the data and minor surface damage suggests that penetration may not be suitable for assessment of curing and more study would be needed before further field implementation (Vandenbossche, 1999).

Figure A.12: Concrete pavement after penetration testing (Choi and Won, 2008)

Ground Penetration Radar

Ground-penetrating radar (GPR) is used to assess differences in structure profiles as determined by the response of a transmitted radar frequency to assess the dielectric constant (DC) arrival time and amplitude (Maierhofer, 2003). GPR is suitable for ice, soil, and pavement structures where the reflected pulses, display the DC and thicknesses of the layers within the pavement (Joshaghani and Zollinger, 2021). Since radar attenuates on liquid water, the DC is highly correlated with the moisture content contained in soil or concrete. If the water evaporates from the concrete surface, this will cause the DC values to decrease accordingly. By assessing the relationship between DC and water content over time, evaporation rate under laboratory and field conditions can be determined (Joshaghani and Zollinger, 2017; Joshaghani, 2019). Therefore, DC measurements could be an excellent technique to determine the moisture retention capability of various curing methods (Figure A.13). A correlation was reported between the dielectric constant and the efficiency of a given curing compound with the moisture retention capability based on a laboratory study performed by Zollinger and Sun (2015).

Figure A.13: GPR equipment used for dielectric constant measurement (Joshaghani and Zollinger, 2021)

The advantages of using GPR are, it is safe for use in public spaces and many project sites, can detect metal and non-metal objects and voids, and underground irregularities, and is highly sensitive to moisture. GPR can be used evaluate the effectiveness of a curing compound application by determining the dielectric constant and associated with the free moisture content and the degree of hydration of concrete. When using GPR for concrete and especially curing effectiveness, a signal reflected from a metal plate used as reference (Joshaghani and Zollinger, 2017). The dielectric constant values can be determined using equation A.3:

$$\varepsilon_{r,1} = \left(\frac{1 + \left(\frac{A_0}{A_p}\right)}{1 - \left(\frac{A_0}{A_p}\right)} \right)^2 \quad \text{(A.3)}$$

Where: Ɛ_(r,1): is Dielectric constant of the first layer, A_o is amplitude of surface reflection and A_p is the amplitude of the GPR wave, which can be obtained by calibration with a metal plate.

EVALUATION INDEX

The evaluation index (EI) is a comprehensive evaluation technique with combines observed relative humidity and evaporation with laboratory evaporation behavior and GPR assessment to provide a complete understanding of curing effectiveness (Sun and Zollinger, 2015). EI determines curing effectiveness by compares relative humidity and evaporation of ambient conditions from the construction environment, sealed conditions from the portion of the concrete not impacted by curing, and filtered conditions in the cure-affected zone. On-site evaporation can be measured directly or estimated using American Concrete Institute (ACI) 308 shown in Figure A.14 or calculated using Equation A.4.

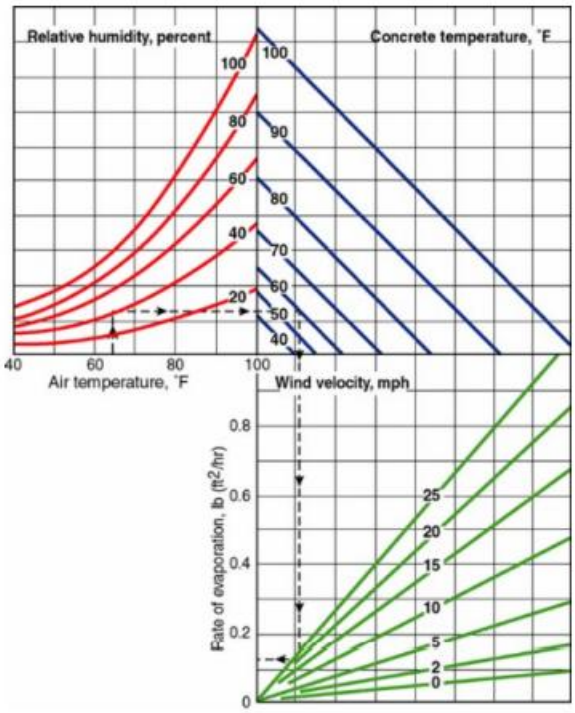

Figure A.14: Nomograph for estimating the maximum potential rate of evaporation (ACI, 2016)
Potential evaporation can be calculated using the Equation A.4.

$$\boldsymbol{PE} = \boldsymbol{70^{2.5} - \left(\frac{RH}{100} * T^{2.5}\right) * (1 + 0.4 * 4) * 0.00001} \quad \text{(A.4)}$$

Where: PE: the potential evaporation rate, RH: the ambient relative humidity (%), T is Temperature (F) and W: The wind velocity (mph).

EI and RH are used in conjunction with predetermined reference curves developed under laboratory testing conditions to determine the appropriate rate of application of a given curing combination under given conditions (Figure A.15). EI can be determined using Equation A.5.

EI=(t_f-t_a)/(t_s-t_a) (A.5)

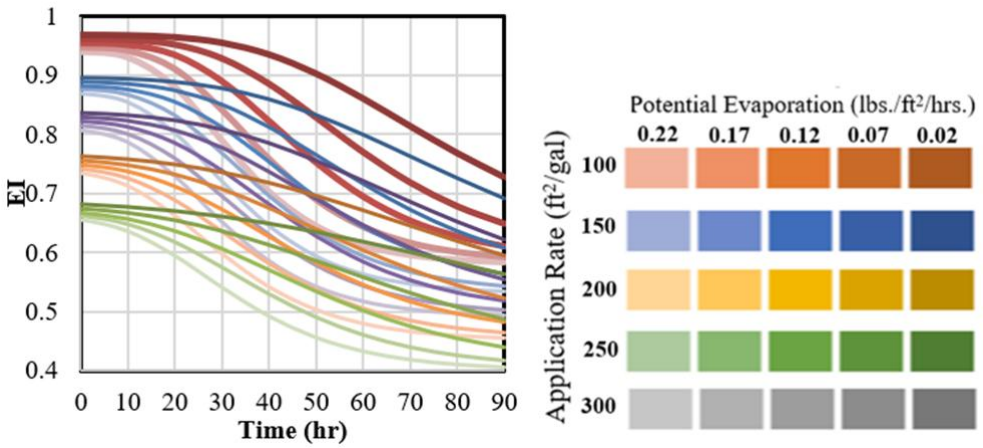

Figure A.15: Influence on EI of Evaporation Rate and Application Rate over Time

Combining the ground-truth weather station results with predicted or measured ambient conditions allows assessment of the evaporation rate in the cure-affected zone and prediction of future increases in application rate to control unwanted drying (Figure A.16). EI can pair with GPR to determined if the desired application rate has been achieved.

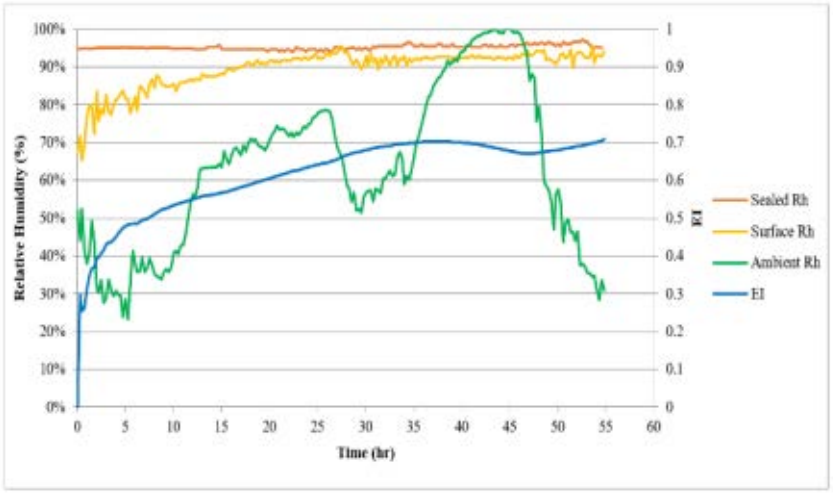

Figure A.16: Example of relative humidity and evaluation index

Ultrasonic pulse velocity

Another common non-destructive technique for assessing hardened concrete which may show promise for curing evaluation is Ultrasonic Pulse Velocity (UPS). When the velocity of a particular concrete specimen is known, the time between transmitting and receiving a reflected signal can be used to locate and voids, honeycomb, cracks, delamination, and other defects. UPV can be used to predict the strength of early age concrete based on measuring the velocity of compression stress waves (Kewalramani and Gupta, 2006) and has been used to determine setting time and strength relative to sawing operations (Taylor et al., 2016; Crovetti and Kevern, 2018). The rapid increase in UPV as concrete hardens may be utilized to assess quality of curing as early drying results in a more rapid increase whereas higher UPV after set (24 hrs) indicative of denser microstructure and better curing. More research is needed to evaluate if UPV is able to provide a useful signal for curing.

Capillary suction

The measurement of capillary suction is common in agricultural fields to assess available moisture for root uptake. As water evaporates the surface tension of the remaining film surrounding the soil particles attempts to pull the particles together. In the same fashion, the buildup of capillary pressure in the pore system of fresh concrete due to the loss of water causes drying shrinkage (Whittmann, 1976). While capillary pressure has been positively correlated to reduced plastic shrinkage cracking for internally-cured concrete (Vosoughi et al., 2017) near surface measurement on fresh concrete may be used to make decisions concerning the timing of concrete curing measures and to evaluate the effect of such measures (Slowik et al., 2014).

Summary of Curing Assessment Techniques

Overall, Table A4 presents a summary of the potential techniques to evaluation the effectiveness of curing compounds. Other details such as timing of assessment, cost, advantages, and drawbacks are also included.

Table A4: Summary of Evaluation Techniques

Technique	Timing after MFCC Application	Relative Cost	Advantages	Disadvantages
Visual	Immediate	Low	Requires no equipment	Difficult to quantify
Rate of application	Immediate	Low	Can provide semi-real time changes to curing application rate	Significant data collection and verification Cannot identify small areas
Moisture Retention	Early age	Low	Well-established methodology	High variability between labs Not a field test
Penetration resistance	Early age	Moderate	Correlated to strength	Semi-destructive
Reflectance	Immediate	Moderate	Quantifiable	Small area tested
Image analysis	Immediate	Low	Fast Low cost equipment	Covers small area Requires AI calibration
Relative humidity	Early age	Low	Direct measure of property of concern	Sensors currently not able to measure in appropriate range and depth
Ultrasonic pulse velocity	Early age	Low	Good indicator of strength	Unknown performance related to curing
Capillary suction	Early age	High	Early age indication of potential issues	Small area tested Unknown performance related to external curing
Ground penetration radar	Immediate	High	Direct assessment of moisture	Many passes required for full coverage
Evaluation index	Early age	Low	EI provides information needed to determine application rate.	It depends on the data provide by GPR or other technics.

6.2 Appendix B- Lab Testing Data

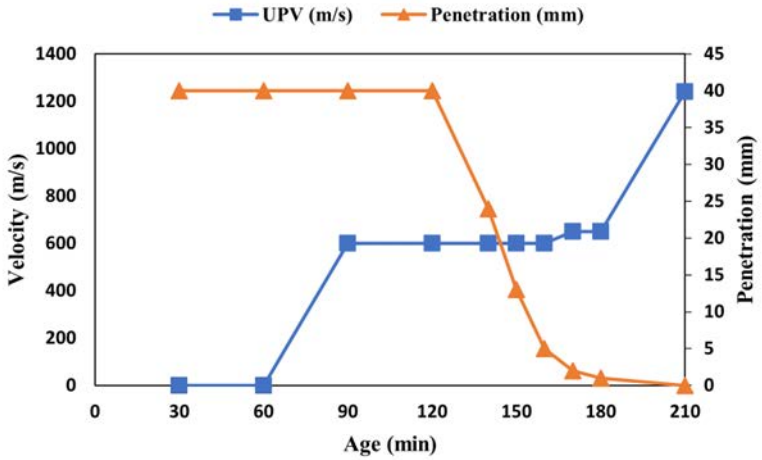

Figure B.1. Representative Setting Time Results for Lab Mixture

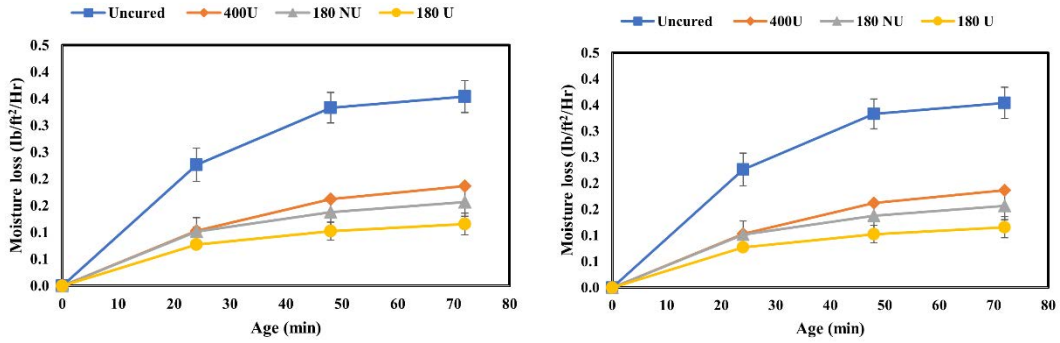

Figure B.2. Moisture retention results for 50F and 50 % RH (Left: Before setting; Right: After setting)

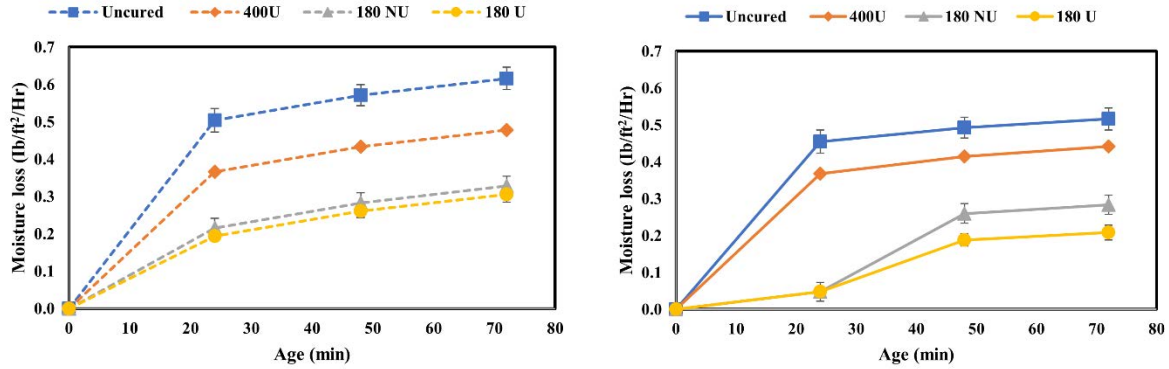

Figure B.3. Moisture retention results for 70F and 32 % RH (Left: Before setting; Right: After setting)

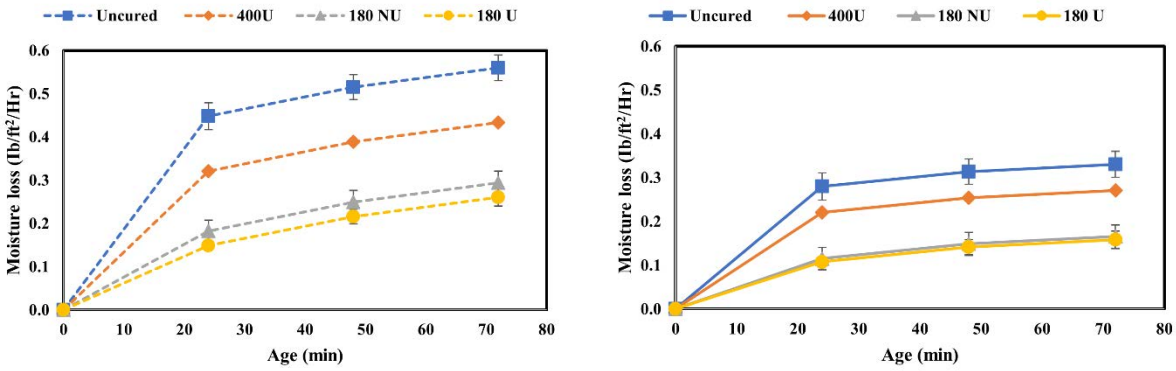

Figure B.4. Moisture retention results for 70F and 50 % RH (Left: Before setting; Right: After setting)

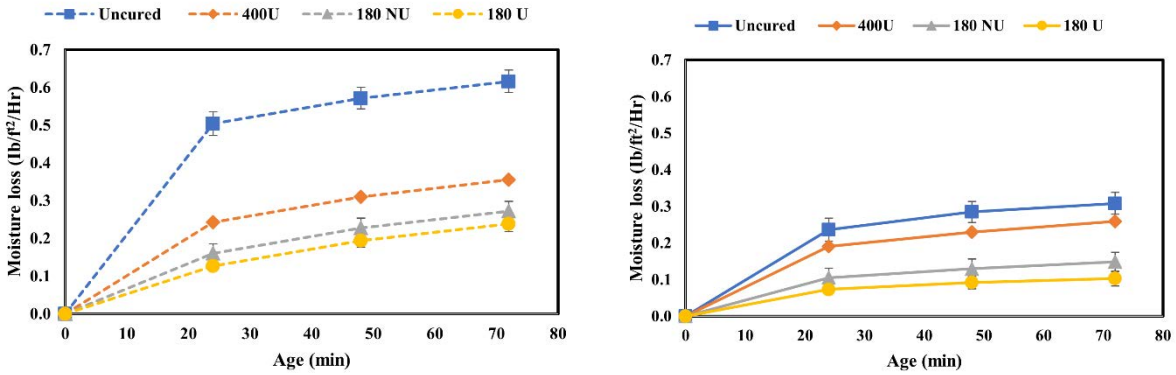

Figure B.5. Moisture retention results for 70F and 75 % RH (Left: Before setting; Right: After setting)

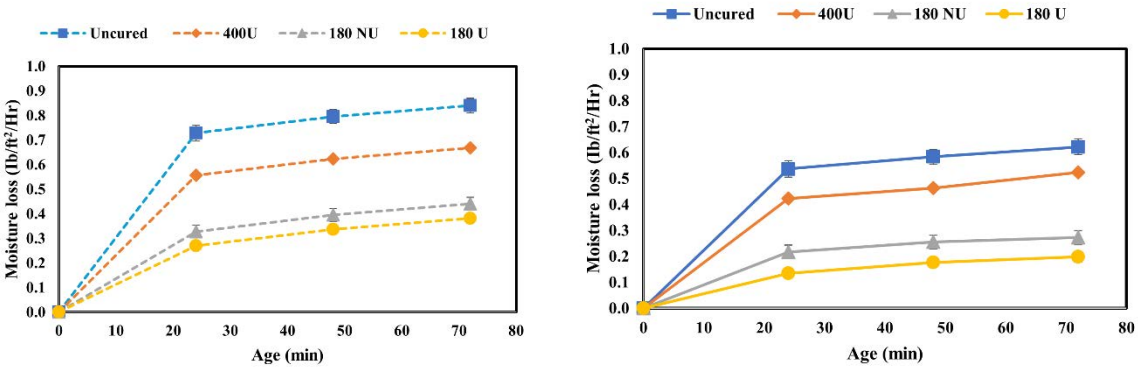

Figure B.6. Moisture retention results for 90F and 32 % RH (Left: Before setting; Right: After setting)

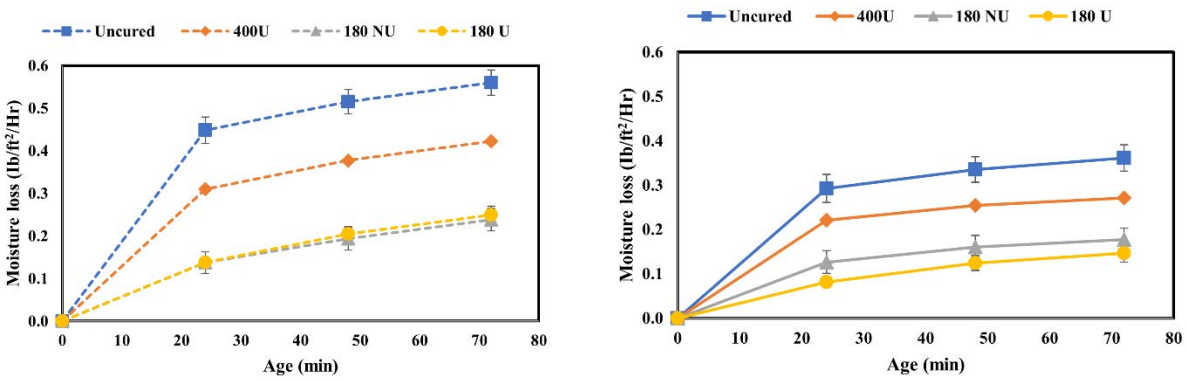

Figure B.7. Moisture retention results for 90F and 75 % RH (Left: Before setting; Right: After setting)

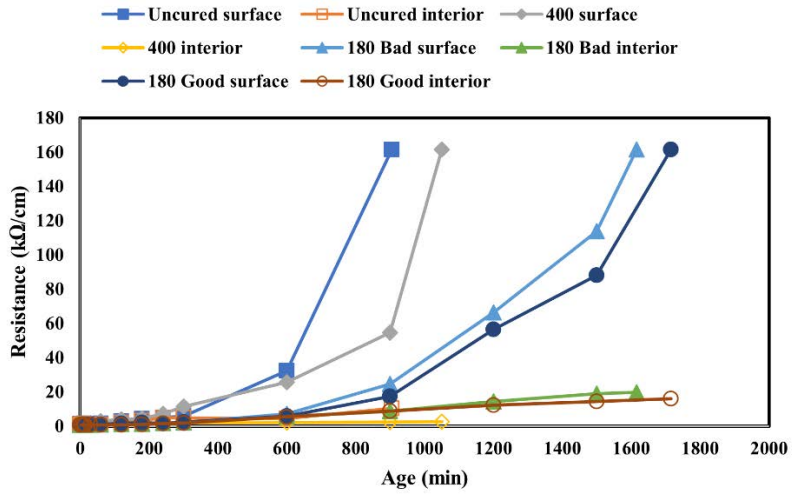

Figure B.8. Embedded resistance data evaporative condition 70F32%

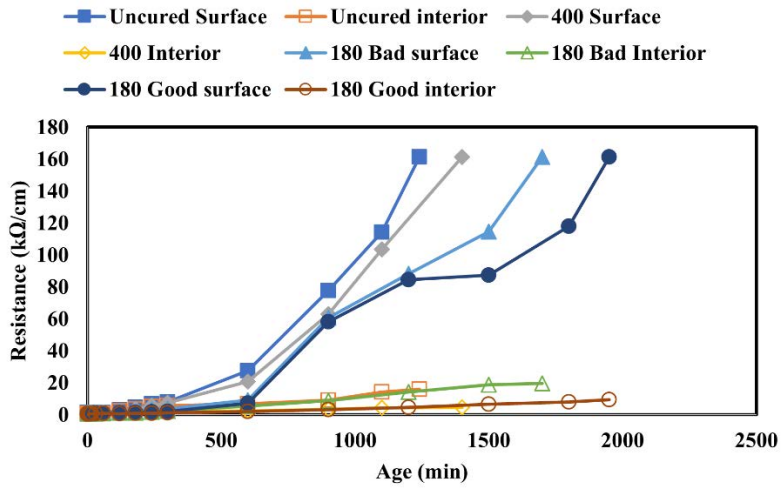

Figure B.9. Embedded resistance data evaporative condition 70F50%

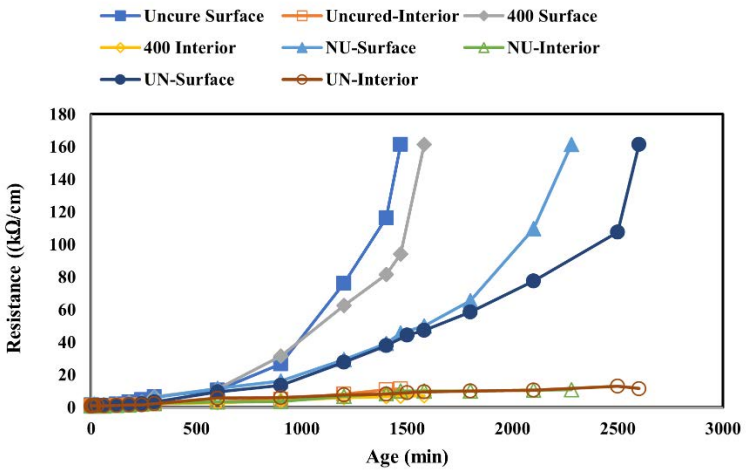

Figure B.10. Embedded resistance data evaporative condition 70F75%

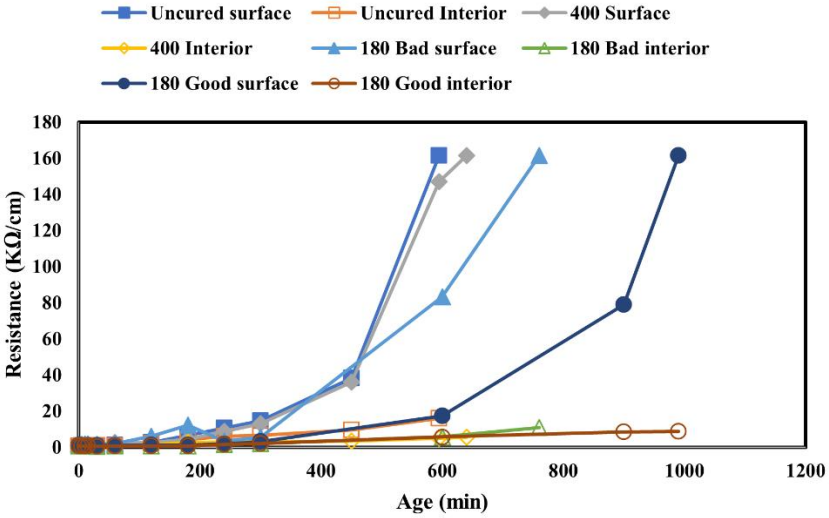

Figure B.11. Embedded resistance data evaporative condition 90F32%

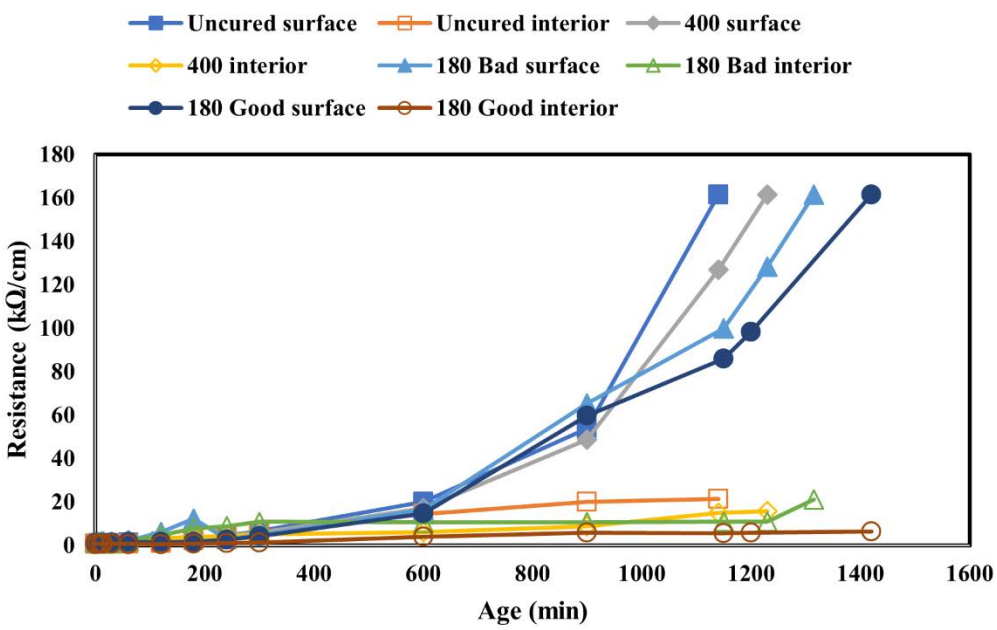

Figure B.12. Embedded resistance data evaporative condition 90F75%

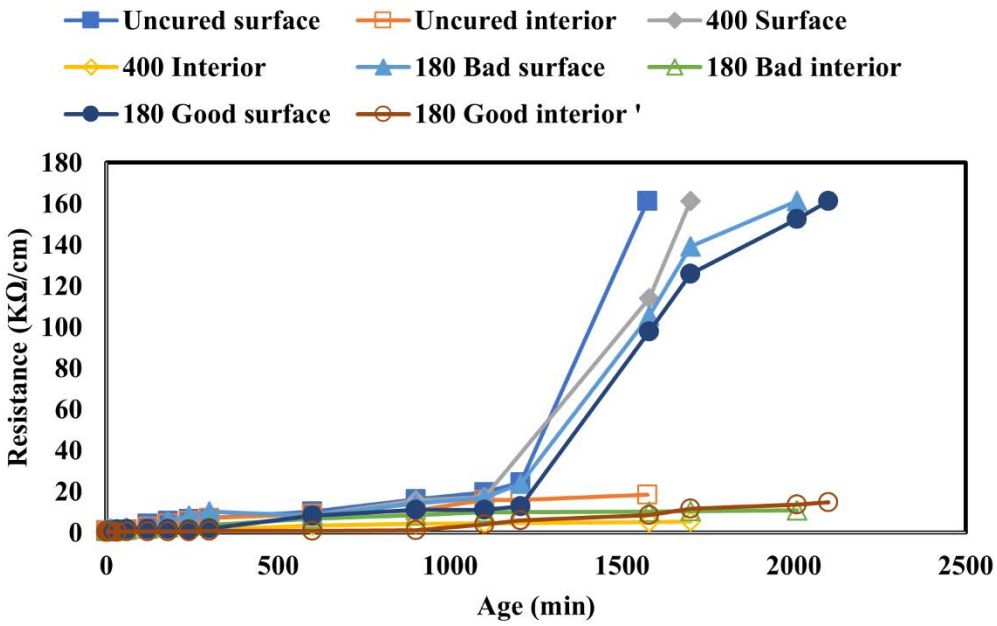

Figure B.13. Embedded resistance data evaporative condition 50F50%

6.3 Appendix C- Karsten Tube Field Testing Data

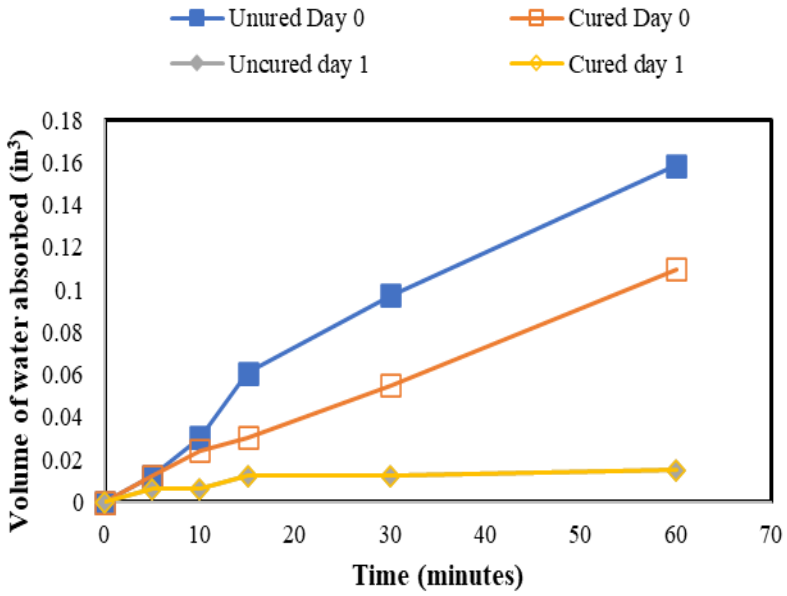

Figure C.1. I-43: Karsten tube results

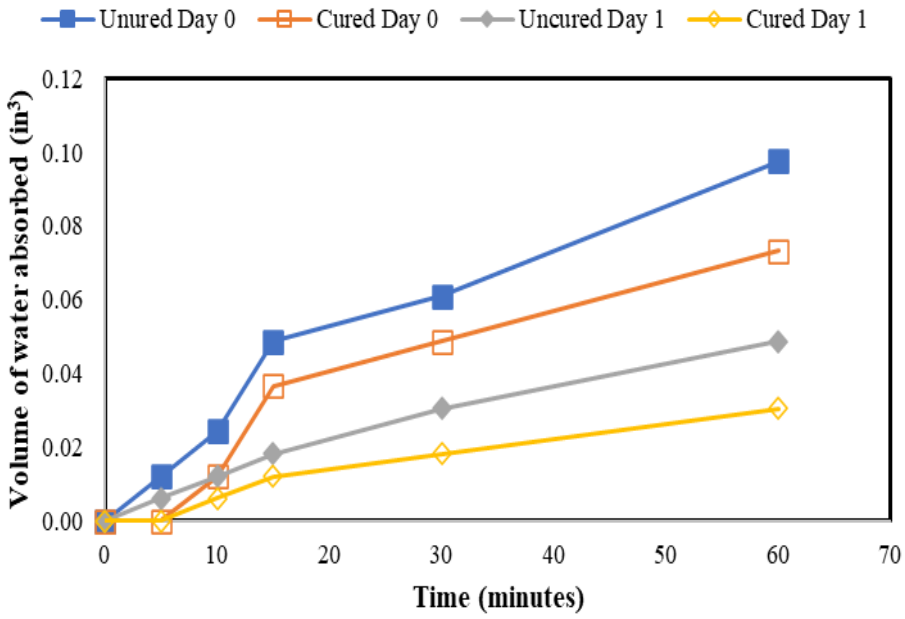

Figure C.2. STH 15: Section A Karsten tube results

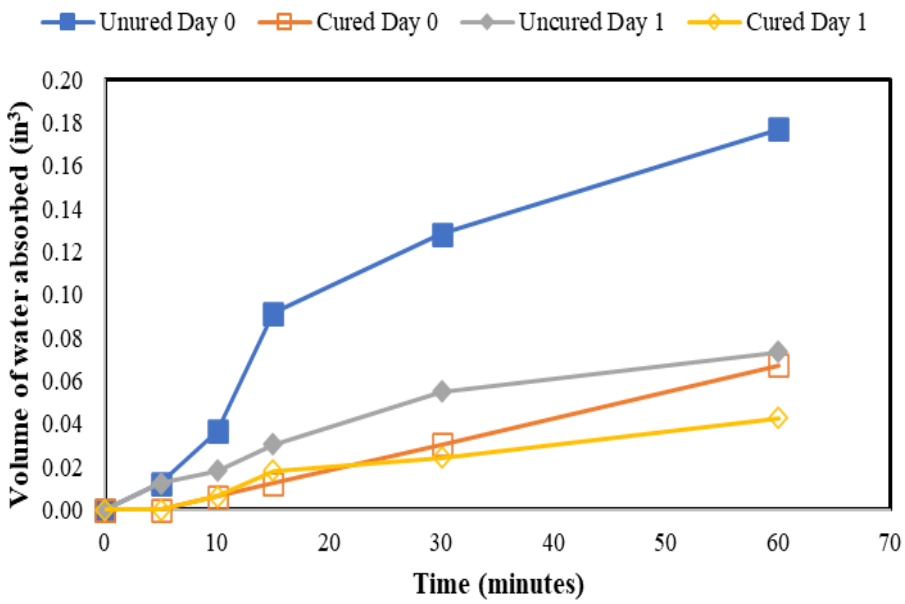

Figure C.3. STH 15: Section C Karsten tube results

6.4 Appendix D- Chilled Mirror Data

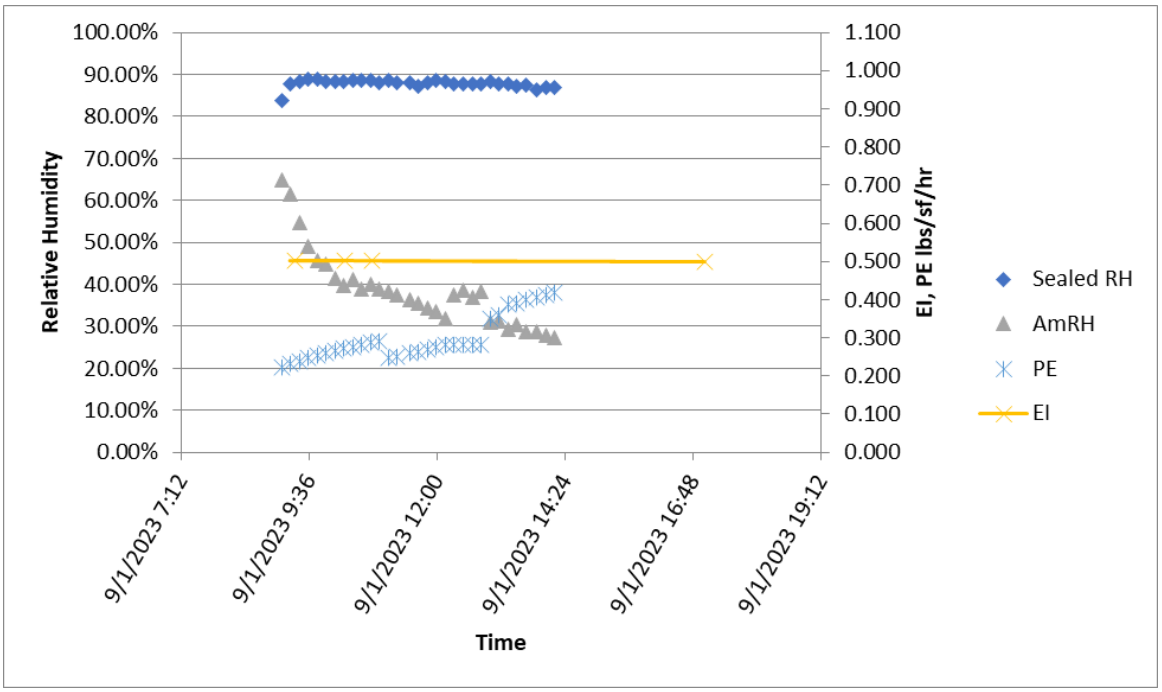

Figure D.1 STH 29 Section C – Morning, Aug 31, 2023; 2 hr Delay, AR=219 sf/g.

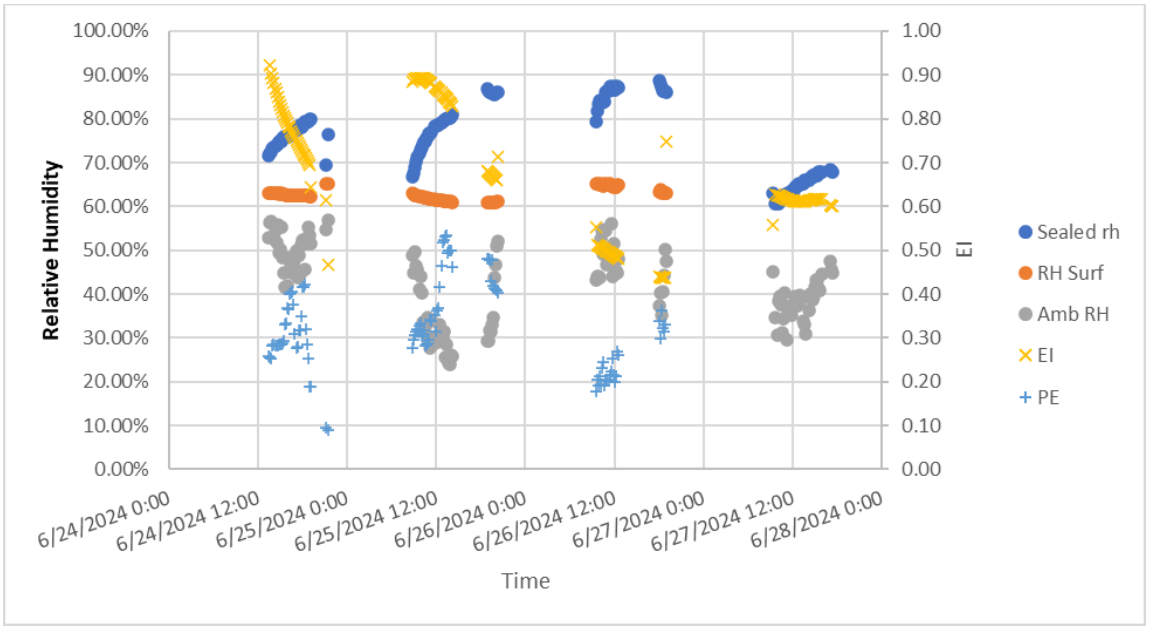

Figure D.2 STH 53 Sta 2934 – Morning, June 24, 2024; 1 hr Delay, AR=230 sf/g.

6.5 Appendix E – GPR Data

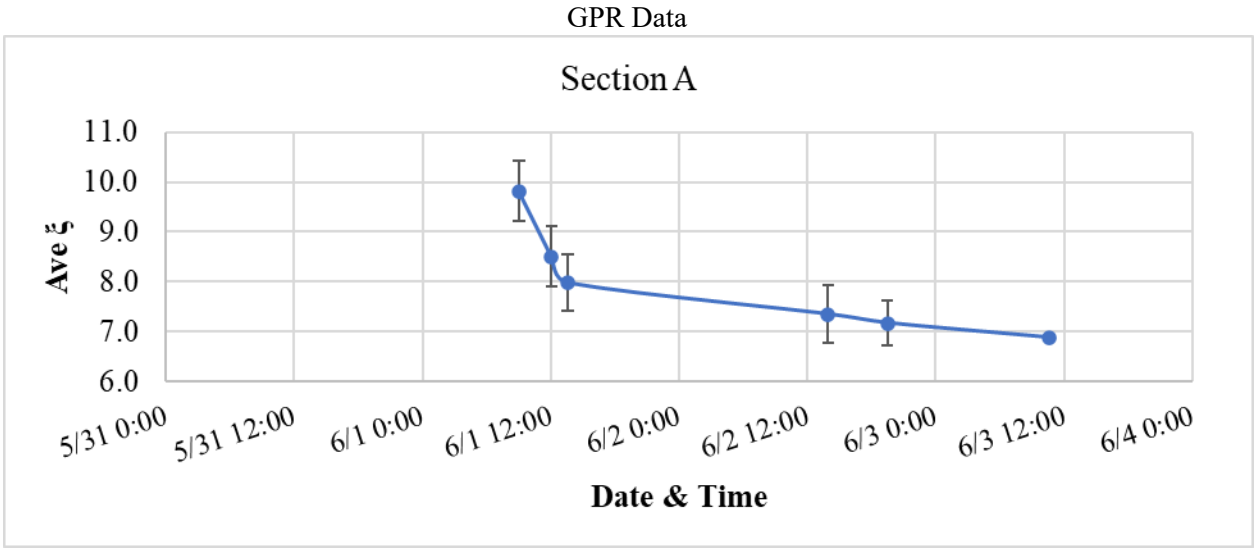

Figure E.1 STH 15 Section A – 2 hr Delay, AR=299 sf/g.

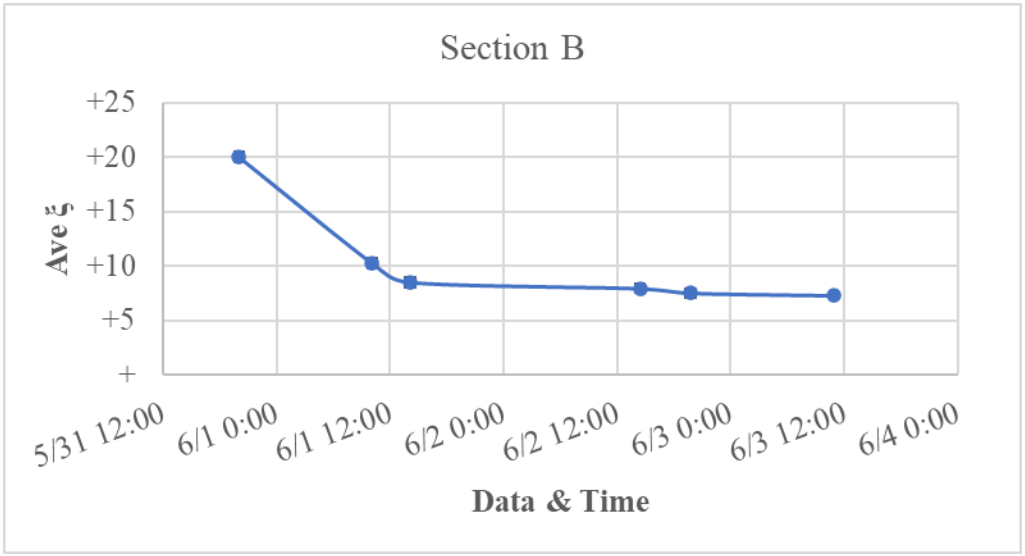

Figure F.2 STH 15 Section B – 2 hr Delay, AR=162 sf/g.

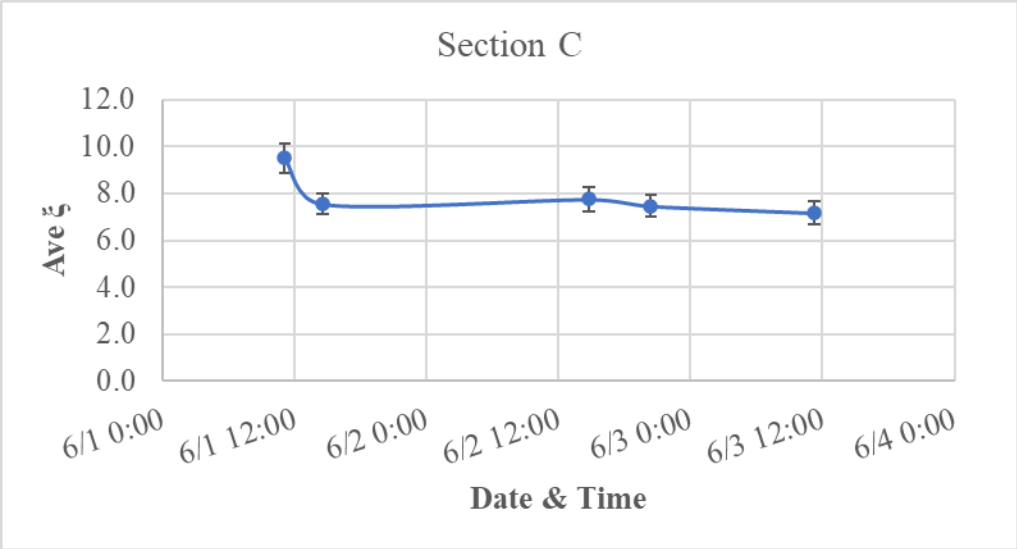

Figure E.3 STH 15 Section C – 2 hr Delay, AR=198 sf/g.

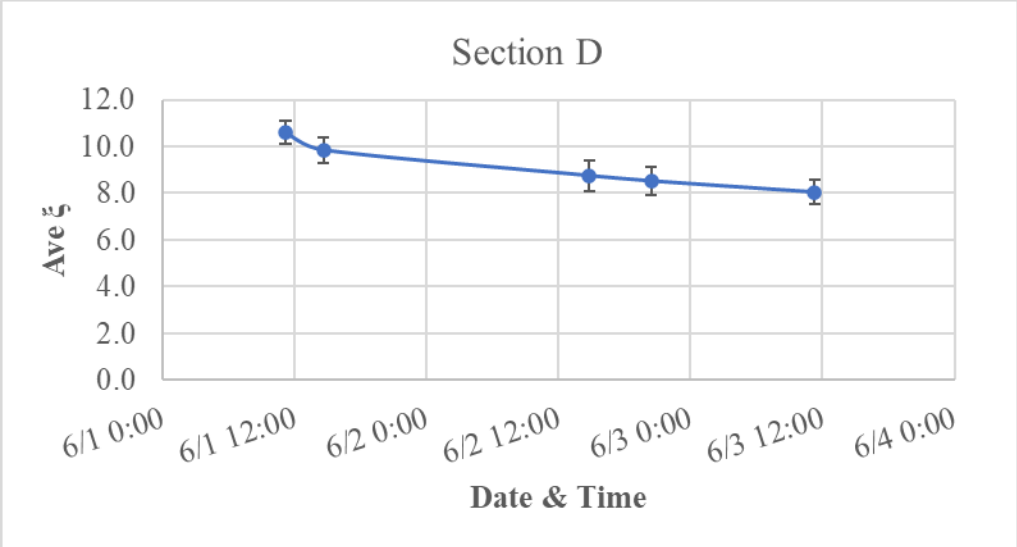

Figure E.4 STH 15 Section D – 2 hr Delay, AR=136 sf/g.

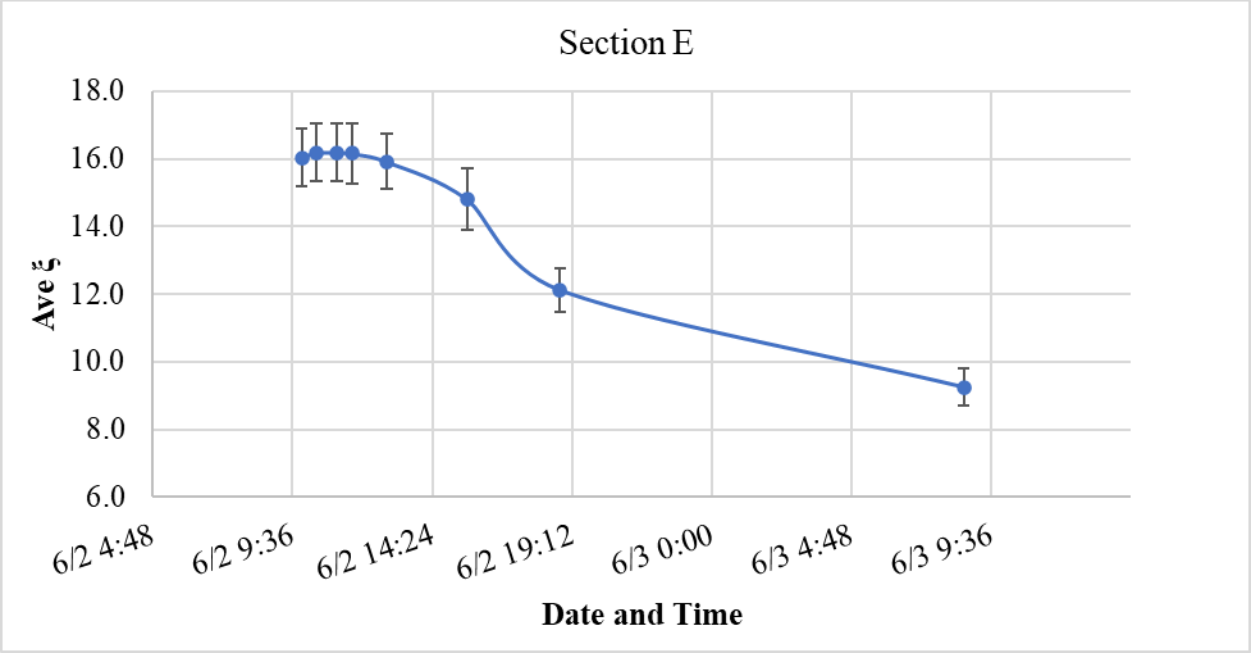

Figure E.5 STH 15 Section E – No Delay, AR=275 sf/g.

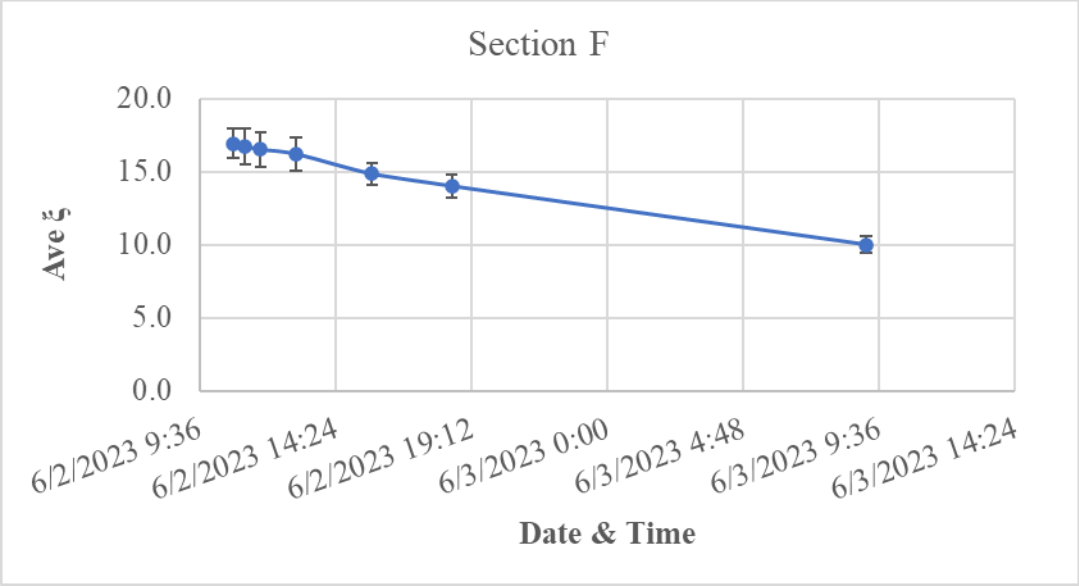

Figure E.6 STH 15 Section F – No Delay, AR=162 sf/g.

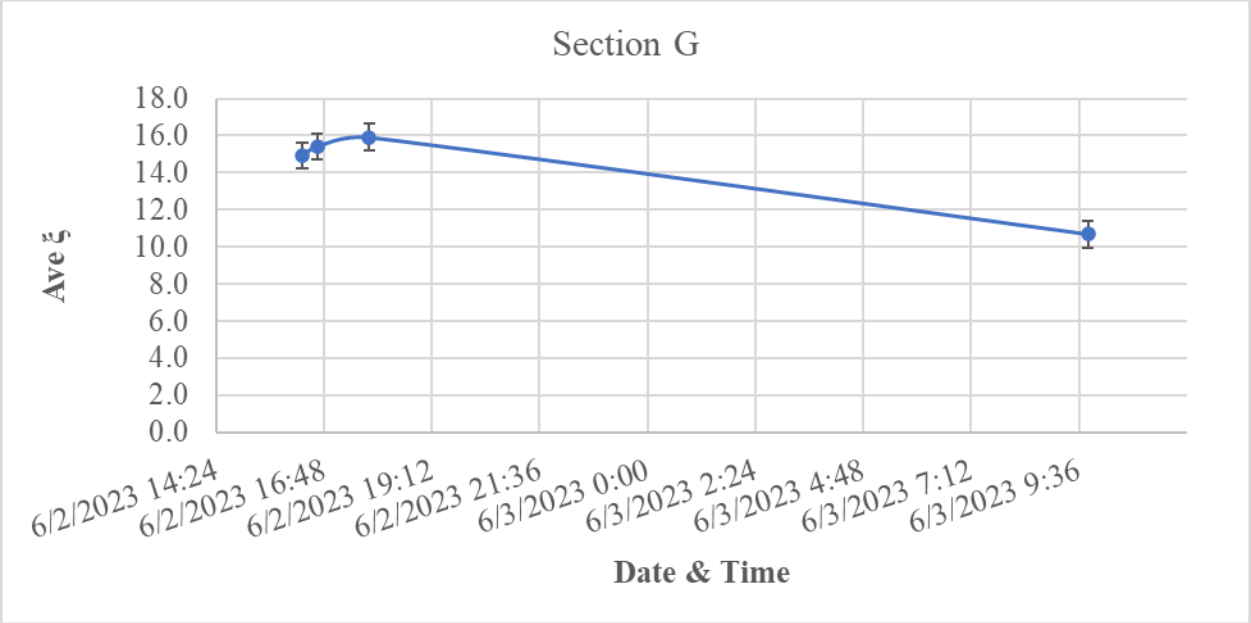

Figure E.7 STH 15 Section G – No Delay, AR=270 sf/g.

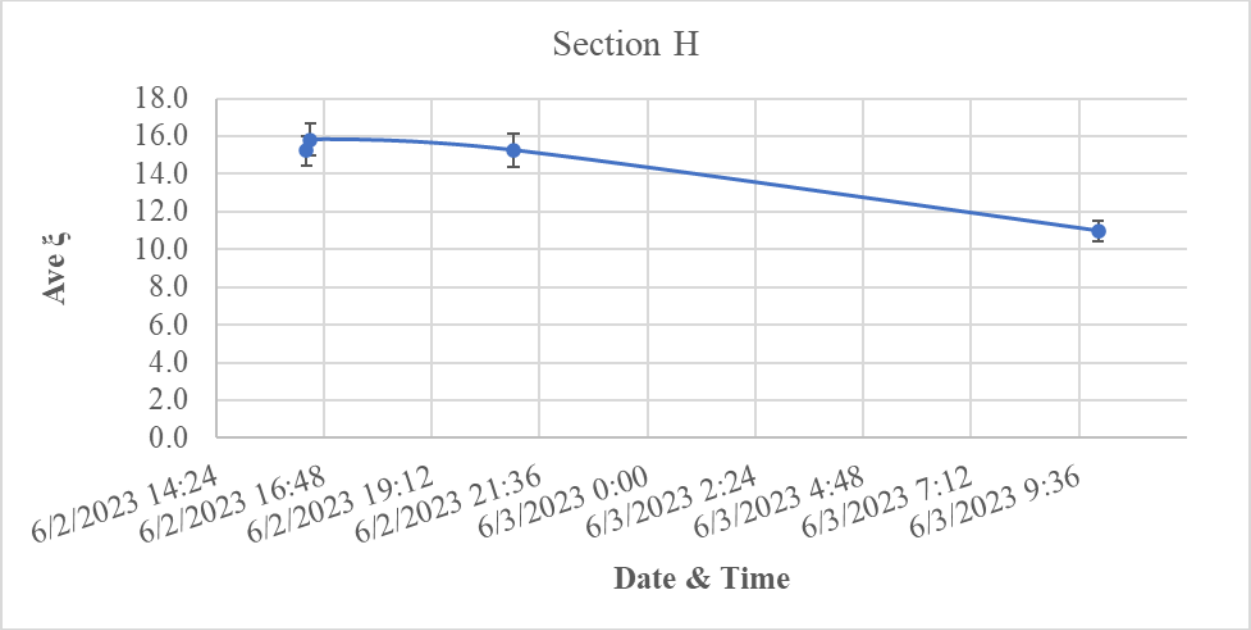

Figure E.8 STH 15 Section H – No Delay, AR=167 sf/g.

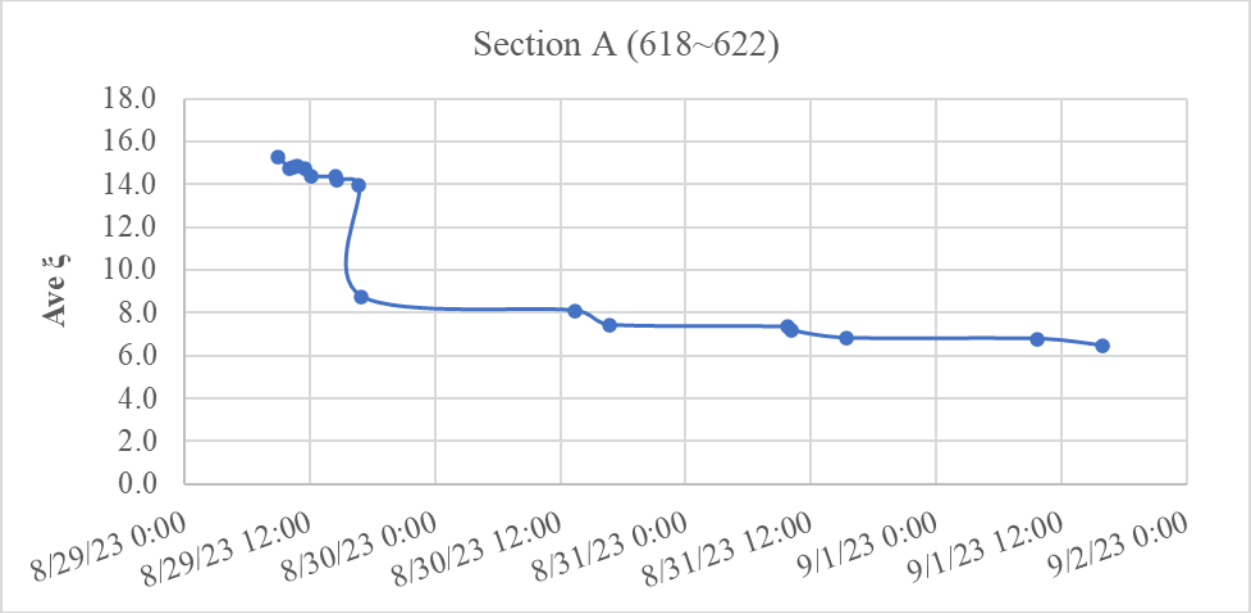

Figure E.9 STH 29 Section A – 2 hr Delay, AR=252 sf/g.

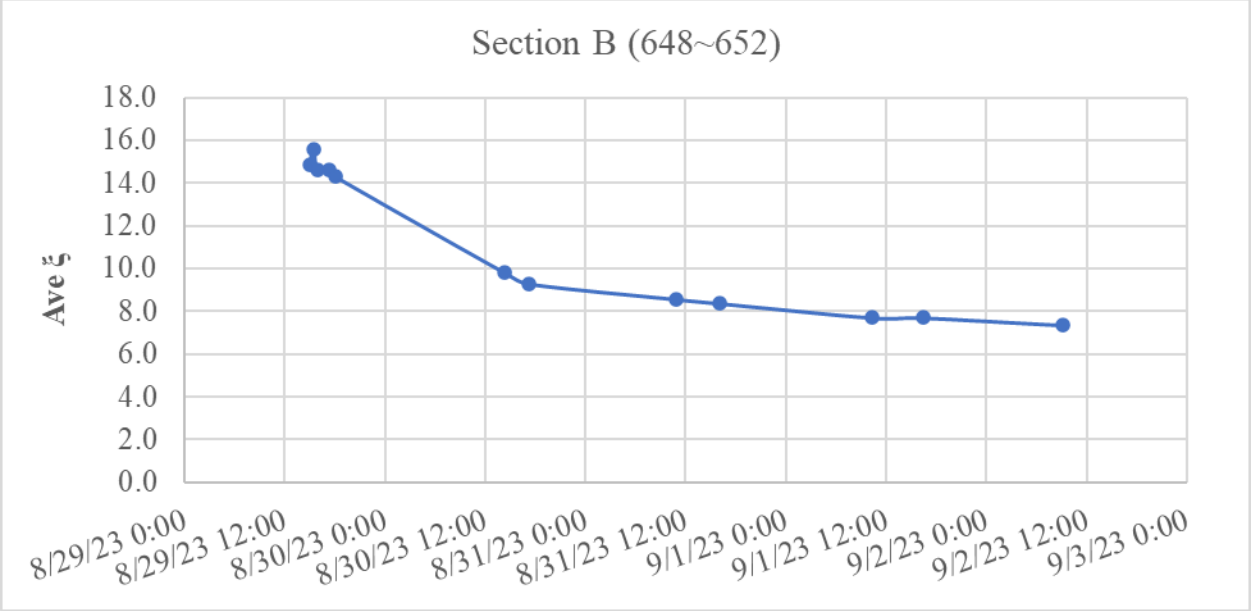

Figure E.10 STH 29 Section B – No Delay, AR=96 sf/g.

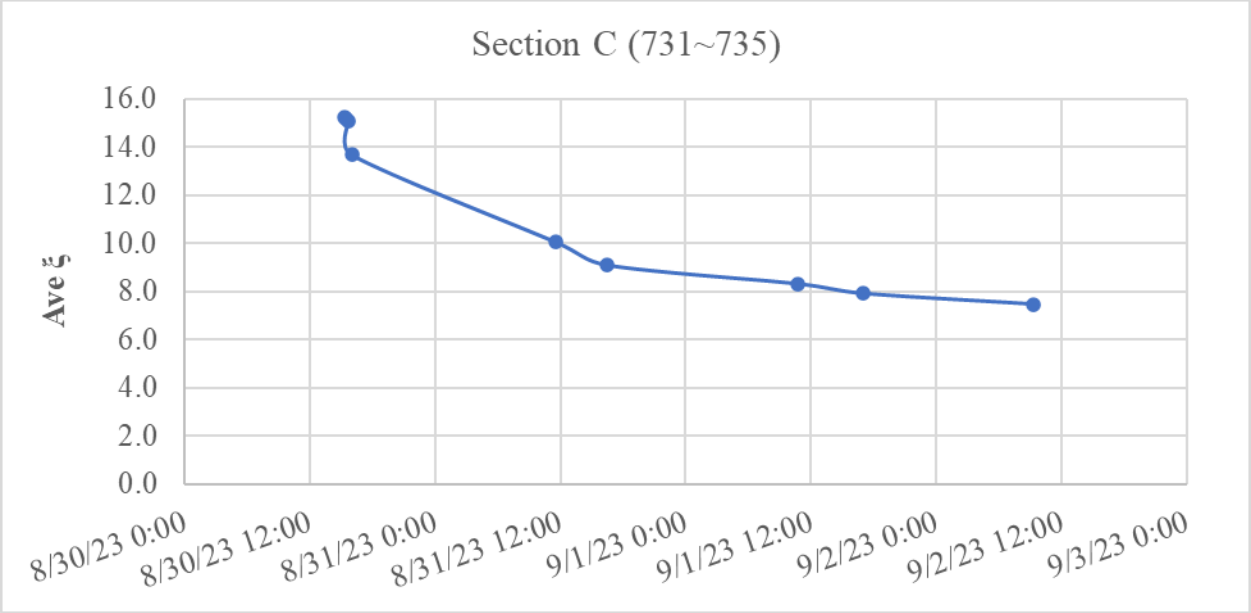

Figure E.11 STH 29 Section C – No Delay, AR=247 sf/g.

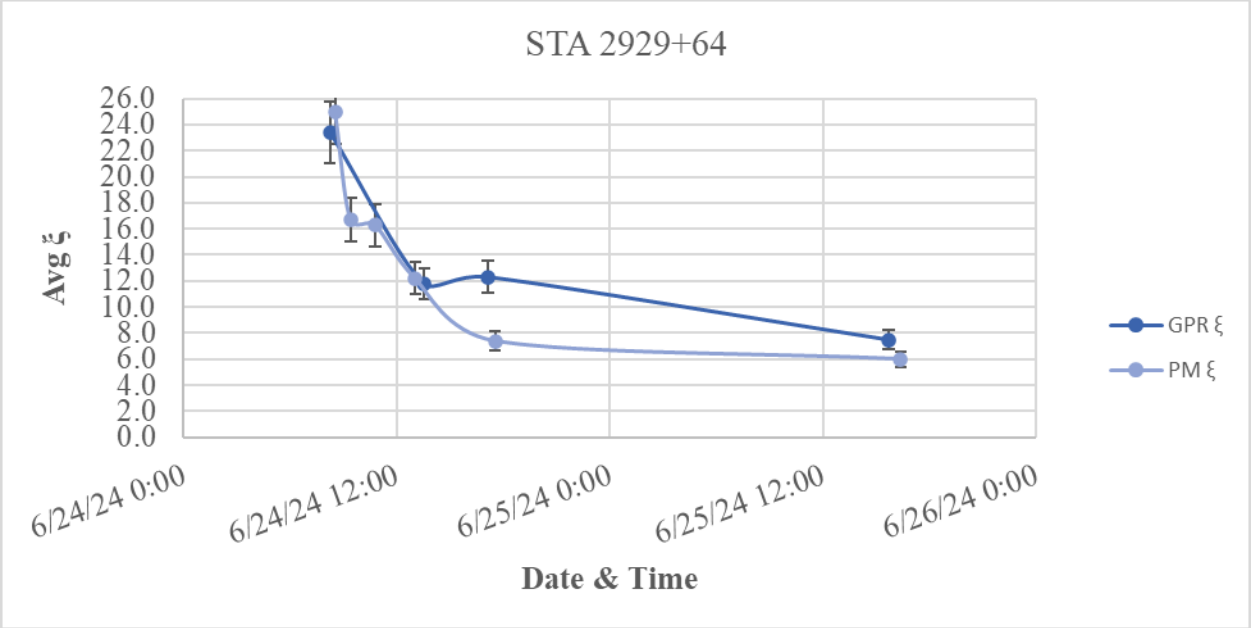

Figure E.12 STH 53 STA 2929+64 – 1 Hour Delay, AR = 150 sf/g.

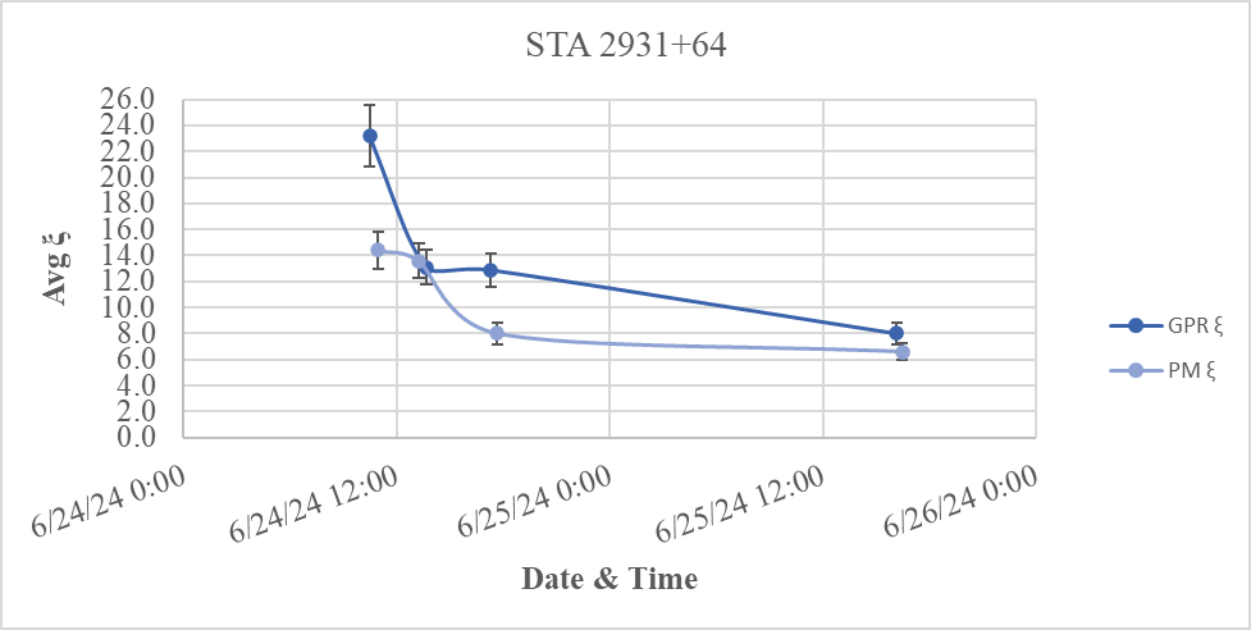

Figure E.13 STH 53 STA 2931+64 – 1 Hour Delay, AR = 115 sf/g.

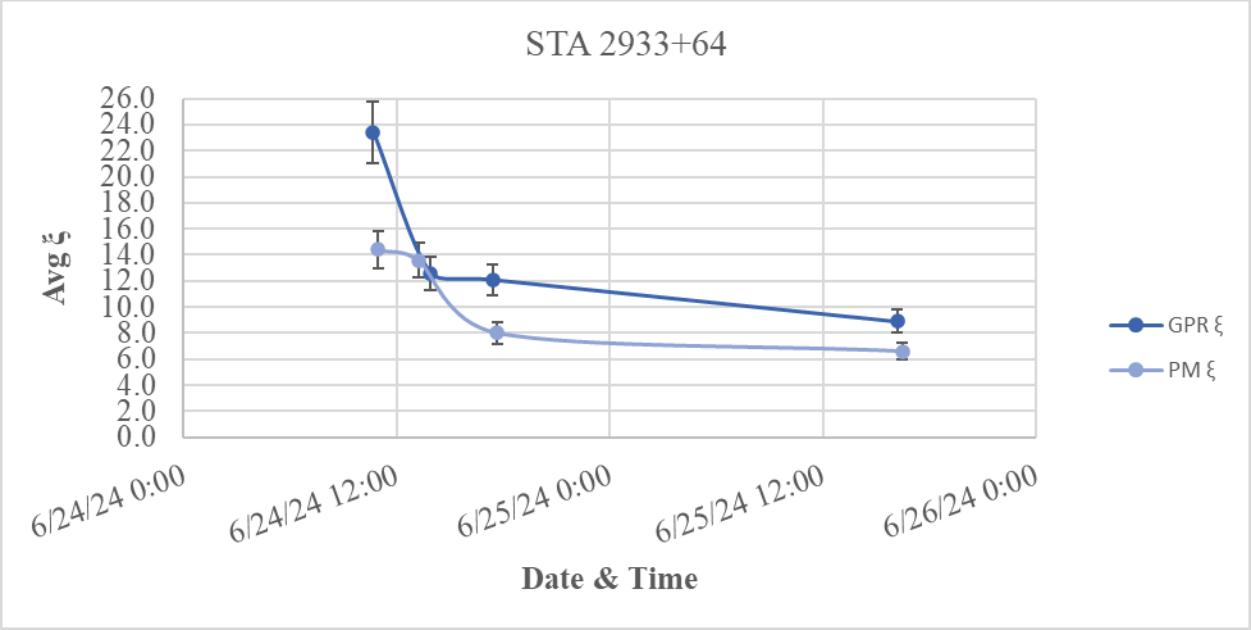

Figure E.14 STH 53 STA 2933+64 – 1 Hour Delay, AR = 230 sf/g.

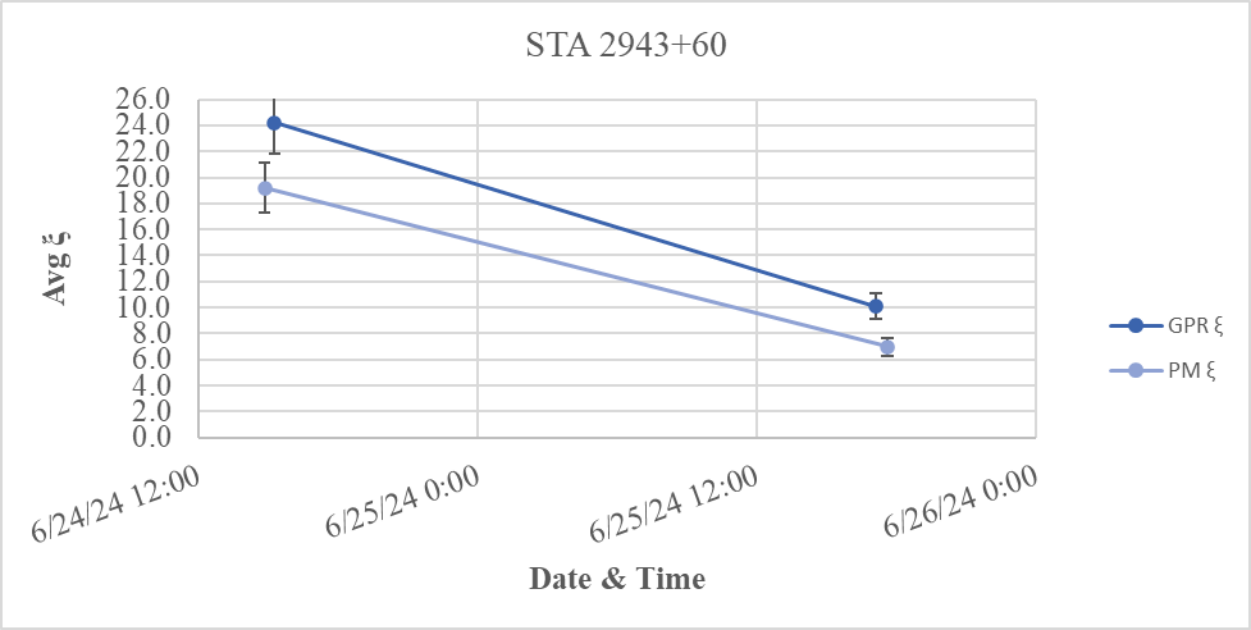

Figure E.15 STH 53 STA 2943+60 – 1 Hour Delay, AR = 150 sf/g.

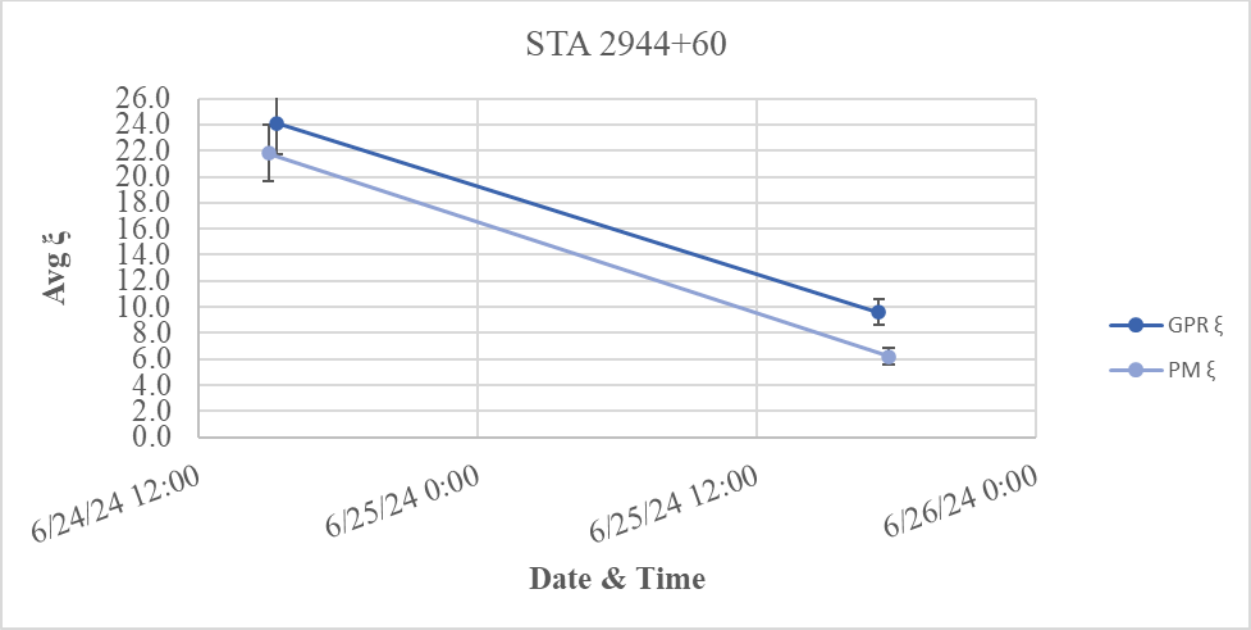

Figure F.16 STH 53 STA 2944+60 – 1 Hour Delay, AR = 115 sf/g.

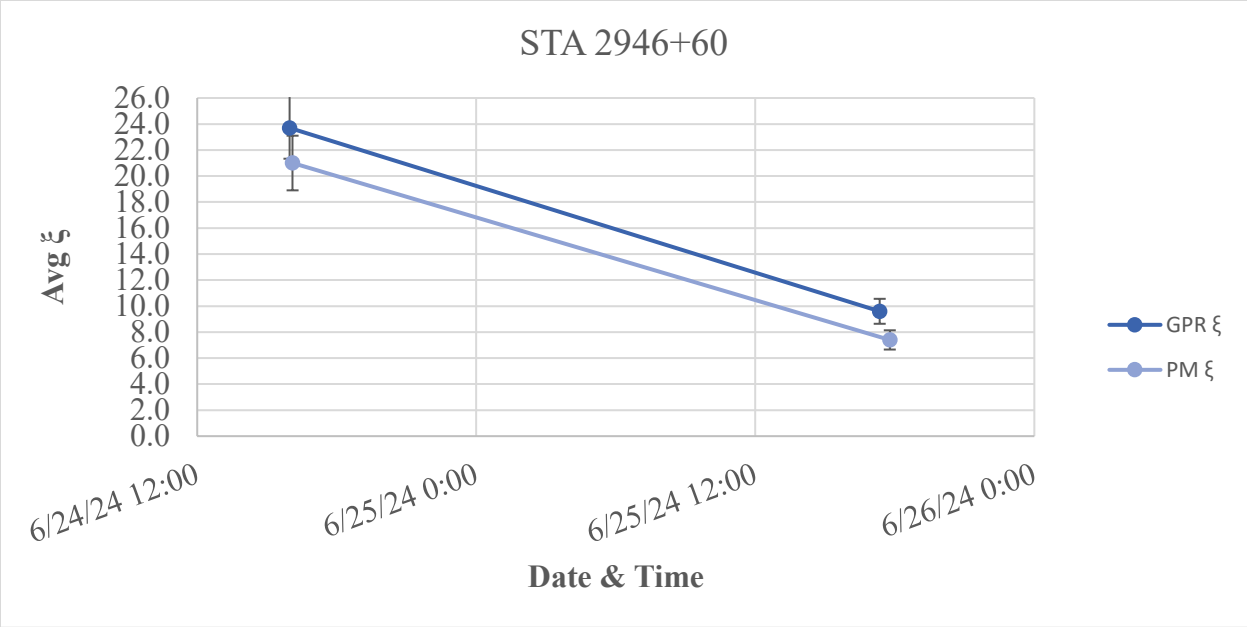

Figure E.14 STH 53 STA 2946+60 – 1 Hour Delay, AR = 230 sf/g.

6.6 Appendix F – Drying Shrinkage Data

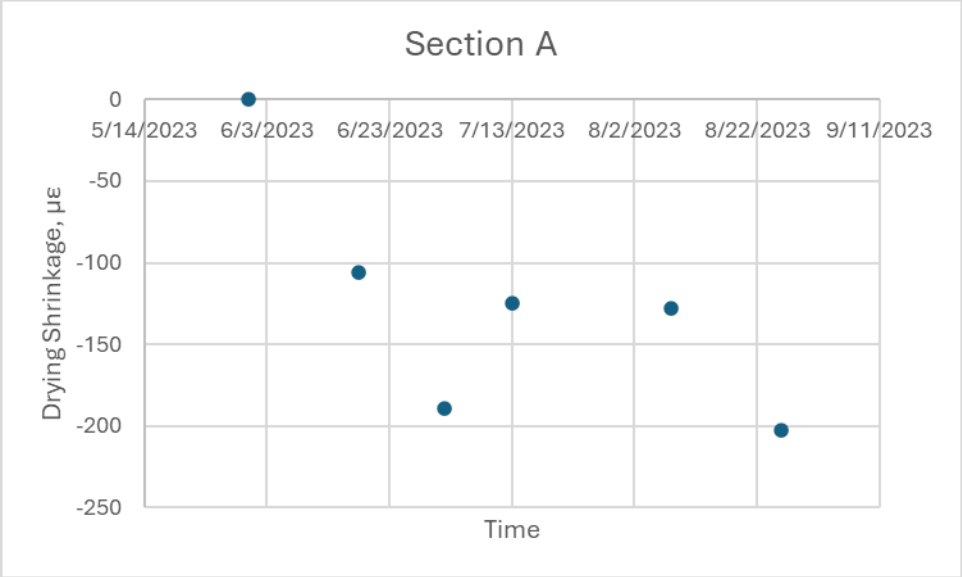

Figure F.1 STH 15 Section A – 2 hr Delay, AR=299 sf/g.

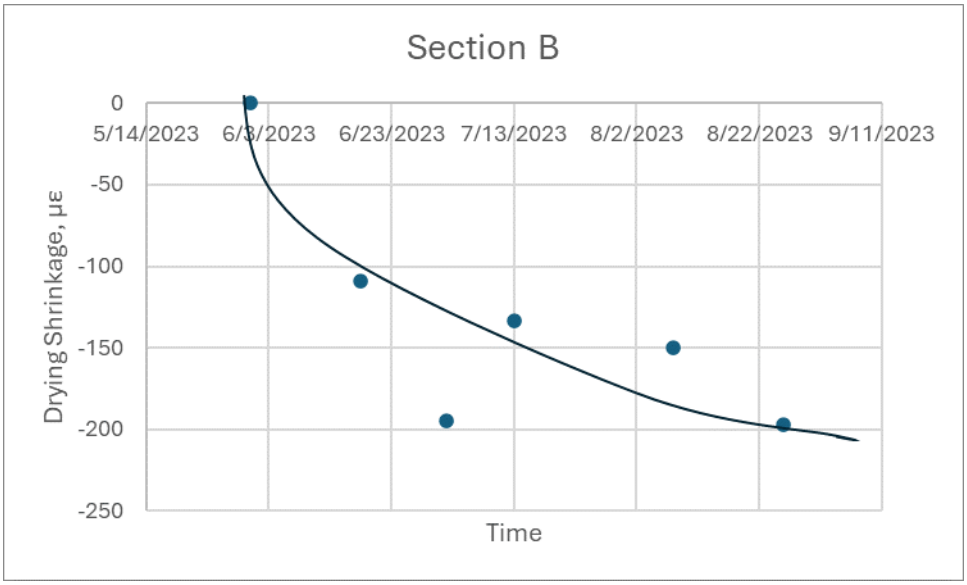

Figure F.2 STH 15 Section B – 2 hr Delay, AR=162 sf/g.

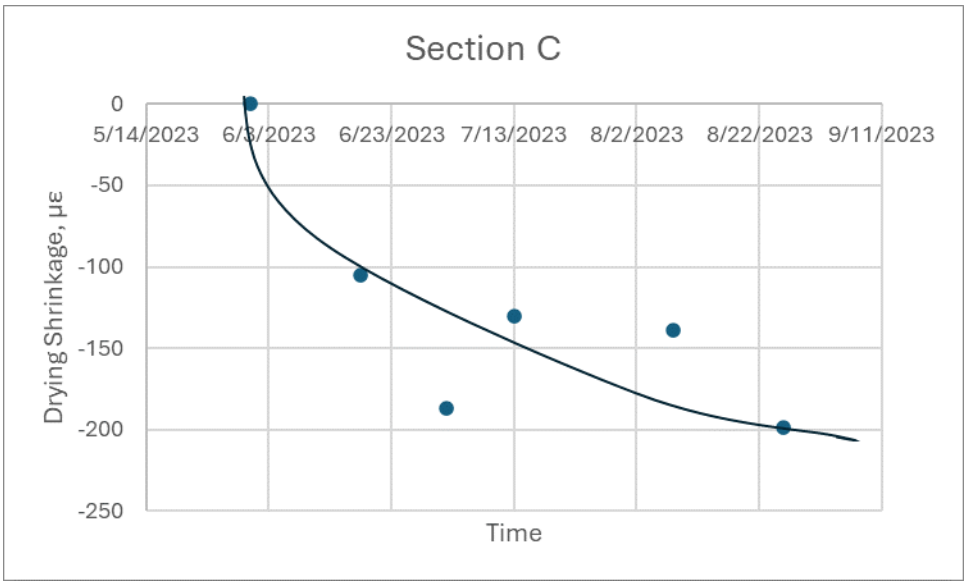

Figure F.3 STH 15 Section C – 2 hr Delay, AR=198 sf/g.

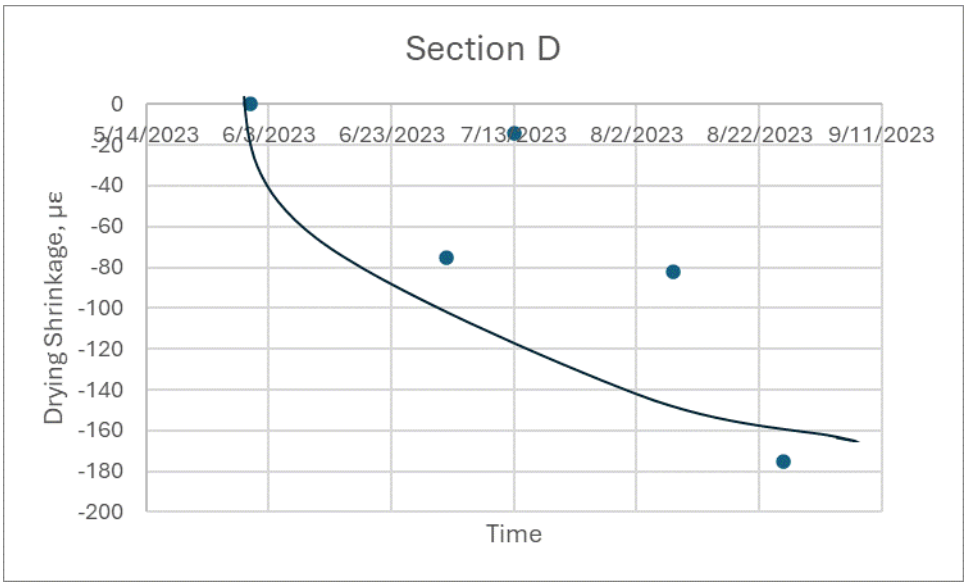

Figure F.4 STH 15 Section D – 2 hr Delay, AR=136 sf/g.

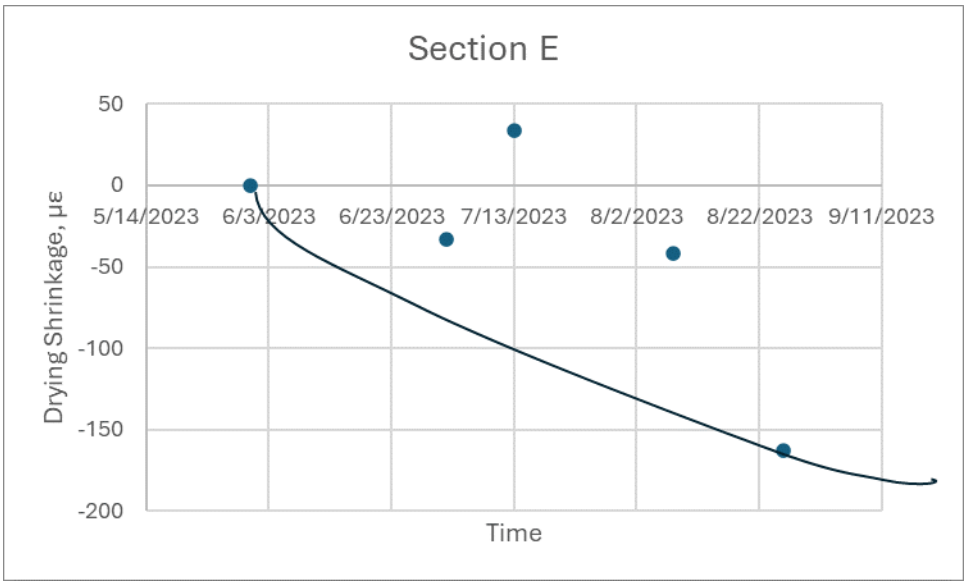

Figure F.5 STH 15 Section E – No Delay, AR=275 sf/g.

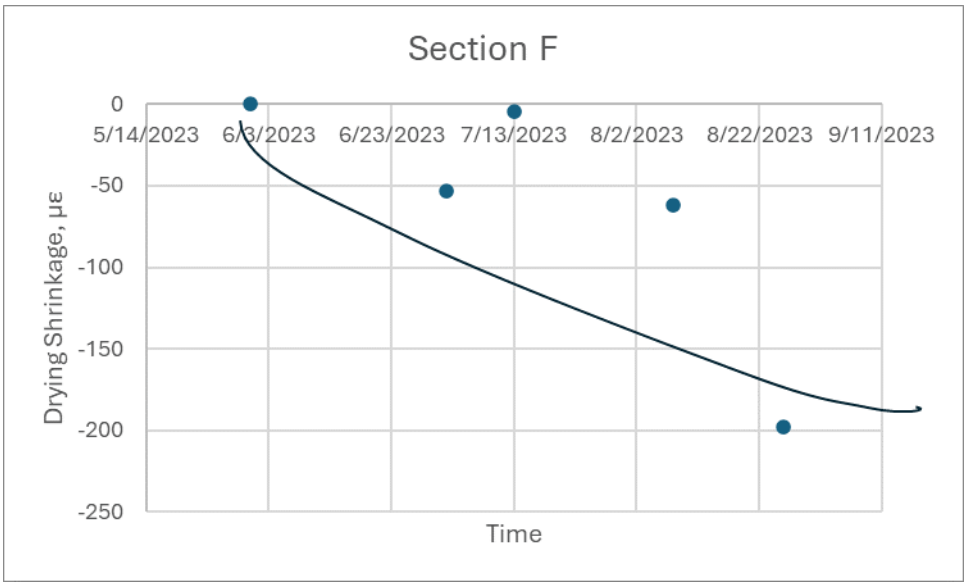

Figure F.6 STH 15 Section F – No Delay, AR=162 sf/g.

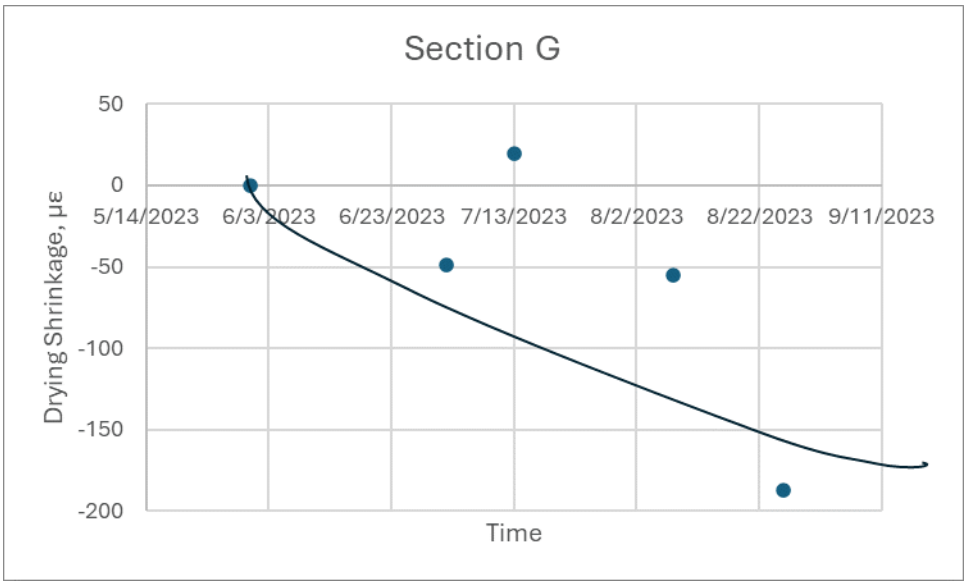

Figure F.7 STH 15 Section G – No Delay, AR=270 sf/g.

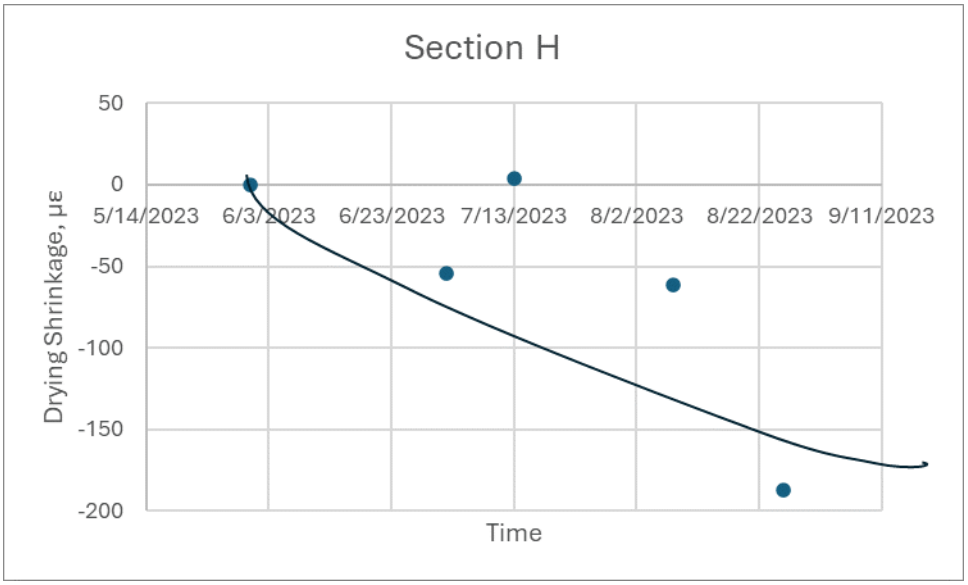

Figure F.8 STH 15 Section H – No Delay, AR=167 sf/g.

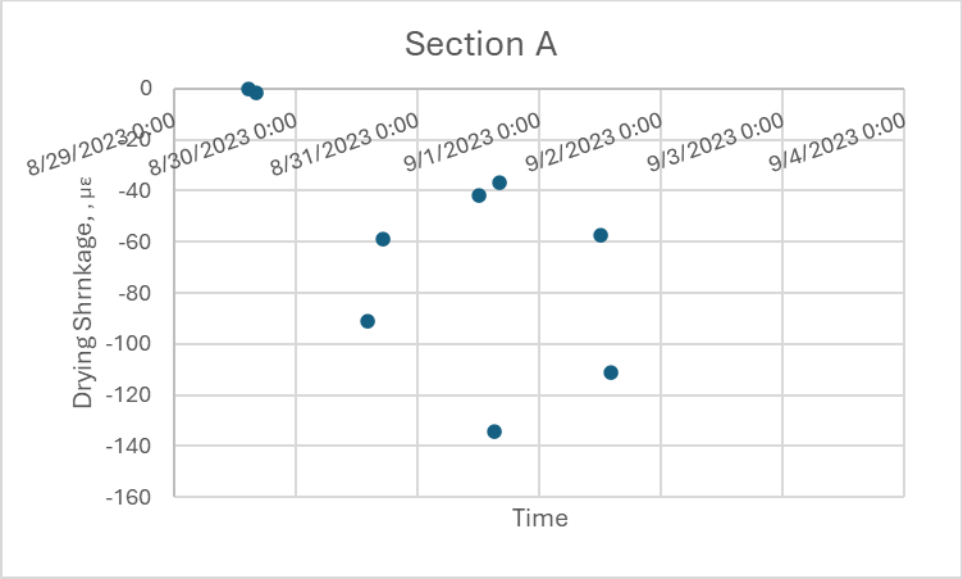

Figure F.9 STH 29 Section A – 2 hr Delay, AR=252 sf/g.

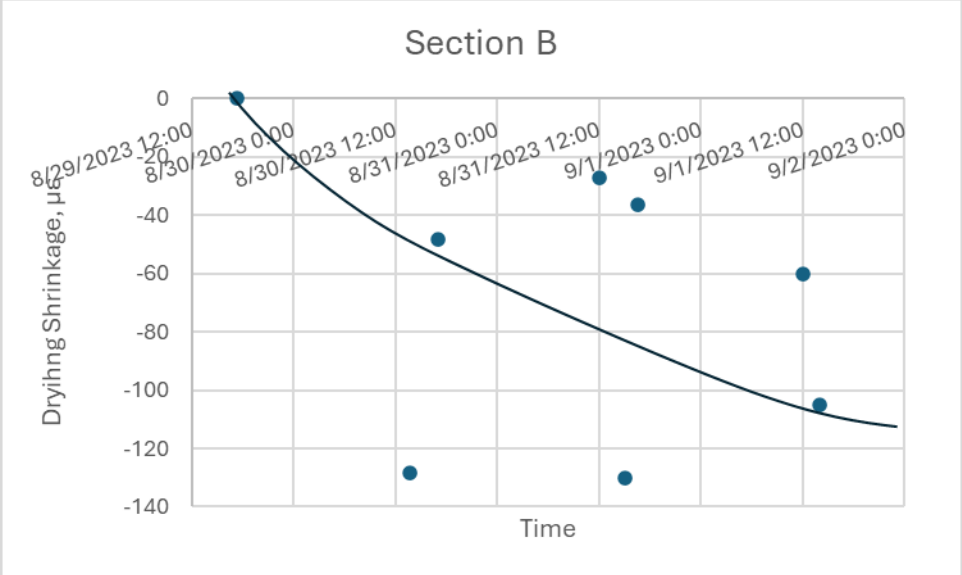

Figure F.10 STH 29 Section B – No Delay, AR=96 sf/g.

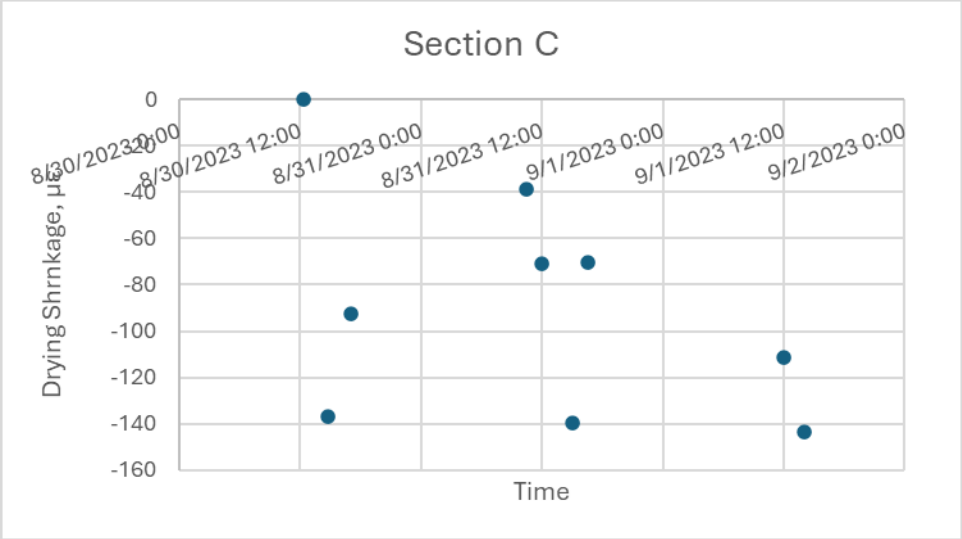

Figure F.11 STH 29 Section C – No Delay, AR=247 sf/g.

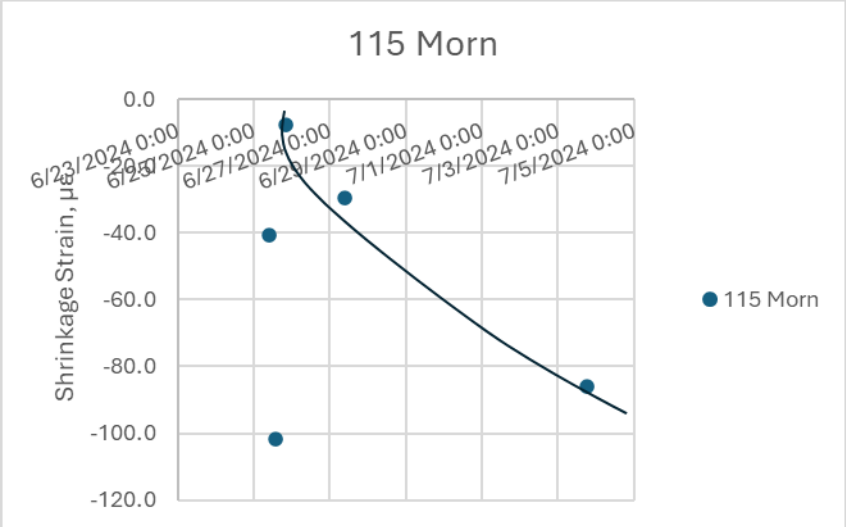

Figure F.12 STH 53 STA 2931+64 – 1 Hour Delay, AR = 115 sf/g

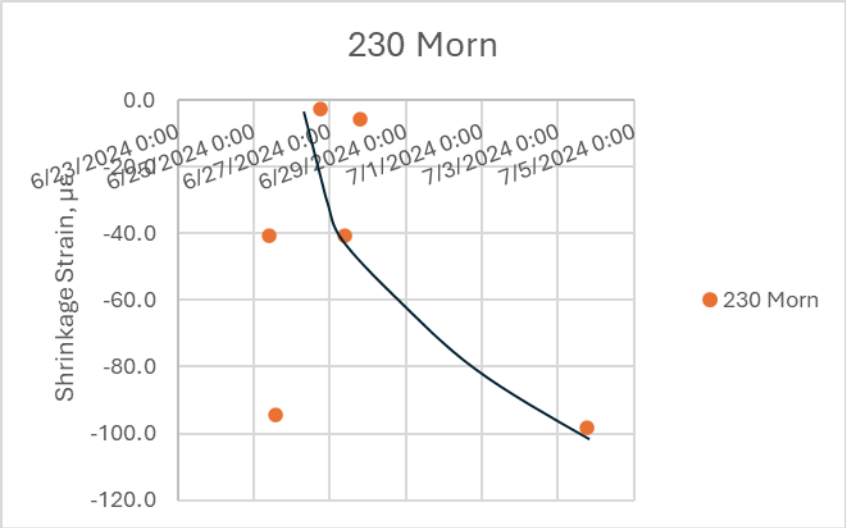

Figure F.13 STH 53 STA 2933+64 – 1 Hour Delay, AR = 230 sf/g

6.7 Appendix G – Drying Shrinkage Behavior

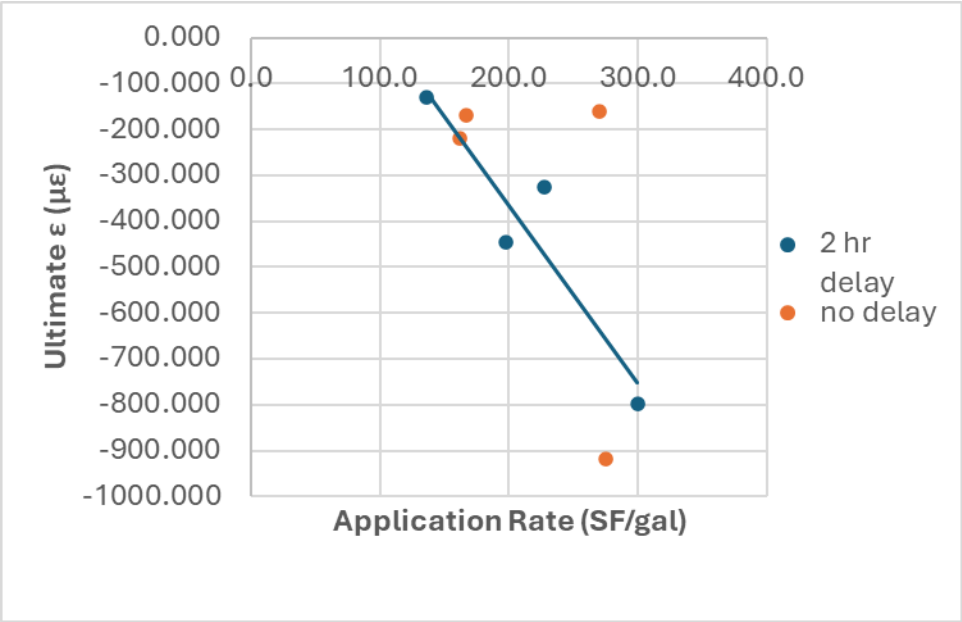

Figure G.1 STH 15: Ultimate Drying Shrinkage vs AR and ToA.

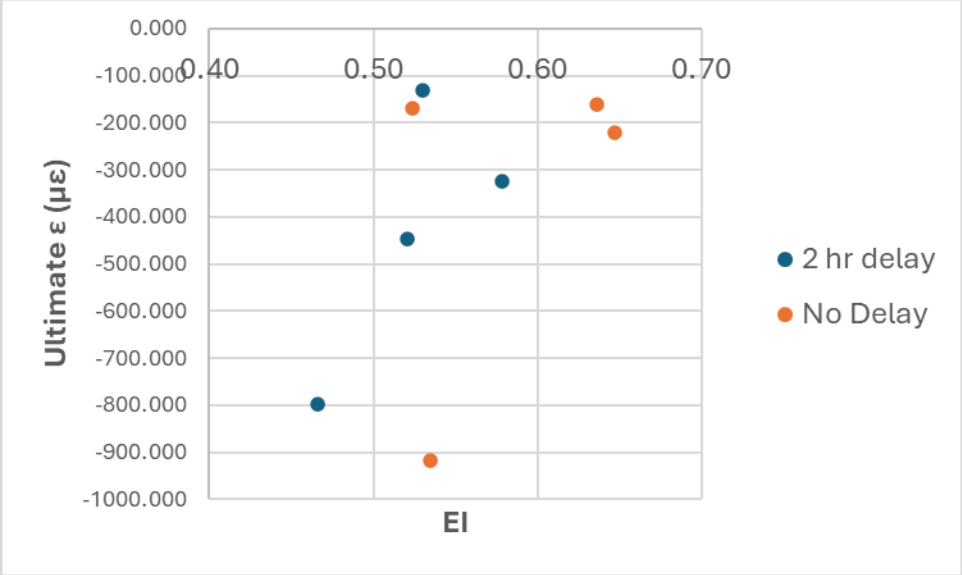

Figure G.2 STH 15: Ultimate Drying Shrinkage vs EI and ToA

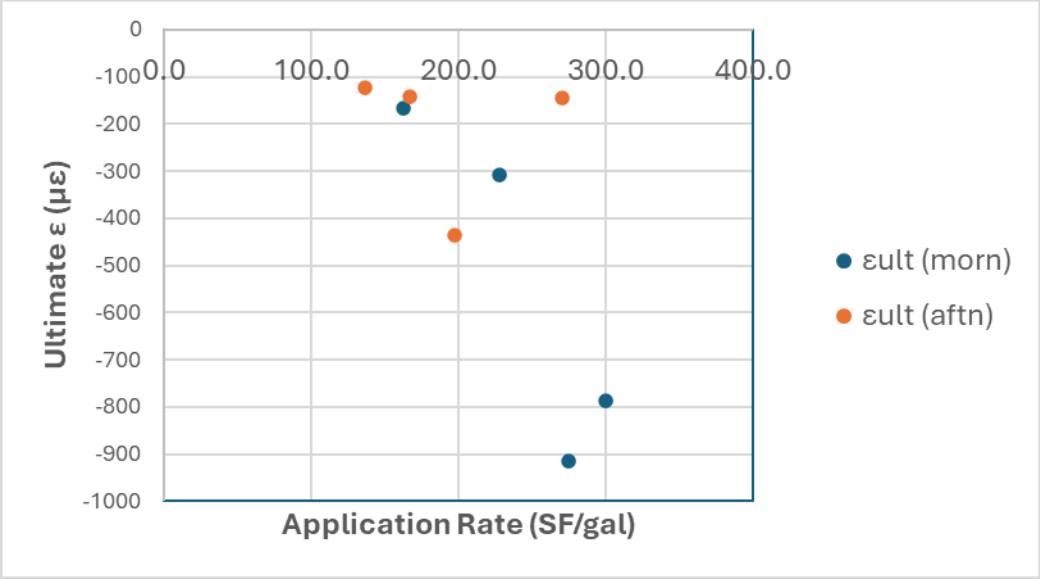

Figure G.3 STH 15: Ultimate Drying Shrinkage vs ToP and ToA

Figure G.4 STH 29: Curing Summary

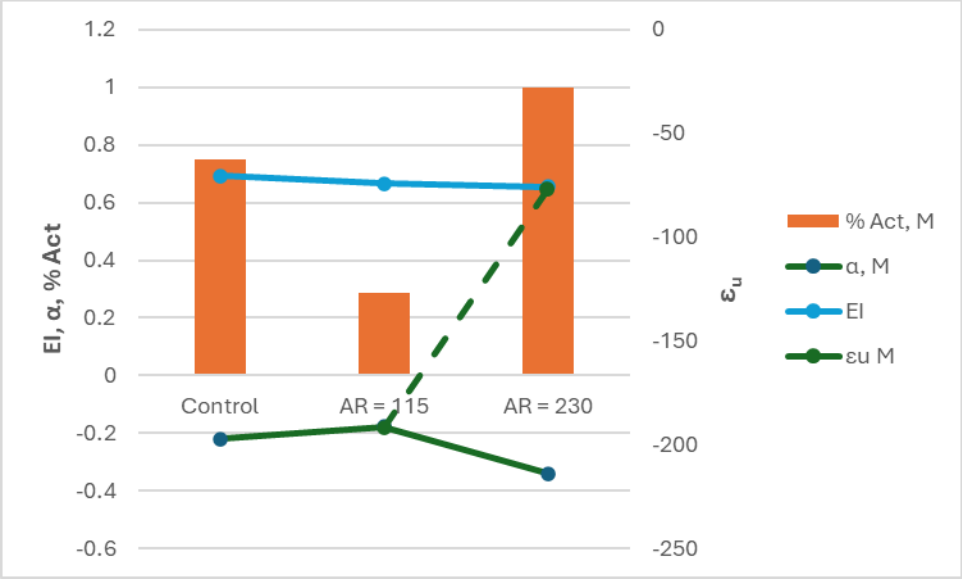

Figure G.5 STH 53: Morning Placement Curing Summary.

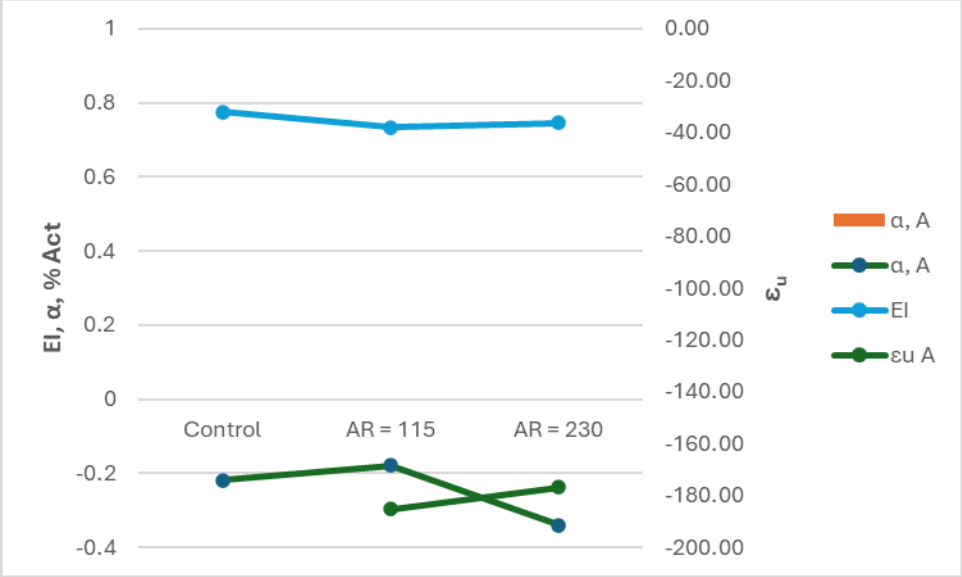

Figure G.6 STH 53: Afternoon Placement Curing Summary.

6.8 Appendix H - Corner Displacement

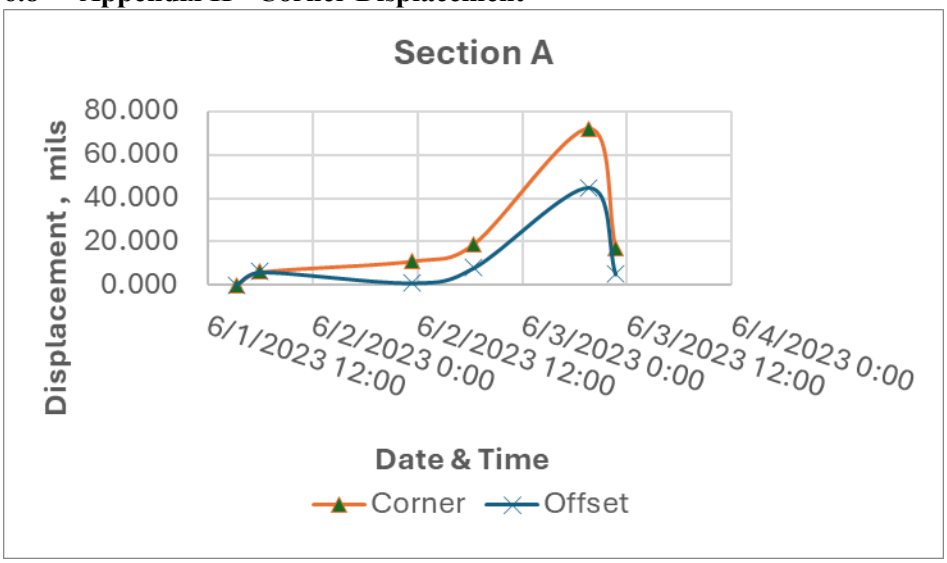

Figure G.1 STH 15 Section A: Corner Displacement Data.

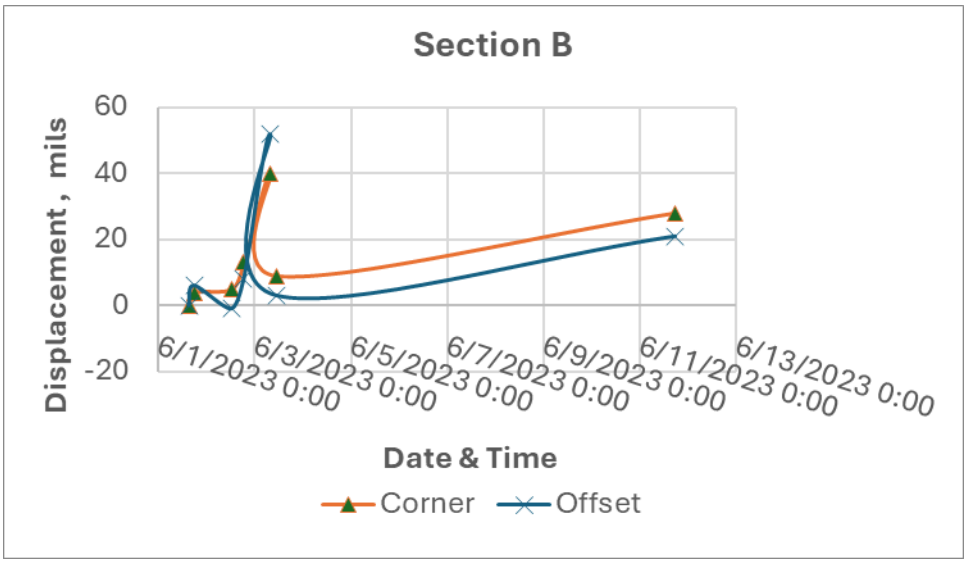

Figure G.2 STH 15 Section B: Corner Displacement Data.

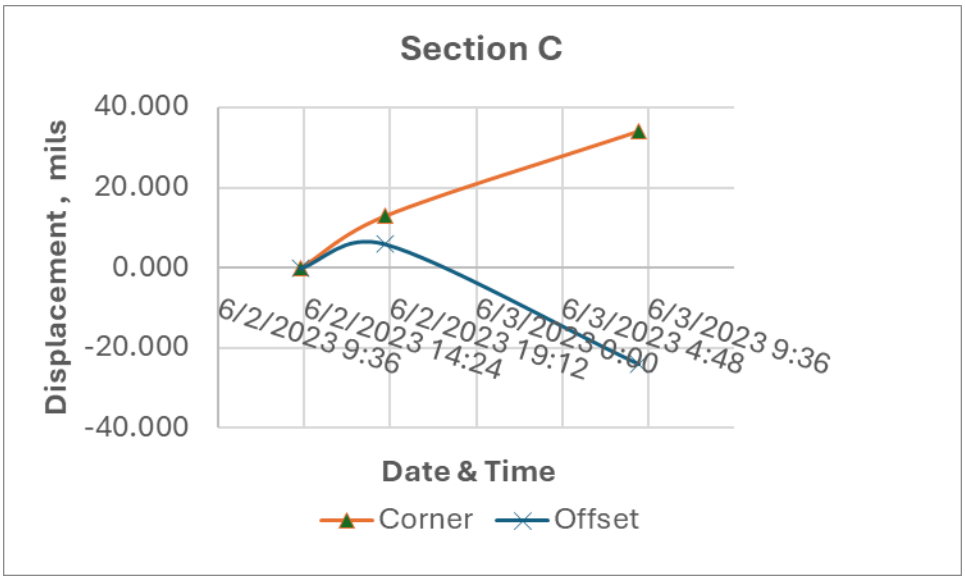

Figure G.3 STH 15 Section C: Corner Displacement Data.

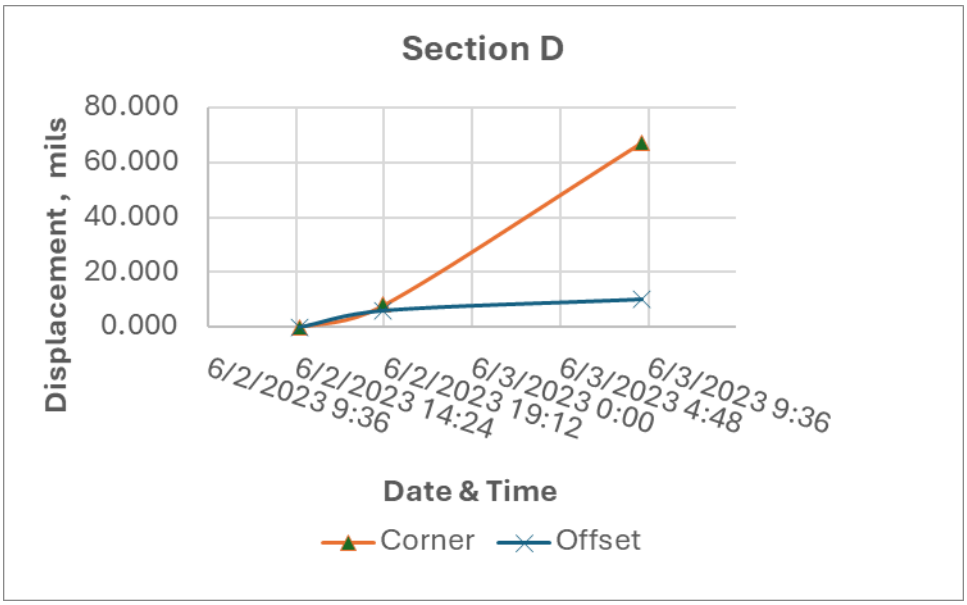

Figure G.4 STH 15 Section D: Corner Displacement Data.

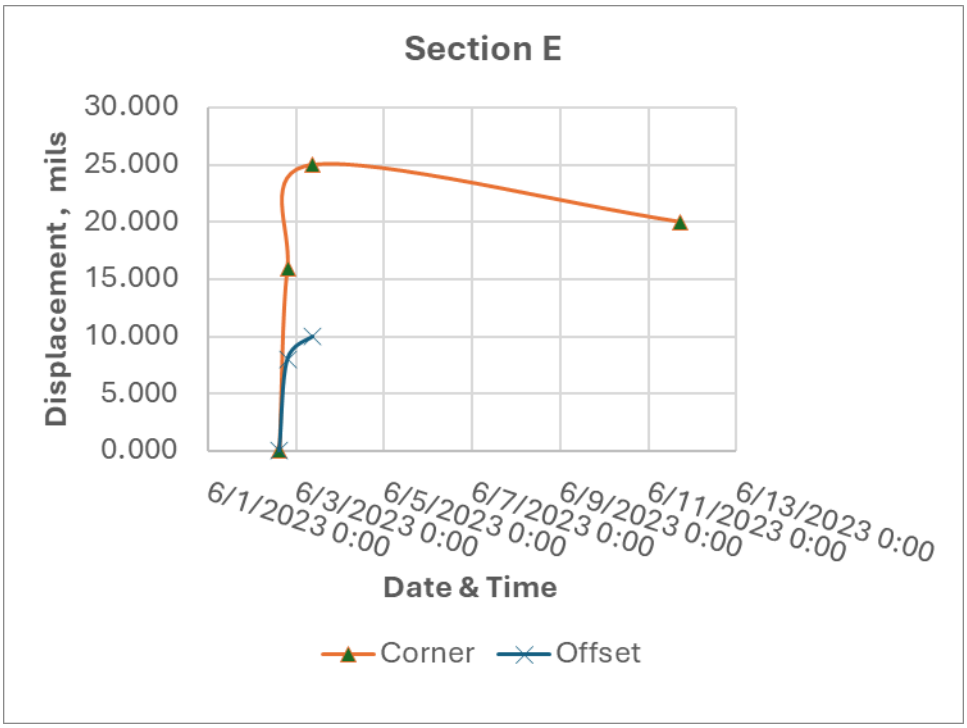

Figure G.5 STH 15 Section E: Corner Displacement Data.

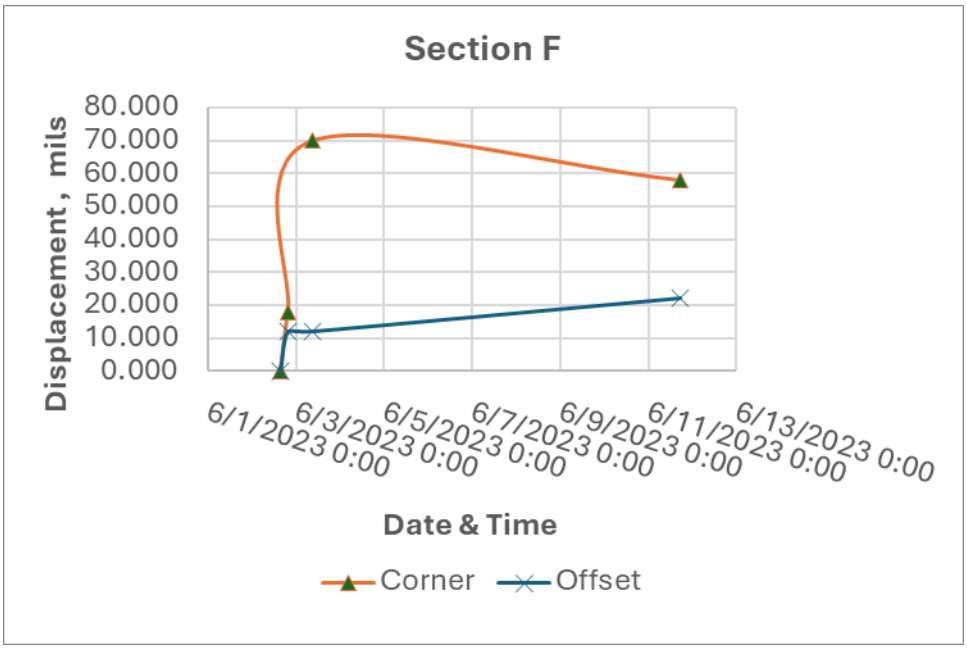

Figure G.6 STH 15 Section F: Corner Displacement Data

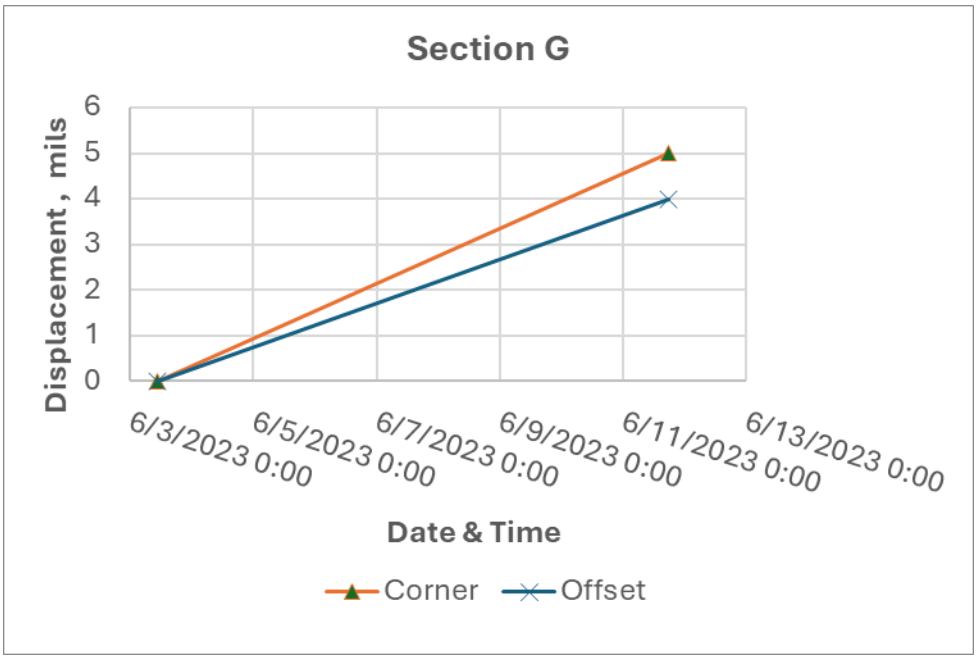

Figure G.7 STH 15 Section G: Corner Displacement Data

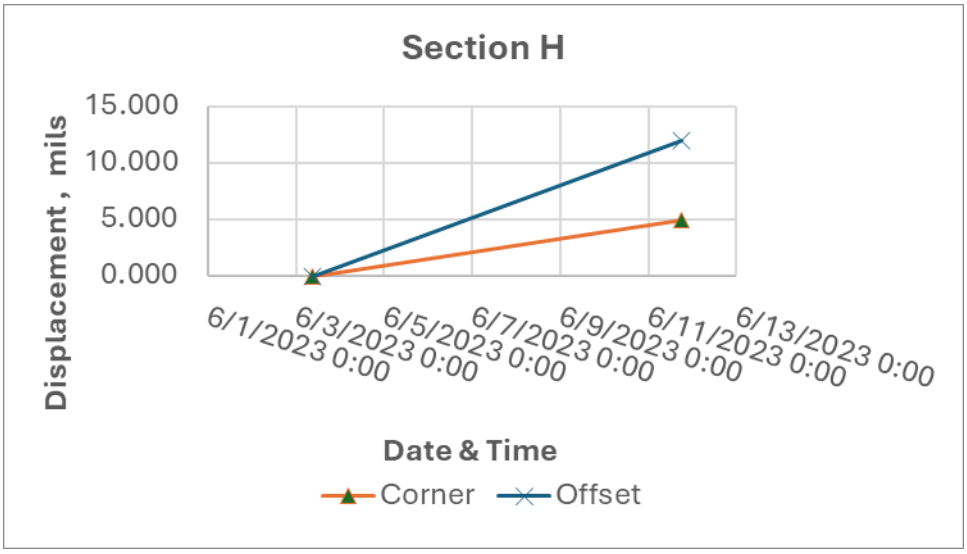

Figure G.8 STH 15 Section H: Corner Displacement Data.

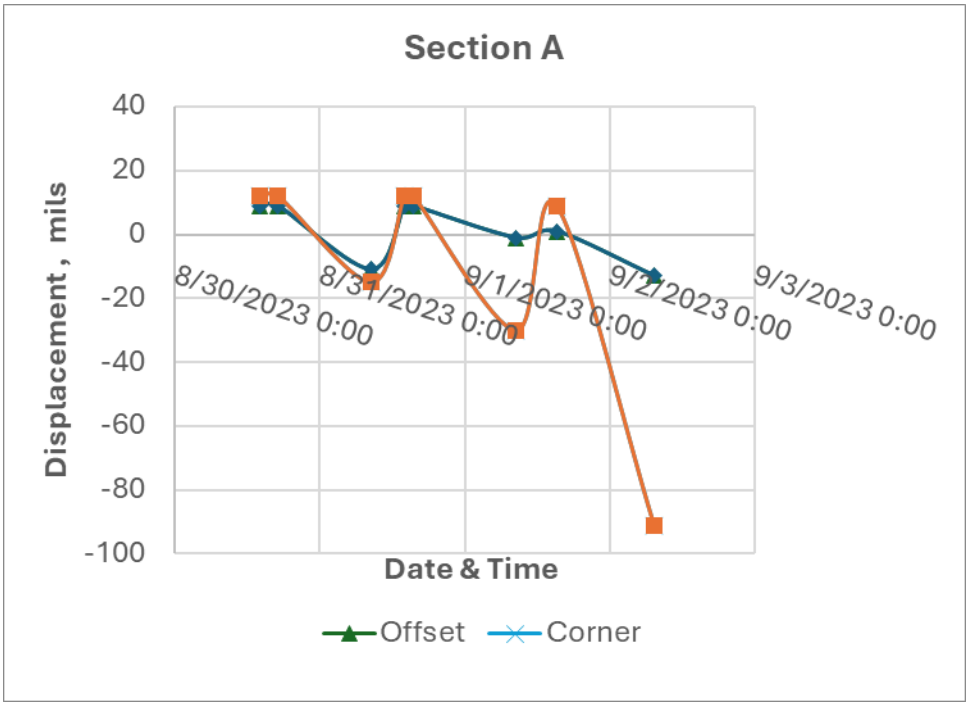

Figure G.9 STH 29 Section A: Corner Displacement Data.

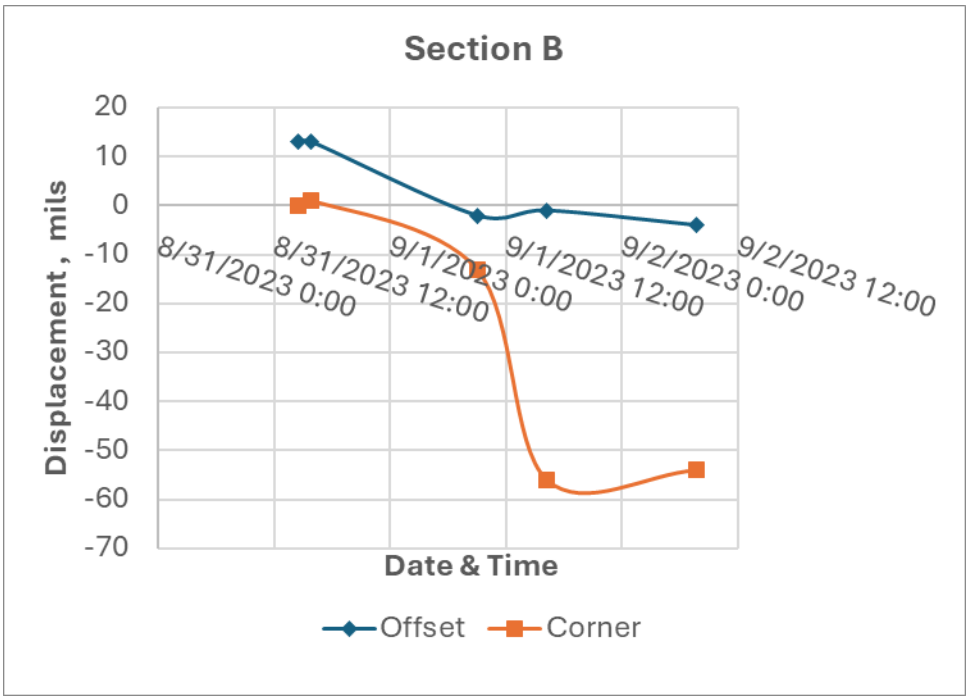

Figure G.10 STH 29 Section B: Corner Displacement Data.

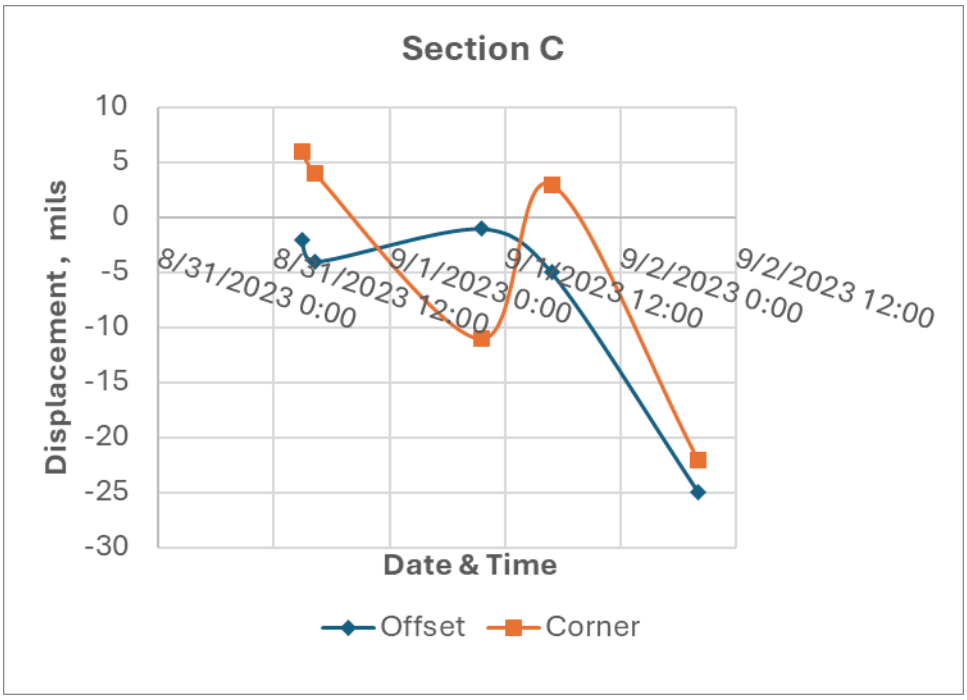

Figure G.11 STH 29 Section C: Corner Displacement Data.

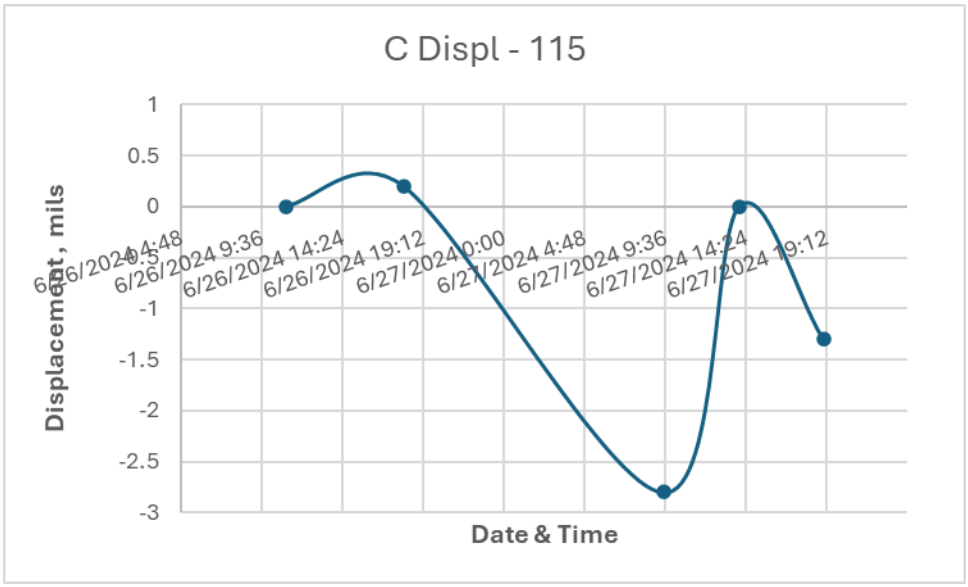

Figure G.12 STH 53 AR=115 sg/g: Corner Displacement Data.

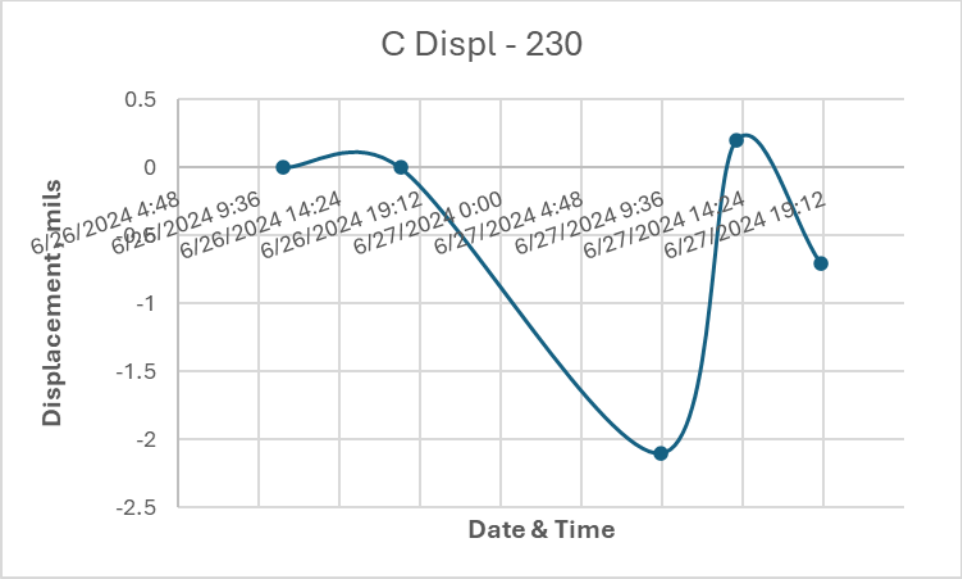

Figure G.13 STH 53 AR=230 sg/g: Corner Displacement Data.

6.9 Appendix I - Draft Specification

419.2 Curing

Curing is the maintenance of a sufficient moisture content and temperature throughout the concrete mass to support hydration until the concrete has developed sufficient strength to open it to service. Concrete develops strength due to hydration, a chemical reaction that occurs when portland cement is combined with water. Concrete does not harden as it dries; quite the contrary, if freshly placed concrete dries out, hydration ceases, and the concrete stops gaining strength. Optimum durability is achieved as the concrete approaches full hydration. Proper curing is critical for the development of strong, durable, high quality concrete. Curing should begin as soon as the free water "sheen" has disappeared from the surface. Paving operations should be slowed or suspended when the contractor's curing operation falls behind.

Membrane forming curing compound is a spray-on material which significantly reduces evaporation from the pavement surface, sealing in the moisture required for hydration and prevent rapid drying of exposed surfaces. Except during cold weather, these materials must be colored white to reflect radiant heat that could cause surface overheating and impose thermal stress on the concrete. In cold weather, black or clear sheeting materials may be used. Two principal types of curing compounds are currently specified for use on WisDOT work:

- Poly-alpha-methylstyrene (PAM) curing compound (standard spec 415.2.4)
- ASTM C309 water based wax curing compound (standard spec 501.2.9). Each of these types of curing compound has different performance characteristics and is appropriate in different applications. PAM may be used in all applications except for pavement that will be overlain. For those pavements use curing compound conforming to standard spec 501.2.9. PAM curing compound has very good water retention characteristics. For WisDOT work the principal use for PAM is concrete pavement on rural highways and on expressways and high-performance concrete (HPC) in urban areas as well. Traditional wax curing compound provides adequate water retention for miscellaneous ancillary items and allow better bonding to items that will be covered up in service. In the concrete pavement area, the principal use for the traditional wax cure is for concrete base and concrete base patching, both items that will be covered up in service. The wax cure wears off faster, and is more easily removed, allowing better bond of the concrete base to the final pavement layer placed on top of it. A concern is that use of PAM or linseed cure would be more likely to cause debonding of the overlay from the concrete base.

Curing compound shall be thoroughly mixed and continually agitated as the white pigment can settle quickly. Larger projects utilize bulk delivery and storage. The bulk storage is normally agitated using pressurized air prior to delivery while the spray machine tank is stirred with electrically driven paddles or continuous pump recirculation. Provide continuous agitation while spraying to ensure uniform consistency and dispersion of pigment within the curing compound during application.

Preparing and maintaining the cure-spraying machine includes flushing the nozzles before operating. Most texturing machines have shields or hoods that shelter the nozzle application operation to prevent spray drift, especially in windy conditions.

Be sure to apply the cure to the vertical slab edges. Re-spray any damaged areas and check that no areas are left uncoated. Cure the edges of the pavement as soon as possible after form removal.

The construction inspector shall perform the following equipment inspection at the beginning of each day of construction or breaks more than 4 hours of curing compound application.

6.10 Appendix J – Construction Inspector Checklist

At the beginning of each day of construction it is important to verify the curing cart is setup and operating correctly.

1. Verify the membrane-curing compound on site is approved for use by comparing the storage container documentation with the approved products list.
2. Verify uniform spray bar height above the pavement.
3. Verify the curing equipment provides continuous agitation during application either through constant mixing or recirculation.
4. Verify rate of application and record test data.
    a. Measure the tank area and the level of the curing compound in the tank before application. Some tanks are semi-translucent and the measurement can be taken from outside of the tank. If the tank is opaque, remove the fill cap and measure from a consistent place typically on the lip of the fill opening.
    b. Have the operator apply curing compound for at least 100 feet. Using a distance wheel, record the exact distance covered. It may be easiest to premark the 100 foot distance and identify to the operator where to stop.
    c. Record the speed setting of the curing. Many curing carts operate using hydrostatic motors controlled by a dial. If the control dial does not have markings, estimate the operational location between 0-100. Typical operations are around 75% or three-quarters of maximum speed.
    d. Record the time the cart took to cover the trial distance.
    e. Measure the level of curing compound after the trial run.
    f. Calculate the application rate in square feet covered per gallon of curing compound.
        i. For example on a 26 ft wide pavement
        ii. Curing tank width 30 in. and length 45 in.
        iii. Curing compound level 3 inches below the top lip of the tank before the spray trial.
        iv. Curing compound level 6 inches below the top lip of the tank after the spray trial
        v. 30 in. x 45 in. x (6 in.-3 in.) = 4140 cubic inches = 2.4 cubic feet = 17.9 gallons (1 cubic foot = 7.48 gallons)
        vi. A 100 ft trial length at 26 ft wide is 2,600 sf.
        vii. 2,600 sf/17.9 gallons = 145 sf/gallon
    g. Calculate the speed of the curing cart in feet per minute.
    h. If the curing application rate is low (>150 sf/gal), perform another trial run of 100 feet at a lower speed. If the curing application rate is high (<150sf/gal), perform another trial run of 100 feet at a higher speed. Once the desired rate has been achieved it is a good practice to ask the curing cart operator to put a mark on the control panel to identify the correct index location.
5. Verify sufficient overlap (30% desired) in spray nozzles
    a. While the rate measurement trial is underway, verify the surface nozzles are providing uniform coverage and nozzles are overlapping 30%. If the nozzles overlap more than 30%, instruct the operator to raise the spray bar. If the nozzles do not overlap at least 30%, instruct the operator to lower the spray bar.
6. Verify side nozzles
    a. While the rate measurement trial is underway, verify that the side nozzles are functioning and providing uniform coverage.